

AN EXPERIMENTAL STUDY OF EXCITED STATE LEVEL POPULATIONS
IN THE ARGON INDUCTIVELY COUPLED PLASMA

By

ZANE HARRY WALKER

B.Sc., Dalhousie University, 1983

A THESIS SUBMITTED IN PARTIAL FULFILLMENT OF
THE REQUIREMENTS FOR THE DEGREE OF
MASTER OF SCIENCE

in

THE FACULTY OF GRADUATE STUDIES
(Department of Chemistry)

We accept this thesis as conforming
to the required standard

THE UNIVERSITY OF BRITISH COLUMBIA

June 1986

© Zane Harry Walker

In presenting this thesis in partial fulfilment of the requirements for an advanced degree at the University of British Columbia, I agree that the Library shall make it freely available for reference and study. I further agree that permission for extensive copying of this thesis for scholarly purposes may be granted by the head of my department or by his or her representatives. It is understood that copying or publication of this thesis for financial gain shall not be allowed without my written permission.

Department of Chemistry

The University of British Columbia
1956 Main Mall
Vancouver, Canada
V6T 1Y3

Date June 11, 1986

ABSTRACT

In an effort to elucidate excitation and ionization of analyte in the inductively coupled plasma, excited state level populations have been determined for three analytes, Fe, Ba, and Cr, from experimentally measured line emission intensities at various rf input powers and spatial positions. Measurement of line intensities was achieved using a 4096 pixel linear photodiode array spectrometer. The photodiode array spectrometer proved to be very advantageous in the collection of data, allowing the simultaneous measurement of line intensities from a wavelength window approximately 50 nm in width.

Population plots were constructed from relative level populations for both atom and ion species of the three analytes and their dependence on rf input power was examined. The spatial dependence of the FeI and FeII populations was also studied. Excitation temperatures determined from the atom and ion level populations of Fe, Ba and Cr were examined.

The results strongly support the existence of partial local thermodynamic equilibrium in the ICP. Such an equilibrium condition is characterized by an overpopulation of low energy atom levels and the presence of Saha equilibrium between high energy atom levels and the ground state ion. The principal means of analyte excitation and ionization appears to be a result of inelastic electron collisions.

TABLE OF CONTENTS

Chapter	Page
1. Introduction	
1.1 Objective.....	1
1.2 The ICP: An Historical Perspective.....	2
1.3 The ICP.....	4
1.4 Analyte Excitation and Ionization.....	8
1.4.1 Collisional Excitation and De-excitation By Electrons.....	9
1.4.2 Collisional Ionization and Three Body Recombination.....	10
1.4.3 Radiative Recombination.....	10
1.4.4 Radiative De-excitation.....	11
1.4.5 Penning Ionization.....	12
1.4.6 Asymmetric Charge Transfer With Argon.....	12
1.5 Thermodynamic Equilibrium in the ICP.....	13
1.5.1 Maxwell Distribution.....	14
1.5.2 Boltzmann Distribution.....	15
1.5.3 Saha Distribution.....	16
1.5.4 Guldberg-Waage Distribution.....	18
1.5.5 Summary.....	19
1.6 Excited State Level Populations.....	20
2. Experimental	
2.1 Instrumentation.....	22

2.2	Computer Interfacing of LPDA and Data Acquisition.....	30
2.3	Software.....	36
2.4	Sample Preparation and Selection of Analyte Concentration.....	37
2.5	Selection of Spectral Lines.....	38
2.6	Measurement of Spatially Resolved Line Intensities.....	38
2.7	Spectral Correction of Spectral Line Intensities.....	40
3.	Excited State Level Populations	
3.1	Introduciton.....	41
3.2	Results.....	49
3.3	Fe Results.....	54
3.3.1	Fe Level Populations at 8 mm Above the Load Coil.....	54
3.3.2	Fe Level Populations at 16 mm Above the Load Coil.....	65
3.3.3	Fe Excited State Level Populations.....	72
3.4	Ba Results.....	77
3.4.1	Ba Excited State Level Populations.....	77
3.5	Cr Results.....	81
3.5.1	Cr Excited State Level Populations.....	82
3.6	Discussion.....	90
4.	Summary.....	100
	References.....	104
	Appendix A.....	109

Appendix B.....	124
Appendix C.....	134
Appendix D.....	141

LIST OF TABLES

Table	Description	Page
I.	LTE temperatures corresponding to measured electron densities.....	53
II.	Emission lines of Fe including wavelength, gA values, and excitation energies.....	55
III.	Emission lines of Ba including wavelength, gA values, and excitation energies.....	78
IV.	Emission lines of Cr including wavelength, gA values, and excitation energies.....	83
V.	CrI and CrII excitation temperatures and LTE temperatures at 0.75 kW, 1.00 kW, 1.25 kW, 1.50 kW and 1.75 kW rf input power.....	91
VI.	Fe, Ba and Cr excitation temperatures at 1.25 kW and 1.75 kW rf input power.....	95

LIST OF FIGURES

Figure	Description	Page
1.	The ICP discharge.....	6
2.	Block diagram of instrumentation.....	23
3.	The ICP torch.....	24
4.	The concentric glass nebulizer.....	25
5.	The ICP torch, spray chamber and concentric glass nebulizer.....	26
6.	Plot of refractive index of fused silica versus wavelength.....	29
7.	Imaging distance of a fused silica lens, with a radius of curvature of 69.80 nm, as a function of wavelength.....	31
8.	Diagram of the interfacing between the LPDA and the CompuPro microcomputer via the transient recorder.....	33
9.	Timing diagram for the acquisition of data from the LPDA.....	34
10.	Timing diagram for the readout of data from the transient recorder.....	35
11a.	A plot of the logarithm of FeI excited state level populations vs excitation energy, from data extracted from Faires, Palmer and Engleman [53]. Populations have been fitted to a second order	

Figure	Description	Page
	polynomial.....	48
11b.	A plot of the logarithm of FeI excited state level populations vs excitation energy, from data extracted from Faires, Palmer and Engleman [53]. Populations have been fitted using linear regression.....	48
12.	A Saha-Boltzmann LTE plot of the logarithm of level populations as a function of energy. E^+ and E^{++} are the ionization energies of atomic and ionic species respectively. The level populations are represented by a single temperature given by the slope of the Saha-Boltzmann lines ($-1/kT$).....	50
13.	A plot of the logarithm of FeI level populations determined at 8 mm above the load coil and at 1.25 kW rf input power as a function of energy. Radial positions of 0 mm and 1.5 mm.....	58
14.	FeI level dependent temperatures calculated from FeI level populations determined at 8 mm above the load coil, at an rf input power of 1.25 kW and at a radial position of 0 mm.....	59
15.	A plot of the logarithm of FeII level populations determined at 8 mm above the load coil and at 1.25 kW rf input power as a function of energy. Radial	

Figure	Description	Page
	positions of 0 mm and 1.5 mm.....	61
16.	A plot of the logarithm of FeI level populations determined at 8 mm above the load coil and at 1.75 kW rf input power as a function of energy. Radial positions of 0 mm and 1.5 mm.....	63
17.	A plot of the logarithm of FeII level populations determined at 8 mm above the load coil and at 1.75 kW rf input power as a function of energy. Radial positions of 0 mm and 1.5 mm.....	64
18.	A plot of the logarithm of FeI level populations determined at 16 mm above the load coil and at 1.25 kW rf input power as a function of energy. Radial positions of 0 mm and 1.5 mm.....	66
19.	A plot of the logarithm of FeII level populations determined at 16 mm above the load coil and at 1.25 kW rf input power as a function of energy. Radial positions of 0 mm and 1.5 mm.....	67
20.	FeI level dependent temperatures calculated from FeI level populations determined at 16 mm above the load coil, at an rf input power of 1.25 kW and at a radial position of 0 mm.....	68
21.	A plot of the logarithm of FeI level populations determined at 16 mm above the load coil and at 1.75	

Figure	Description	Page
	kW rf input power as a function of energy. Radial positions of 0 mm and 1.5 mm.....	70
22.	A plot of the logarithm of FeII level populations determined at 16 mm above the load coil and at 1.75 kW rf input power as a function of energy. Radial positions of 0 mm and 1.5 mm.....	71
23.	A plot of the logarithm of FeI and FeII level populations determined at 8 mm above the load coil, at a radial position of 0 mm and at an rf input power of 1.25 kW. The solid lines represents LTE calculated populations.....	73
24.	A plot of the logarithm of FeI and FeII level populations determined at 8 mm above the load coil, at a radial position of 0 mm and at an rf input power of 1.75 kW. The solid lines represents LTE calculated populations.....	74
25.	A plot of the logarithm of FeI and FeII level populations determined at 16 mm above the load coil, at a radial position of 0 mm and at an rf input power of 1.25 kW. The solid lines represents LTE calculated populations.....	75
26.	A plot of the logarithm of FeI and FeII level populations determined at 16 mm above the load coil,	

Figure	Description	Page
	at a radial position of 0 mm and at an rf input power of 1.75 kW. The solid lines represents LTE calculated populations.....	76
27.	A plot of the logarithm of BaI and BaII level populations determined at 16 mm above the load coil, at a radial position of 0 mm and at an rf input power of 1.25 kW. The solid lines represents LTE calculated populations.....	79
28.	A plot of the logarithm of BaI and BaII level populations determined at 16 mm above the load coil, at a radial position of 0 mm and at an rf input power of 1.75 kW. The solid lines represents LTE calculated populations.....	80
29.	A plot of the logarithm of CrI and CrII level populations determined at 16 mm above the load coil, at a radial position of 0 mm and at an rf input power of 0.75 kW. The solid lines represents LTE calculated populations.....	85
30.	A plot of the logarithm of CrI and CrII level populations determined at 16 mm above the load coil, at a radial position of 0 mm and at an rf input power of 1.00 kW. The solid lines represents LTE calculated populations.....	86

Figure	Description	Page
31.	A plot of the logarithm of CrI and CrII level populations determined at 16 mm above the load coil, at a radial position of 0 mm and at an rf input power of 1.25 kW. The solid lines represents LTE calculated populations.....	87
32.	A plot of the logarithm of CrI and CrII level populations determined at 16 mm above the load coil, at a radial position of 0 mm and at an rf input power of 1.50 kW. The solid lines represents LTE calculated populations.....	88
33.	A plot of the logarithm of CrI and CrII level populations determined at 16 mm above the load coil, at a radial position of 0 mm and at an rf input power of 1.75 kW. The solid lines represents LTE calculated populations.....	89
34.	Calculated Maxwellian distribution of electron energies based on an equilibrium temperature of 8000 K.....	98

ACKNOWLEDGEMENT

I would like to express my sincere thanks to Dr. Michael W. Blades for his sound guidance and invaluable suggestions which he contributed throughout the course of my research. It is also important to acknowledge the contributions made by other members of our research group in the form of constructive criticism and beneficial discussions. I would also like to thank the staff of the machine shop and the electronic shop for their help in the development of much of the instrumentation.

The improvement of the understanding is for two ends:
first, for our own increase of knowledge; secondly, to
enable us to deliver and make out that knowledge to
others.

John Locke

In loving memory of my grandparents; Joseph and Laura
Anderson, and Harry and Myrtle Walker.

Chapter 1

INTRODUCTION

1.1 OBJECTIVE

The inductively coupled plasma (ICP) has become a valuable and reliable atomic emission source for qualitative and quantitative elemental analysis since the early 1970's. It has seen application in the analysis of geological, biological, industrial and environmental samples. There is little doubt that the ICP has lived up to or even exceeded the expectation of its early users.

The early success of the ICP as an analytical tool has not been paralleled by an early understanding of analyte excitation and ionization mechanisms. A number of researchers have compared experimentally measured quantities, such as ion-atom emission intensity ratios, excitation temperatures and electron densities, with those predicted using a local thermodynamic equilibrium (LTE) model. In doing so, several anomalies have been observed including lower than expected analyte ion-atom intensity ratios [1] and disagreement between electron temperatures, ionization temperatures and excitation temperatures [2,3,4] which, under LTE, should all be equal. In order to explain these anomalies, several models were suggested, such as the argon-metastable model [5], radiative trapping model [6], the reaction model [7] and the

ambipolar diffusion model [8].

In an effort to understand some of these anomalies involving analyte excitation and ionization in the ICP, a study based on excited state level populations of three analytes, Fe, Ba and Cr, was undertaken. This thesis will present the results of this study and will discuss these results in terms of possible analyte excitation and ionization processes.

1.2 THE ICP : AN HISTORICAL PERSPECTIVE

The first mention of an inductively coupled plasma in the literature was in 1947 by Babat who described the operation of a low-pressure discharge [9]. Very little work was done on further developing the ICP until 1961 when Reed described the operation of an atmospheric pressure plasma using argon as well as mixtures of argon and either helium, hydrogen or oxygen [10]. The first application of an atmospheric ICP was not for spectroscopic studies, but rather in the growth of single crystals of refractory oxides [10,11]. The author did however recognize that the ICP would find applications wherever dc plasmas were used, such as in the measurement of atomic transition probabilities.

The first report of an ICP being used as a spectroscopic emission source was published in 1964 by Greenfield, Jones and Berry [12]. The torch design used was similar to the one used by Reed [10] and consisted of two concentric quartz tubes open at

one end, with the gas entering tangentially at the other end. A number of distinct advantages of the ICP over existing conventional atomic emission sources such as arcs and sparks were observed. These advantages included the lack of electrodes which gave freedom from contamination, and the extremely weak spectral background produced by the source.

Approximately one year later, Wendt and Fassel published a study on the application of the ICP as a spectrometric excitation source [13]. Unlike the type of torch used previously by Reed and by Greenfield et al. which employed tangential gas flow within the torch, Wendt and Fassel opted to experiment with laminar gas flows. The original claim was that the laminar-flow ICP produced a more stable analytical environment than one produced using the tangential-flow ICP. However, because of the laminar flow of gas entering the torch, the sample tended to flow around rather than through the plasma. This led to severe interferences [14], apparently due to fluctuations in the electrical properties of the discharge [15].

One of the first major studies published on the ICP which clearly demonstrated the practicality of such a system as an analytical tool appeared in 1968 authored by Dickens and Fassel [16]. Detection limits for a number of elements were determined and clearly showed its competitiveness with other spectroscopic techniques. However, it was not until four years later that the first successful commercial ICP atomic emission spectroscopy

(ICP-AES) instrument was marketed.

ICP-AES is used today to analyse a wide range of samples. Types of samples include geological [17,18], industrial [19], biological [20,21,22], agricultural [23], and environmental [24]. In recent years ICP-AES has been used as a multi-element-specific detector for high pressure liquid chromatography [25]. The ICP has been used as an atom/ion source for atomic fluorescence spectroscopy [26] and has also been incorporated as an ion source into the development of plasma source mass spectrometry [27].

Only a brief outline of the development of the ICP has been presented here. For additional information on the topic, a number of literature reviews have been published [28,29,30,31].

1.3 THE ICP

Although plasma is the fourth state of matter and the most abundant in the universe, it is certainly the least encountered on earth. The definition of a plasma provided by Webster's Dictionary is

an ionized gas (as in the atmospheres of stars) containing about equal numbers of positive ions and electrons and differing from an ordinary gas in being a good conductor of electricity and in being affected by a magnetic field [32].

Such a definition, although correct, disparages the complexity of plasmas.

The problem of containing plasma matter, which has a temperature of at least several thousand degrees, was overcome with the development of the ICP torch [10]. It is therefore logical to begin a discussion of the ICP by first discussing the torch. A diagram of a conventional torch is provided in figure 1. The torch consists of two concentric quartz tubes, with a third, smaller aerosol tube, placed on the center axis. Three argon gas flows enter the torch: two of them, the plasma and auxiliary flow, enter tangentially; and the third, the aerosol flow, enters from the base of the torch. The role of the auxiliary flow is to prevent the plasma from coming in contact with the top of the aerosol tube. The aerosol flow is used to carry the sample, usually in the form of an aerosol spray, into the plasma via the aerosol tube. The torch is placed such that the top of the inner concentric quartz tube lies 3 or 4 mm below the first of the three turns of a water-cooled copper tube which comprises the load coil.

The argon atoms entering near the base of the torch begin a tangential motion upwards. At some point in time, the incoming argon gas is seeded with electrons through the use of a tesla coil. A high radio frequency (r.f.) signal is passed through the load coil producing an alternating magnetic field. As the argon gas seeded with electrons enters the alternating magnetic

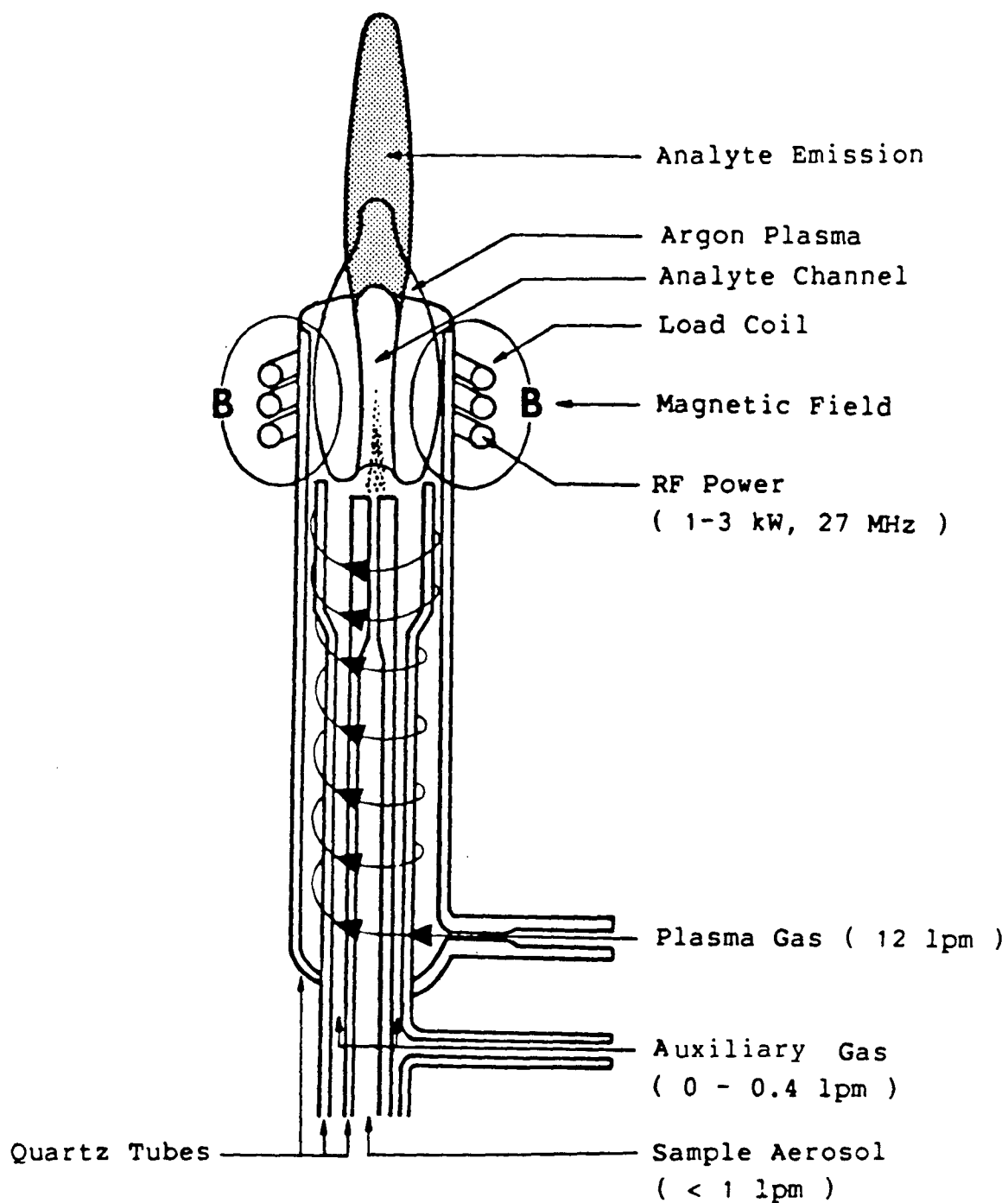


Figure 1. The ICP discharge.

field, the kinetic energy of the electrons is greatly increased. The number of collisions between electrons and argon atoms increases resulting in the formation of more electrons and argon ions



As the electron number density increases the reverse process to (1), three body recombination, is observed



A second possible process leading to a decrease in argon ion population is two body recombination



In this process, Ar^{*} represents an excited state of an argon atom and the excess energy of the process is carried away in the form of electromagnetic radiation, $h\nu$. Once these electron producing and electron consuming processes reach steady state the plasma is sustained, assuming the r.f. signal being passed through the load coil remains uninterrupted. It is important to note that the source of energy needed to sustain the plasma does not arise from the breaking of chemical bonds, as is the case in flames, but

rather from a transfer of the energy applied to the load coil in the form of r.f. power.

It is also worth stressing the importance of the tangential motion of argon gas up through the torch. This motion leads to the following conditions: (1) vortex stabilization, which is apparent by the extension of the plasma further "upstream" above the load coil region and (2) the centering of the plasma which prevents contact with the walls of the torch and aids in cooling the torch [10].

There are a number of methods for introducing a sample into the plasma, the most common of which is to pass a sample in the form of an aqueous (or organic) solution through a nebulizer forming an aerosol gas. However it is also possible to introduce powdered samples [33,34] and solid samples [35,36,37] using the appropriate techniques. The aerosol gas punches a hole through the base of the plasma resulting in the formation of an analyte channel (see figure 1). The further the sample travels up the analyte channel, the greater is its radial diffusion. A change in the aerosol flow rate will change the amount of sample entering the plasma and will alter the characteristics of the analyte channel.

1.4 ANALYTE EXCITATION AND IONIZATION

If a sample is introduced into the base of the plasma in the

form of an aqueous aerosol gas, the sample will first undergo a process of desolvation, then vapourization and finally dissociation upon which atomic species are formed. These analyte atoms can interact through elastic and inelastic collisions with both free electrons and various argon species present in the plasma. In elastic collisions, the total kinetic energy of the colliding particles is conserved and no change in the internal energies of the individual particles is observed. Of more interest to the spectroscopist are the inelastic collisions which result in changes in the internal energies of the particles as they are excited to higher energy states.

The following sections describe what are believed to be the principal processes leading to excitation and ionization of analyte in the ICP [38]. There are, however, other possible processes which may make minor contributions to the excitation and ionization of analyte [7].

1.4.1 COLLISIONAL EXCITATION AND DE-EXCITATION BY ELECTRONS

An analyte atom, X , or ion, X^+ , may be excited to a higher energy level through a collision with an electron



In the forward process, lost kinetic energy of the electron is transferred to the internal energy of the analyte. The atom X, (or ion X^+) may be in its ground state, or in an excited state which is lower in energy than X^* (or X^{+*}). In the reverse process, internal energy which is lost through de-excitation is transferred to the electron in the form of kinetic energy.

1.4.2 COLLISIONAL IONIZATION AND THREE BODY RECOMBINATION

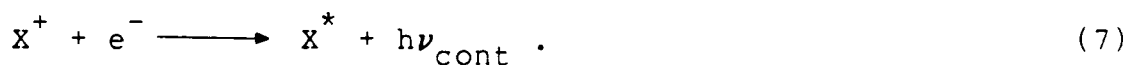
If the energy of the colliding electron is sufficient, ionization of the analyte is possible



The analyte atom X may be in its ground state or in one of its excited states. The resulting ion, X^+ , formed in this reaction may also be in an excited state, although it is more likely to be found in its ground state. In the reverse process excited state atoms can be formed through three body recombination.

1.4.3 RADIATIVE RECOMBINATION

It is also possible to observe recombination processes in which the excess energy resulting from a collision is carried away in the form of electromagnetic radiation



The products resulting from this collision are excited state atoms, X^* , and a continuum photon ($h\nu_{\text{cont}}$) whose energy, $E_{h\nu}$, is given by

$$E_{h\nu} = E_e^- + (E_{X^+} + E_i - E_{X^*}) \quad (8)$$

where,

E_e^- = energy of the electron

E_{X^*} = excitation energy of the atom

E_{X^+} = excitation energy of ion

E_i = ionization potential of analyte X.

1.4.4 RADIATIVE DE-EXCITATION

The most significant process in terms of the analytical capabilities of the ICP is radiative de-excitation of excited state atoms and ions



The energy of the photon emitted is directly related to the energy difference between the upper state q and the lower state

p. Because each element has a unique atomic structure, the resulting atomic spectrum, that is the collection of photons ($h\nu_{\text{line}}$) over all energies, is also unique. Thus it is possible to qualitatively analyse an unknown sample for its elemental composition.

1.4.5 PENNING IONIZATION AND EXCITATION

It is possible to encounter analyte excitation and ionization resulting from collisions with metastable argon atoms



The excess energy in this process is carried away by the electron in the form of kinetic energy. The importance of Penning ionization and excitation has been controversial, being supported by some [39,40] and discarded by others [38,7].

1.4.6 ASYMMETRIC CHARGE TRANSFER WITH ARGON

Excitation of an analyte atom is possible through charge transfer with an argon ion



The likelihood of this process occurring is greater when the energy defect, ΔE , is small. This excess energy is simply carried away in the kinetic energy of the two colliding particles.

1.5 THERMODYNAMIC EQUILIBRIUM IN THE ICP

In the preceding section, a number of elementary processes present in the plasma were outlined. It is now possible to mathematically describe the distribution of states produced in these processes and relate these distributions to a common parameter T , temperature.

Under conditions of detailed balancing the production of each elementary state (or forward process) is exactly balanced by its destructive (or reverse) process. Such a condition leads to a state of thermodynamic equilibrium (TE). However, in an emission source such as the ICP, TE is not achieved due to the presence of high concentration and temperature gradients and the loss of energy from the plasma boundary through radiative processes (7,9,10). The absorption of this radiation is unfavourable because of the relatively small cross sections for the interaction of radiation with matter and the low optical density of the ICP. Thus the term local thermodynamic equilibrium (LTE) is introduced to describe the equilibrium that exists locally for all distributions except for the

distribution of radiation. To put it simply, under LTE one unique temperature can be used to satisfy the Maxwell distribution of particle velocities, the Boltzmann distribution of level populations, the Saha distribution of atoms and ions of a given species, and the Guldberg-Waage distribution of molecular species.

The following distribution functions are well established and widely accepted; hence detailed derivations of these equations are beyond the scope of this thesis and have been omitted.

1.5.1 MAXWELL DISTRIBUTION

Maxwell's equation describes the velocity (or energy) distribution of particles involved in elastic collisions by

$$f(V) dV = (m/2\pi kT_g)^{3/2} \exp (-mv^2/2kT_g) 4\pi v^2 dV \quad (13)$$

where,

$f(V)dV$ = probability that a particle has a
velocity in the region V and $V + dV$

m = the mass of the particle

T_g = gas kinetic temperature of the particle

k = Boltzmann's constant.

Perhaps a more meaningful form of equation (13) in the context of

this thesis is obtained by using the expression relating kinetic energy, KE, to velocity,

$$KE = 1/2 m v^2 \quad (14)$$

which upon substitution into equation (13) yields

$$f(E) = 2\pi^{1/2} (1/kT_g)^{3/2} \exp (-E/kT_g) E^{1/2} dE \quad (15)$$

where,

$f(E) dE$ = the probability function that a particle has
an energy in the region of E and $E + dE$

m = mass of particle (kg)

T_g = gas kinetic temperature (K)

k = Boltzmann's constant (8.617×10^{-5} eV K⁻¹)

E = energy of particle (electron volts, eV).

When the particle in question is an electron, then $f(E)$ yields the energy distribution of electrons and T_g is the electron temperature, T_e .

1.5.2 BOLTZMANN DISTRIBUTION

For processes involving the excitation of atomic species (both neutral atoms and charged ions), the ratio of number

densities of atoms (or ions) in two energetically different bound states is given by the ratio of Boltzmann distributions

$$n_q/n_p = g_q/g_p \exp (-(E_q - E_p)/kT_{exc}) \quad (16)$$

where,

n_p, n_q = number density of particles in states p and q
 g_q, g_p = statistical degeneracies of states p and q
 E_q, E_p = excitation energies of excited states p and q
 T_{exc} = excitation (or Boltzmann) temperature of the species.

It is also possible to relate the number density of a particular atomic (or ionic) excited state n_p , to the total number density of atoms (or ions) n_T with the following form of the Boltzmann distribution

$$n_p/n_T = g_p/Q(T) \exp (-E_p/kT_{exc}) \quad (17)$$

where,

$Q(T)$ = the partition function of the species.

A method for estimating the partition function for most elements, at various temperatures, has been published [41].

1.5.3 SAHA DISTRIBUTION

For ionization / recombination processes of the type



the equilibrium constant, $S_n(T)$, is given by

$$S_n(T) = n_q^+ n_e / n_p \quad (19)$$

where,

- n_q^+ = number density of ions in state q
- n_p = number density of atoms in state p
- n_e = number density of electrons.

The equilibrium constant may be written as

$$\begin{aligned} S_n(T) &= n_q^+ n_e / n_p \\ &= 2g_p^+ / g_q \left(2\pi m_e kT_i / h^2 \right)^{3/2} \\ &\quad \exp \left(-(E_i + E_{nq}^+ - E_{np}) / kT_i \right) \end{aligned} \quad (20)$$

where,

- h = Planck's constant
- m_e = mass of electron
- E_i = ionization potential of species X

E_{nq}^+ = excitation energy of ionic state q

E_{np} = excitation energy of atomic state p.

If numerical substitutions are made for the constants, the resulting expression, assuming densities are measured in cm^{-3} , is given as

$$n_q^+ n_e / n_p = (g_q^+ / g_p) (4.84 \times 10^{15}) T_i^{3/2} \exp(-E / kT_i) \quad (21)$$

where,

$$E = E_i + E_{nq}^+ - E_{np}.$$

If partition functions for all ion and atom species are included ($Q^+(T)$ and $Q(T)$ respectively), the Saha expression may be written for the total number density of ions (n_T^+) and atoms (n_T) as follows :

$$n_T^+ n_e / n_T = (4.84 \times 10^{15}) T_i^{3/2} (Q^+(T) / Q(T)) \exp(-E_i / kT_i) . \quad (22)$$

The Saha equation holds for any two levels p and q between any two adjacent ionization stages.

1.5.4 GULDBERG - WAAGE DISTRIBUTION

For reactions of the type



the Guldberg - Waage equation gives a relationship between the number densities of the products A and B, n_A and n_B , and the number density of the molecule AB, n_{AB} , by the expression

$$\frac{n_A n_B}{n_{AB}} = \frac{Q_A(T)Q_B(T)}{Q_{AB}(T)} \left(\frac{m_A m_B}{m_A + m_B} \right)^{3/2} \frac{(2\pi k T_d / h^2)^{3/2}}{\exp(-E_{AB}/k T_d)} \quad (24)$$

where,

- $Q_A(T)$ = internal partition function for A
- $Q_B(T)$ = internal partition function for B
- $Q_{AB}(T)$ = internal partition function for AB
- m_A, m_B, m_{AB} = masses of species A, B, and AB
- E_{AB} = dissociation energy of molecule AB
- T_d = dissociation temperature.

1.5.5 SUMMARY

As was seen in the preceeding sections 1.5.1 through to 1.5.4, a number of temperatures can be defined : a Maxwellian temperature, T_g , defining the kinetic energy distribution of

particles; an electron temperature, T_e , defining the Maxwellian energy distribution of electrons; an excitation temperature, T_{exc} , defining the atomic excited state populations (here the term atomic includes both neutral and charged species); an ionization temperature, T_i , defining the distribution of atom and ion populations; and a dissociation temperature, T_d , defining the distribution of molecules and their dissociation products. Each of these temperatures can be experimentally determined and one finds that under conditions of LTE,

$$T_g = T_e = T_{exc} = T_i = T_d . \quad (25)$$

However it has become widely accepted that the ICP is not in LTE. The type and extent of departure from LTE will not be discussed here, but rather in context with excited state level populations in chapter 3.

1.6 EXCITED STATE LEVEL POPULATIONS

The emission intensity, I_{pq} , of a spectral line resulting from a transition from an excited state p to a lower state q , where states p and q lie within the same ionization stage, is given by [42]

$$I_{pq} = (A_{pq} hc / 4\pi \lambda_{pq}) n_p \quad (26)$$

where,

A_{pq} = transition probability

c = speed of light

λ_{pq} = wavelength of the transition

n_p = number density of excited state p.

After rearranging this equation and dividing both sides by the degeneracy g , it can be shown that

$$I_{pq} \lambda_{pq} / g A_{pq} \propto n_p / g_p. \quad (27)$$

From this relationship, it is possible to determine the relative population of an excited state p by experimentally measuring the relative line intensity resulting from the transition from states p to q and then multiplying the intensity by the factor λ_{pq} / gA .

Using expression (27) which relates excited state level populations to experimentally determined emission intensities, the following study was undertaken. Excited state level populations were determined for three analytes, Fe, Ba and Cr, at various rf input powers and spatial positions. The instrumentation required to measure the emission intensities is discussed in chapter 2 with the results presented in chapter 3. A summary of this work is provided in chapter 4.

CHAPTER 2

EXPERIMENTAL

2.1 INSTRUMENTATION

A Block diagram of the instrumentation is provided in figure 2. The ICP unit consisted of a Plasma-Therm Inc. (Kreeson, N.J.) HFP-2500E rf generator, an AMN-2500E automatic matching network, an APCS-1 automatic power control unit and a PT-2500 plasma torch assembly. The rf generator operated at a frequency of 27.12 MHz and delivered up to 2.5 kW of rf input power to the load coil. All ICP torches used in this study were constructed at the Department of Chemistry Glass Shop, U.B.C., from precision-bore quartz tubing. Introduction of samples, in the form of aqueous solutions, was achieved using a Plasma-Therm GN 5601 concentric glass nebulizer. Diagrams of the torch and glass nebulizer are provided in figures 3 and 4 respectively. The spray chamber used was of the conventional concentric barrel type manufactured by Plasma-Therm Inc. (Model SC-5037). A diagram of the complete torch, spray chamber and nebulizer assembly is provided in figure 5. The following ICP gas flows were maintained for all experiments: plasma gas - 12 lpm, auxiliary gas - 0.4 and 0.0 lpm, and aerosol gas - 0.9 lpm. In the measurement of iron spectral line intensities, no auxiliary flow was used. However this led to severe degradation of the ICP torch and as a result

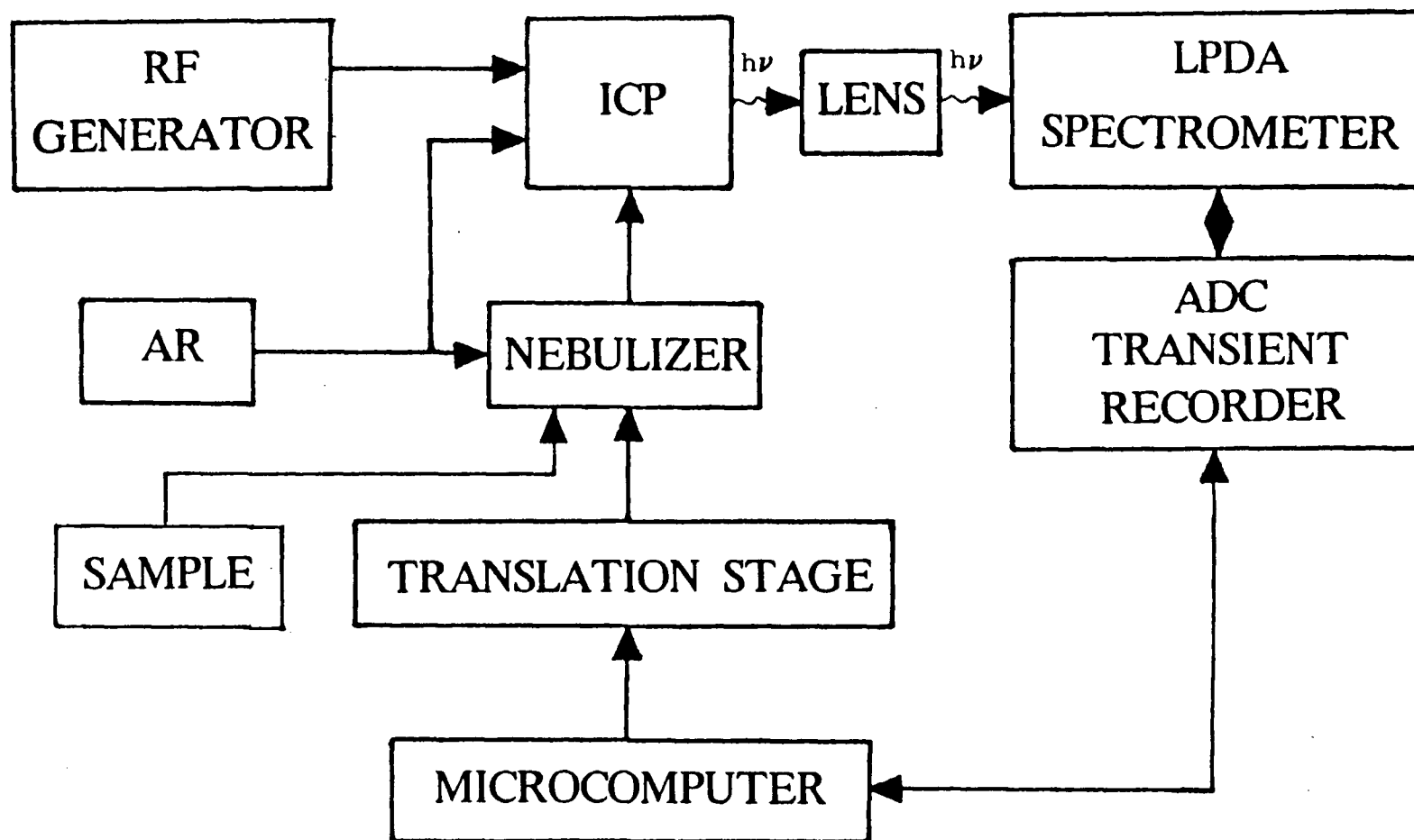


Figure 2. Block diagram of Instrumentation.

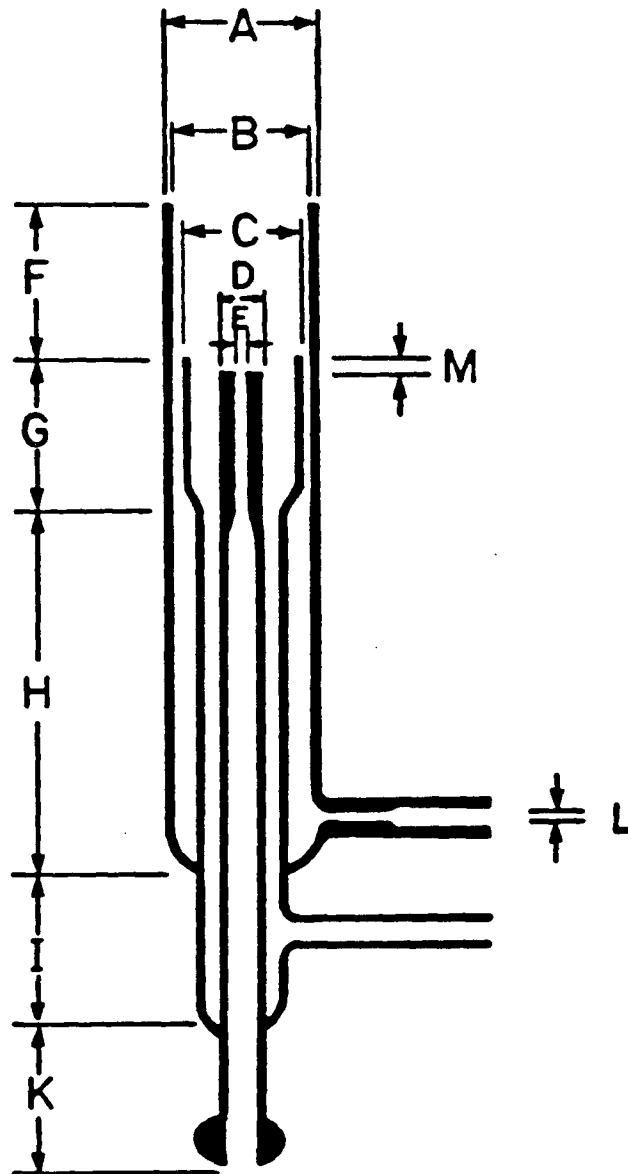


Figure 3. The ICP torch.

Dimensions: A=20.37 mm, B=17.39 mm, C=15.86 mm, D=5 mm, E=1.48 mm, F=20 mm, G=20 mm, H=43 mm, I=20 mm, K=25 mm, L=1 mm, M=3 mm.

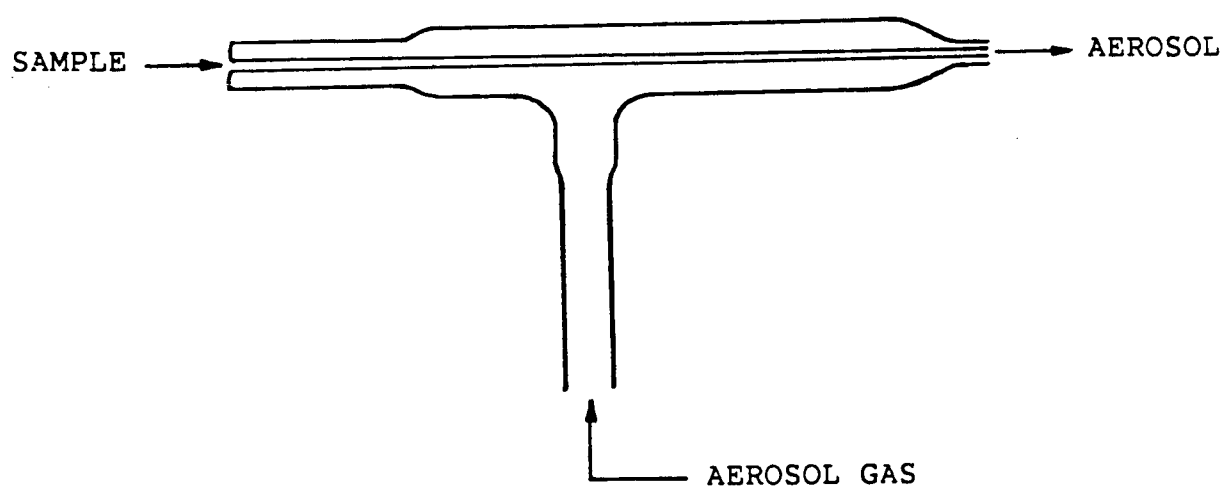


Figure 4. The concentric glass nebulizer.

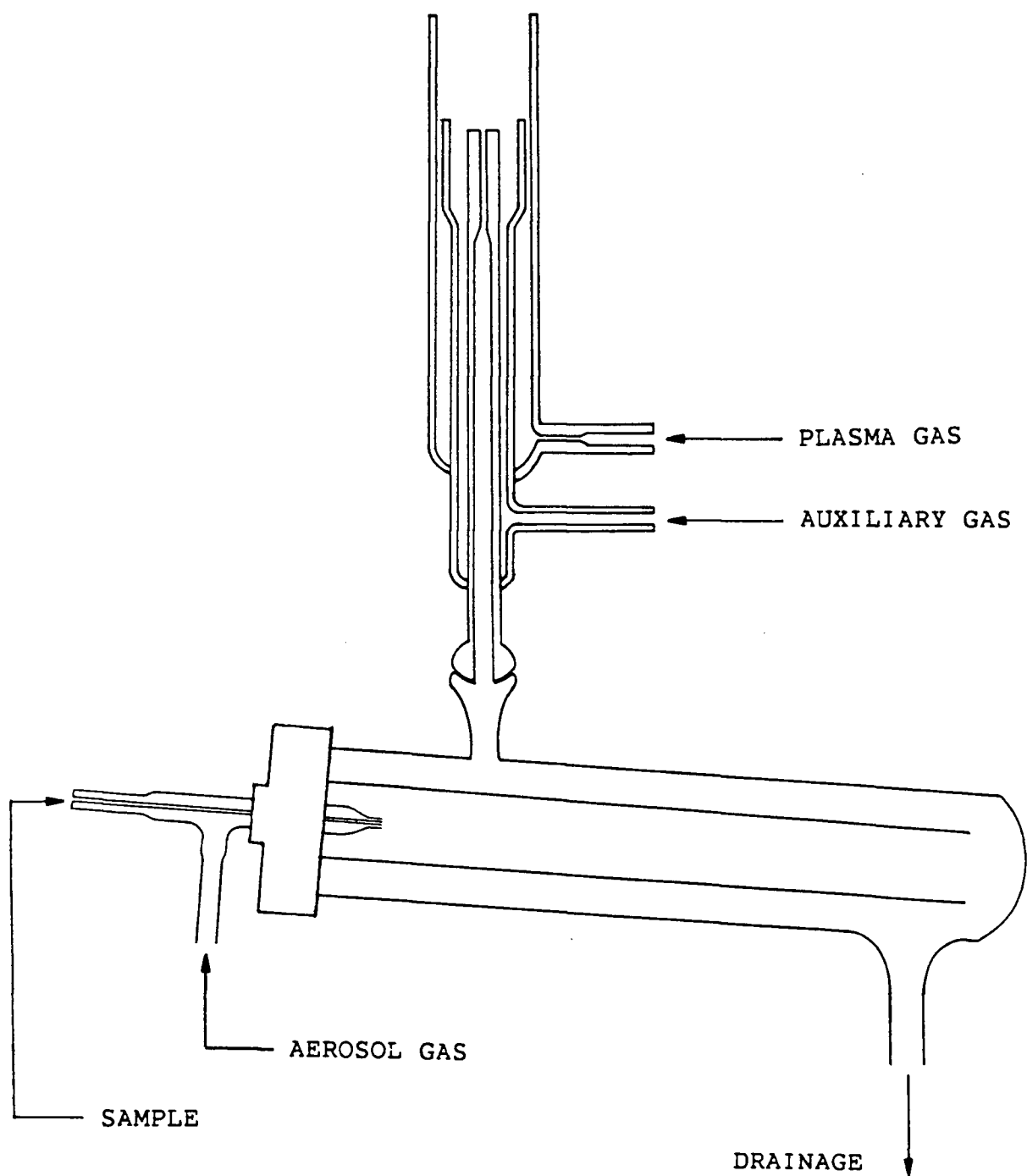


Figure 5. The ICP torch, spray chamber and concentric glass nebulizer.

an auxiliary flow of 0.4 lpm was implemented for the remaining barium and chromium intensity measurements. The entire plasma torch assembly was mounted on a linear translation stage driven by a Daedal Inc. (Harrison City, Pa) Model 4979 stepper motor which provided horizontal movement perpendicular to the optical axis in increments of 0.0127 mm.

A Schoeffel-McPherson (Acton, Ma) Model 2061, 1-meter, Czerny Turner monochromator was used as the dispersive system. The monochromator was equipped with a Schoeffel-McPherson Model AH-3254, 120 x 140 mm, holographic grating with 1200 lines/mm. The reciprocal linear dispersion of the LPDA spectrometer was equal to 0.833 nm/mm. All line intensity measurements reported in this thesis were performed using a Reticon (Sunnyvale, Ca) Model RL-4096S linear photodiode array (LPDA). This LPDA consisted of 4096 discrete photodiodes 7 μ m wide and mounted on 15 μ m centers. The height of each photodiode was 0.5 mm and the overall length of the light-sensitive area of the array was 61.44 mm. The use of the LPDA permitted the simultaneous measurement of spectral lines from a wavelength window approximately 50 nm wide. A Melcor (Treton, N.J.) Model CP1.4-71-10L thermoelectric (Peltier) cooler was mounted to the backside of the LPDA, allowing the array to be cooled to -15 C. Cooling the array eliminated a great deal of the dark current which is usually observed at room temperature, thus permitting the use of longer integration times. The LPDA was purged with nitrogen to prevent

the formation of ice on its surface. Readout of the array was accomplished using a Reticon Model RL-4096S-3 evaluation board.

The LPDA was experimentally determined to have a resolution (full width at half maximum) of 0.037 nm using an entrance slit width of 60 μm . Under these conditions the number of pixels sampling the full width half maximum intensity is 5. Assuming a Lorentzian line shape, the amount of error in the measured spectral line intensities is less than 0.1 % [43].

The emission from the ICP was focussed with 1:1 imaging onto the entrance slits of the monochromator using an Oriel (Stratford, Ct) Model 41775 plano-convex fused silica lens. The lens had a diameter of 150 mm and a radius of curvature, R, of 69.80 mm. The focal length of the lens was corrected for achromatic response using the following procedure. Literature values for the refractive index of fused silica at various wavelengths [44] were plotted as a function of wavelength and fitted with a fifth order polynomial as shown in figure 6. The imaging distance, which is twice the focal length, was then calculated as a function of wavelength using the equation

$$1/f(\lambda) = (n(\lambda) - 1) (1/R_1 - 1/R_2) \quad (28)$$

where,

$f(\lambda)$ = focal length at wavelength

$n(\lambda)$ = refractive index of fused silica at wavelength

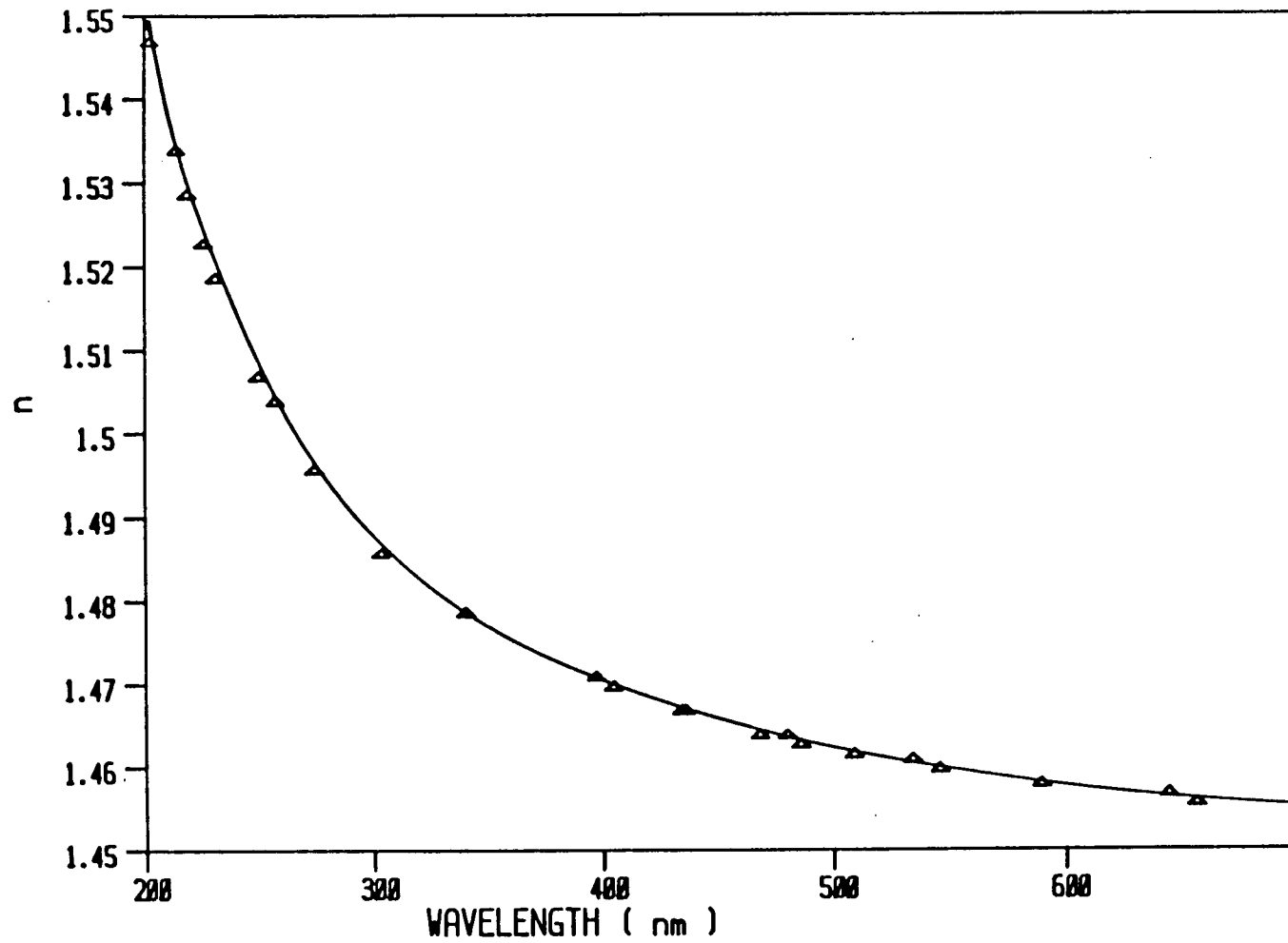


Figure 6. Plot of refractive index of fused silica versus wavelength.

R_1 = radius of curvature for lens surface facing
emission source

R_2 = radius of curvature for lens surface facing
emission source

For the lens used, $R_1 = 69.80$ mm and $R_2 = \infty$. The imaging distance has been plotted as a function of wavelength in figure 7.

2.2 COMPUTER INTERFACING OF LPDA AND DATA ACQUISITION

The Reticon evaluation board provides two control lines, a start and a clock, which are used in reading out the array data. The start line carries the start pulse which indicates the array has completed its integration and initiates readout from the 4096 individual array pixels. The time between start pulses controls the length of time the array is allowed to integrate electromagnetic radiation. Integration times can be chosen from between 10.6 msec and 43.5 sec in increments of 10 msec by setting the proper sequence of 12 binary switches, located on the back panel of the diode array housing. The clock line controls the rate at which data is read from the array and the rate at which digitization and storage of the analog signal takes place. A third, video line carries the analog readout signal from the array. Due to the relatively fast diode array controlled clock

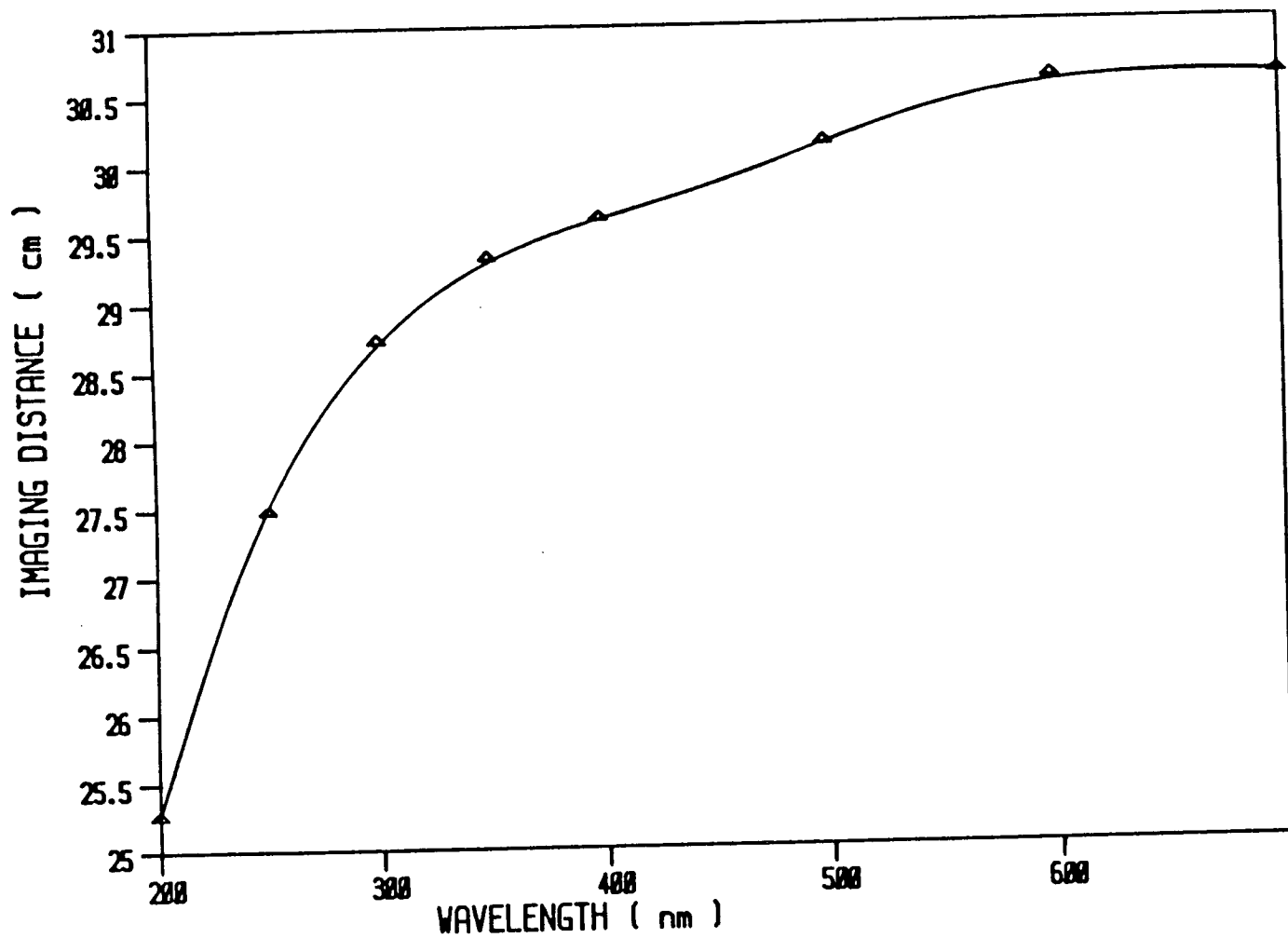


Figure 7. Imaging distance of a fused silica lens, with a radius of curvature of 69.80 mm, as a function of wavelength.

rate of 400 kHz, the analog signal must first be sent to a transient recorder, which was constructed in the Department of Chemistry Electronic Shop, U.B.C. The analog video signal from the array was digitized by a 12-bit analog-to-digital converter and then stored in the transient recorder's read write random access memory (RAM). The digitized data stored in the RAM of the transient recorder was then read, at a slower clock rate, into a CompuPro (Viasyn, Hayward, Ca) system 816 microcomputer equipped with a 68000 CPU, 1 Mbyte of RAM, a 1.2 Mbyte 8 inch floppy disc, and a 40 Mbyte hard disc. The interfacing between the transient recorder and the microcomputer was achieved through the use of three parallel ports located on a CompuPro Interfacer*4 card. A complete diagram outlining the interfacing of the LPDA to the computer, via the transient recorder, is provided in figure 8.

The acquisition of data from the LPDA can be broken down into two operations. Firstly, the acquisition of data from the array and subsequent digitization and storage in the RAM of the transient recorder, and secondly the transfer of data from the RAM of the transient recorder to the RAM of the computer. For a better understanding of these operations, timing diagrams have been provided, one corresponding to the acquire mode, figure 9, and the second corresponding to the readout mode, figure 10.

In order to acquire data, the acquire line, ACQ, is set high from within the software. Once in the acquire mode, a

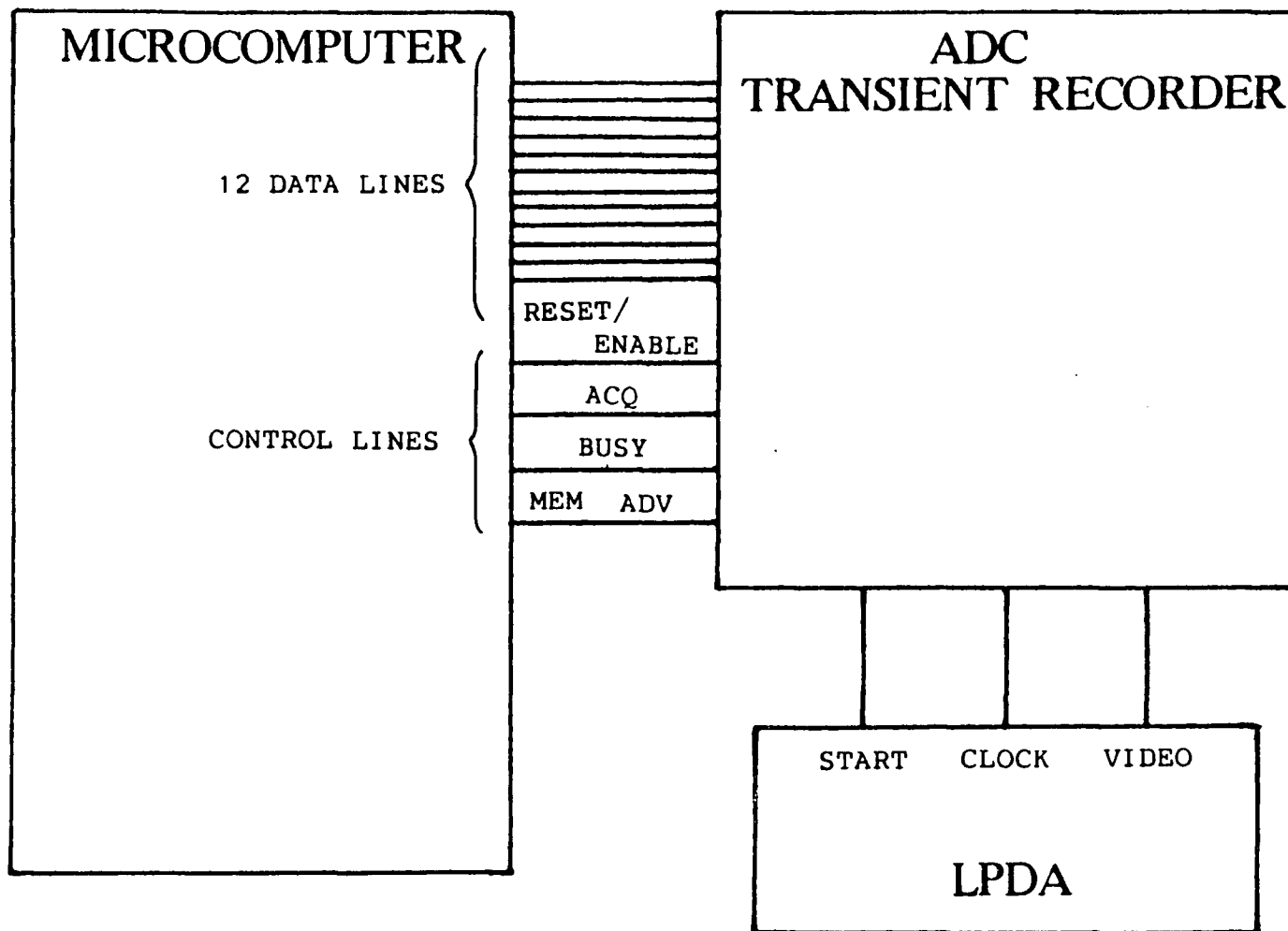
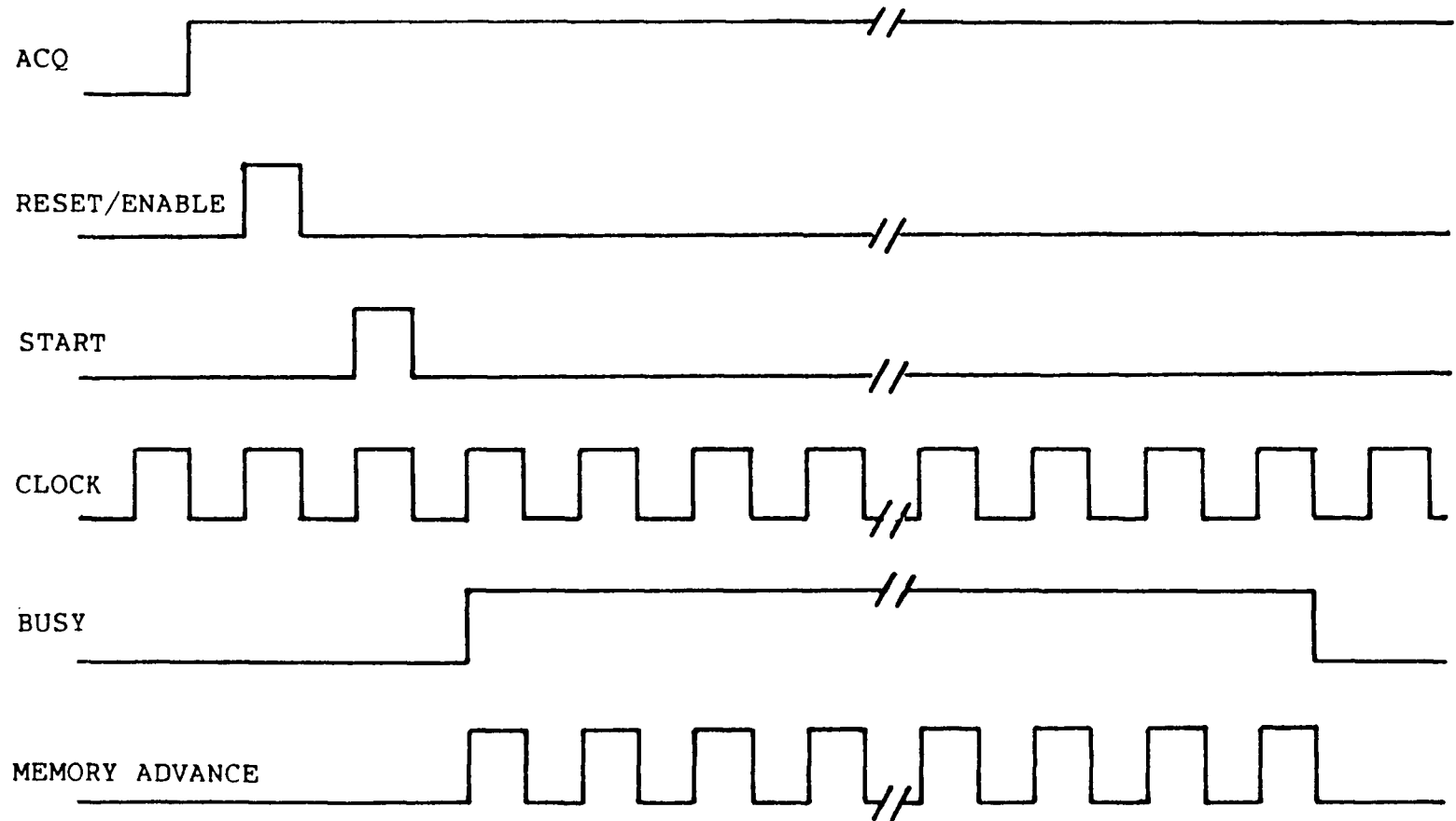


Figure 8. Diagram of the interfacing between the LPDA and the CompuPro microcomputer via the transient recorder.

MICROCOMPUTER

TRANSIENT RECORDER

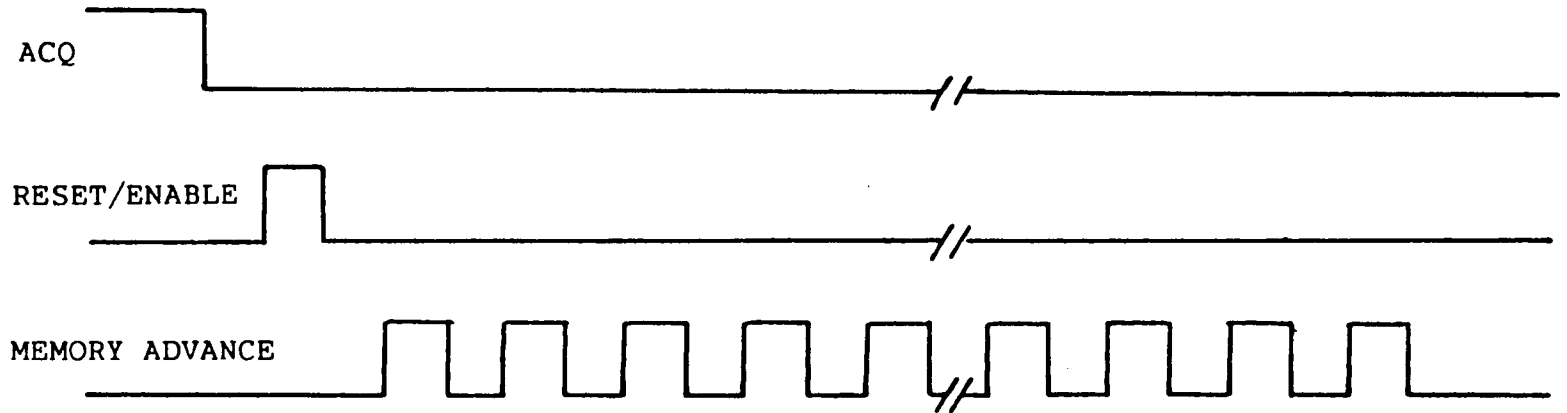


34

Figure 9. Timing diagram for the acquisition of data from the LPDA.

MICROCOMPUTER

TRANSIENT RECORDER



35

Figure 10. Timing diagram for the readout of data from the transient recorder.

reset/enable pulse is sent to the transient recorder, which resets the counter to memory location 0. The transient recorder then awaits the arrival of a start pulse from the LPDA evaluation board. Once the start pulse has arrived, the transient recorder begins digitization and storage of the first analog signal as the first clock pulse, following the start pulse, arrives and steps through all 4096 analog signals with the arrival of each successive clock pulse. The busy line, which was set high as the first clock pulse was received, is set low once the 4095th clock pulse is received indicating to the computer that the acquisition process has been completed.

Readout of the data to the computer is achieved by first setting the ACQ line low (see figure 10) followed by the sending of a reset/enable pulse which resets the counter to memory location 0. Starting with the first memory location, the stored digitized data is sent via the 12 data lines to the parallel port and subsequently stored in the computer's RAM. Once the first data point is successfully read and stored, a pulse is sent via the memory advance line, which increments the counter to the second location and the process of reading and storing the data is repeated. This continues until all 4096 memory locations have been read.

2.3 SOFTWARE

All software used in the acquisition of experimental data and the subsequent computations was written in Fortran-77 (Silicon Valley Software, Cupertino, Ca) and run on the CompuPro 816 system microcomputer, with one exception. The software controlling I/O (input/output) communications between the transient recorder and the CompuPro microcomputer was written in 68000 assembly language. This permitted a much faster rate of data transfer from the RAM of the transient recorder to the RAM of the microcomputer than possible using Fortran programming. The Fortran program used to control the collection of lateral emission intensities and the assembly language program used to control the transfer of data from the LPDA to the microcomputer are provided in Appendix A.

2.4 SAMPLE PREPARATION AND SELECTION OF ANALYTE CONCENTRATION

All solutions were freshly prepared from reagent grade chemicals, namely $\text{FeSO}_4 \cdot 7\text{H}_2\text{O}$, $\text{BaCl}_2 \cdot \text{H}_2\text{O}$ and $\text{Cr}(\text{NO}_3)_3 \cdot 9\text{H}_2\text{O}$, and distilled water. The Fe solution was made up in 0.1 N HNO_3 to inhibit the formation of iron oxides.

The following concentrations of analyte were used throughout this study: 5000 ppm Fe, 2000 ppm Ba, and 5000 ppm Cr. In order to obtain sufficient intensity from high energy lines, these

relatively high analyte concentrations were required. To avoid problems, such as self absorption and changes in nebulizer efficiency, associated with using high analyte concentrations, working curves were constructed and the analyte concentrations then chosen from within the linear portion of the working curve.

2.5 SELECTION OF SPECTRAL LINES

The following procedure was performed in selecting suitable atom and ion emission lines for measurement of Fe, Ba and Cr spectral line intensities. For each of the three analytes, a number of "spectral windows", 50 nm in width, were chosen. The number of windows and the wavelength on which they were centered depended upon the richness of the analyte's atomic spectrum, and the particular wavelengths which offered the highest concentration of spectral lines. In choosing lines from these windows, a number of criteria were followed : (1) no significant spectral overlaps of the lines should occur, (2) the excitation energies of the various lines should span as wide an energy range as possible, and (3) the lines should be sufficiently intense as to provide reasonable signal-to-noise ratios.

2.6 MEASUREMENT OF SPATIALLY RESOLVED LINE INTENSITIES

In order to determine spatially resolved, relative level

populations, the following procedure was used. The ICP torch enclosure, mounted on the translation stage, was moved to a position such that the focussed image of the plasma appeared just to the right of the entrance slits of the spectrometer. The translation stage was moved, via the stepper motor, to 150 horizontal positions, each separated by 0.0762 mm. As the focused image of the plasma was stepped across the entrance slit, the emission intensities from the spectral lines of interest were measured at each of the 150 horizontal positions. Generation of foreground minus background line intensities was achieved in one of two ways, either through spectral stripping or "dynamic" background subtraction. In the case of Fe and Cr line intensities, a water blank was run and the measured "background" intensities were stripped from the foreground intensities. In the case of Ba, which required several spectral windows at several integration times, the more time efficient dynamic background subtraction was employed. As a spectrum was collected at each horizontal position, off-line, baseline intensities were subtracted from the peak intensity. Note that due to the extremely weak intensities from many of the Cr atom and ion lines, sufficient off-axis intensity was not available and as a result spatially resolved intensity measurements were not possible. The line profiles, resulting from the collection of 150 lateral line intensities, were smoothed using a 13-point simplified least squares procedure [45]. To obtain radial

intensities, these smoothed lateral profiles were then subjected to an Abel inversion procedure using an asymmetric Abel inversion [46]. The end result was the generation of spatially resolved line intensities based on experimentally measured lateral intensities.

2.7 SPECTRAL CORRECTION OF SPECTRAL LINE INTENSITIES

The spectral response of the LPDA spectrometer was established over the range 250 to 700 nm using an Electro Optics Associates (Palo Alto, Ca) Model L-10 quartz-iodine, tungsten filament standard lamp supplied with an Electro Optic Associates Model P-101 power source [47]. Measured intensities were corrected for spectral response to compensate for non-linearity in the LPDA response and changes in its sensitivity over the wavelength range.

CHAPTER 3

EXCITED STATE LEVEL POPULATIONS

3.1 INTRODUCTION

One approach taken in studying analyte excitation and ionization in the ICP has been the measurement of the excitation and ionization temperatures which characterize these processes. Under conditions of LTE, these two temperatures, along with all other temperatures characterizing the various distributions in the ICP, will be equal. Thus a simple method of confirming or disproving the existence of LTE in the ICP is possible through the comparison of experimentally determined temperatures.

Mermet [4] reported excitation temperatures determined from Ar, Fe and Ti line intensities and found them to be comparable with each other. However, electron densities measured in the same study from Stark broadening (also known as collisional broadening) of the $H\beta$ line, suggested a much higher excitation temperature, assuming Saha equilibrium.

Kalnicky et al. [48] calculated electron densities based on the measured ion-atom emission intensity ratios of five analytes, Ca, Mg, Fe, Cd, and Zn, via the Saha equation using an Fe(I) excitation temperature as the Saha temperature. These electron densities were found to be 30-50 times less than densities determined using a second method, namely Stark broadening of the

H β line.

In a study published by Jarosz et al. [3], excitation temperatures determined from Fe, Ti and V were found to be considerably less than the ionization temperature determined from Ar, assuming LTE.

The conclusion from these and other similar studies was that significant deviations from LTE exist in the ICP. However the information provided by these measurements was insufficient to give a clear insight into the nature and extent of the deviations.

A second approach to understanding analyte excitation and ionization in the ICP has been through the measurement of analyte ion-atom intensity ratios. In two studies by Caughlin and Blades [49,50], ion-atom emission intensity ratios were measured experimentally, $(I_i/I_a)_{\text{EXP}}$, for five analytes, Sr, Ca, Mg, Cd, and Zn. The experimental ratios were compared to the corresponding LTE ratios, $(I_i/I_a)_{\text{LTE}}$, calculated using the appropriate equations and electron temperatures determined from electron densities. The ratio of $(I_i/I_a)_{\text{EXP}}$ to $(I_i/I_a)_{\text{LTE}}$, referred to as the b_r value, was determined for r.f. input powers ranging from 1.0 to 2.0 kW. The b_r values for Cd, Mg and Zn showed a moderate dependence on rf input power increasing from 0.2 to 0.5 for Mg and Zn and from 0.6 to 0.8 for Cd upon going from 1.00 kW to 2.00 kW. The b_r values for Sr and Ca, which have the two lowest ionization potentials of the five analytes,

expressed a strong dependence on rf input power increasing from 0.2 for both elements at 1.0 kW to 1.2 for Ca and 1.5 for Sr at 2.0 kW. Degree of ionization, α , was also determined from the ion-atom intensity data and compared to values calculated under conditions of LTE. By constructing a plot of α versus ionization potential it was observed that all five analytes were underionized with respect to an LTE model. The results of this study clearly indicated the absence of LTE in the ICP and suggested that the contribution of radiative de-excitation and recombination, which results in the loss of energy from the system, may be the root cause for the departures.

One shortcoming of measuring excitation and ionization temperatures and ion-atom emission intensity ratios, is the assumption of Boltzmann populated excited states. Excitation, or Boltzmann, temperatures are usually determined using the two line method which involves experimentally measuring the line intensity from two emission lines within the same ionization stage. An excitation temperature can then be determined from these measured intensities using the Boltzmann formula given in equation (16). Ionization, or Saha, temperatures are determined by measuring the line intensity of an atom and an ion emission line. An ionization temperature can then be determined using these line intensities and a measured electron density via the Saha equation (21). In both cases the assumption is made that the population of excited states proceeds according to the Boltzmann

distribution. In other words by measuring only two atom or ion lines in the case of excitation temperatures, or only one atom and one ion line in the case of ionization temperatures, it is assumed that the temperatures determined will be independent of the excitation energy of the lines chosen. Similarly, in the studies using ion-atom ratios only one atom and one ion emission line was chosen for each of the five analytes. Thus any departures in the Boltzmann population of excited states, which might exist for some or all of the analytes studied, would go undetected. In light of the evidence supporting the absence of LTE, it may be naive to assume that the excited states are populated according to the Boltzmann distribution and that deviations do not exist.

A more advantageous approach would be to measure as many atom and ion emission lines as possible and to use these intensities to determine excited state level populations for both ionization stages. By doing so it would be possible to detect any deviations, which might exist, in the Boltzmann population of excited states or in the Saha equilibrium between atom and ion ionization stages. Also since these level populations are dictated by the mechanisms causing excitation, information obtained as a result of these measurements will help to elucidate excitation mechanisms in the ICP.

One of the first comprehensive studies of excited level state populations was reported in 1980 by Alder, Bombelka and

Kirkbright [51]. A plot was constructed of excited state level populations, $\ln(I\lambda/gA)$, determined from 20 Fe(I) measured line intensities, versus the excitation energies of those levels which ranged from 3.33 to 6.91 eV. These plots were constructed for intensities collected at three vertical positions, 10, 20 and 30 mm above the load coil. Excitation temperatures were calculated from the resulting non-linear distribution of points by subdividing the 20 data points into 3 groups according to their individual energies. This treatment of the data yielded 3 excitation temperatures of increasing magnitude, the lowest temperature being derived from the set of low excitation energies and the highest temperature from the set of high excitation energies. Their results indicated an overpopulation of the lower energy levels and it was suggested that this overpopulation proceeds by radiative decay of the upper levels down to the lower levels, which is not balanced by the inverse absorption processes. As a result of the non-linear population plots observed, it was apparent that the two-line temperature measurements using two low lying energy levels could not be relied upon to reflect the unique excitation temperature in the ICP.

Using some of the data published by Alder, Bombelka and Kirkbright on excited level state populations [51], Kornblum and Smeyers-Verberke re-examined the approach taken by the authors in interpreting their data [52]. They felt it more reasonable to

postulate a continuous and gradual change in excitation temperature between neighbouring energy levels instead of the three temperature structure proposed by the authors. Using a statistical approach they found the scatter around the three partial straight lines not to be significantly less than the scatter around the straight line drawn through all 20 data points. Instead of trying to force the data to a linear fit, the authors tried various higher order polynomial fits and found a second order fit yielded the smallest degree of scatter. Level dependent temperatures were calculated for each FeI level and plotted against excitation energy. The temperatures were found to increase with increasing excitation energy, qualitatively the same conclusion arrived at by Alder, Bombelka and Kirkbright.

A second study involving FeI excited state level populations using a Fourier transform spectrometer was carried out by Faires, Palmer and Engleman [53] in order to construct a vertical profile of FeI excitation temperatures in the ICP. The authors chose to interpret their level population plots as being linear and calculated an unique excitation temperature for each vertical position. From the population plot provided in figure 4 of this paper [53], population/energy values have been extracted. Various linear regression and higher order fitting programs were applied to this data, the best result coming from a second order polynomial fit, and not from a linear fit. The FeI population plot fitted using both the second order polynomial fit and the

original linear regression fit are provided in figure 11A and 11B respectively. The variance calculated from these fits revealed that the second order fit produced a variance value half that calculated from a linear regression fit. This result can also be qualitatively confirmed upon visual inspection of the two plots. The level dependent temperatures calculated from the second order fit yielded values comparable to those found by Kornblum and Smeyers-Verberke [52].

Furuta recently reported a study of ionization and excitation temperatures in the ICP in which excitation temperatures were determined from FeI excited state level populations [2]. Unfortunately only 7 of the 20 emission lines measured were used in constructing the population plot and 6 of these lines had excitation energies which fell into one of two small energy ranges. As a result their population plot consisted of only three clusters of points which made interpretation of the plot difficult. The author chose to divide the 7 data points into 2 groups yielding two excitation temperatures, one corresponding to low energy levels, the other to high energy levels. The conclusion was also reached that the low energy atom levels appeared to be overpopulated with respect to the high energy atom levels.

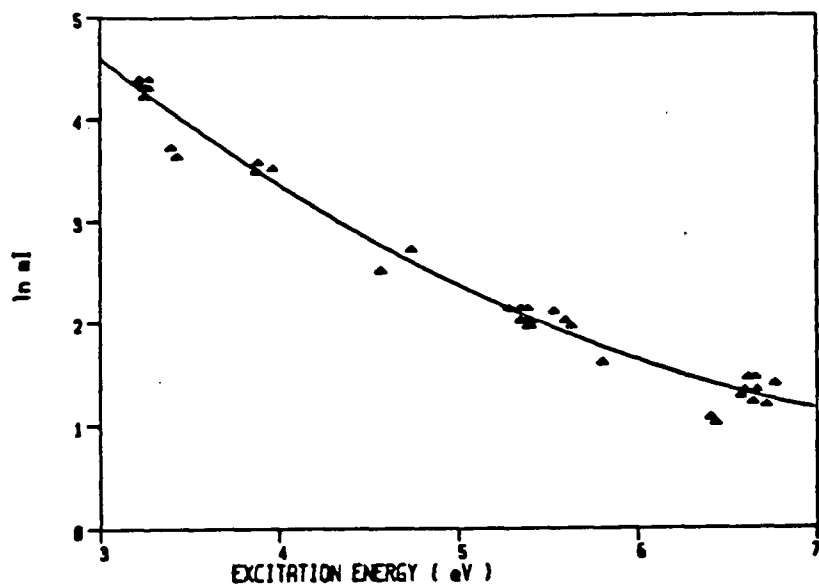


Figure 11a. A plot of the logarithm of FeI excited state level populations vs excitation energy, from data extracted from Faires, Palmer and Engleman [53]. Populations have been fitted to a second order polynomial.

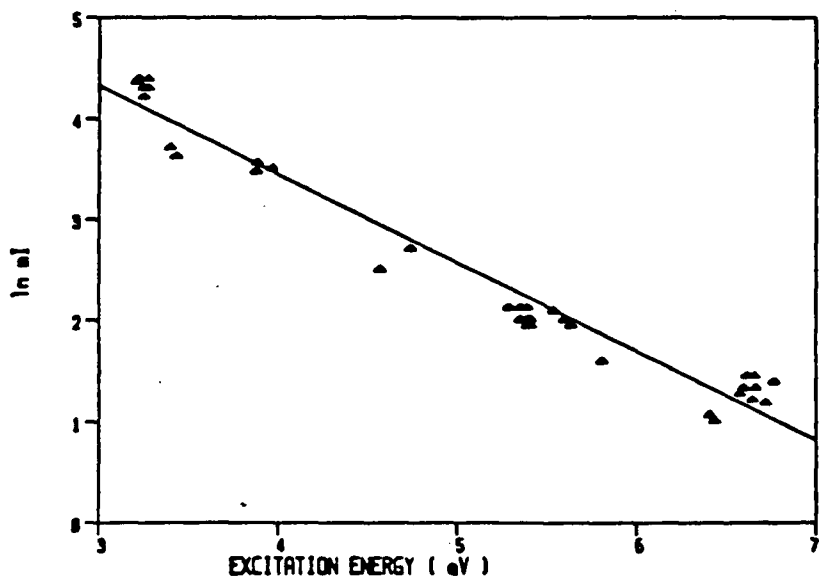


Figure 11b. A plot of the logarithm of FeI excited state level populations vs excitation energy, from data extracted from Faires, Palmer and Engleman [53]. Populations have been fitted using linear regression.

3.2 Results

Before discussing the results, the structure of an excited state level population plot will be briefly examined. For an analyte system in LTE with its surroundings, a population plot similar to the one provided in figure 12 will be observed. The vertical line drawn at E^+ corresponds to the ionization potential of the analyte thus dividing the populations into those of atom levels on the left and those of ion levels on the right. Under conditions of LTE the excited state levels will be populated according to the Boltzmann distribution, thus a plot of the natural log of the excited state level population, $\ln (I\lambda/gA)$, versus excitation energy, E_{exc} , will be linear with a slope equal to $-1/kT_{exc}$, where T_{exc} is the excitation temperature. The slope of the plot, and therefore T_{exc} , will be the same for both atom and ion levels. The relative separation between the two Boltzmann plots will yield the ionization temperature, T_i , via the Saha equation, which under LTE will be equal to the excitation temperature. If the analyte and plasma are not in LTE, then deviations from this plot are to be expected.

Excited state level populations have been determined for three analytes, Fe, Ba, and Cr from experimentally measured emission line intensities. The choice of these three analytes was made after careful consideration of the following criteria;

- (1) The analyte should have a rich emission spectrum with the

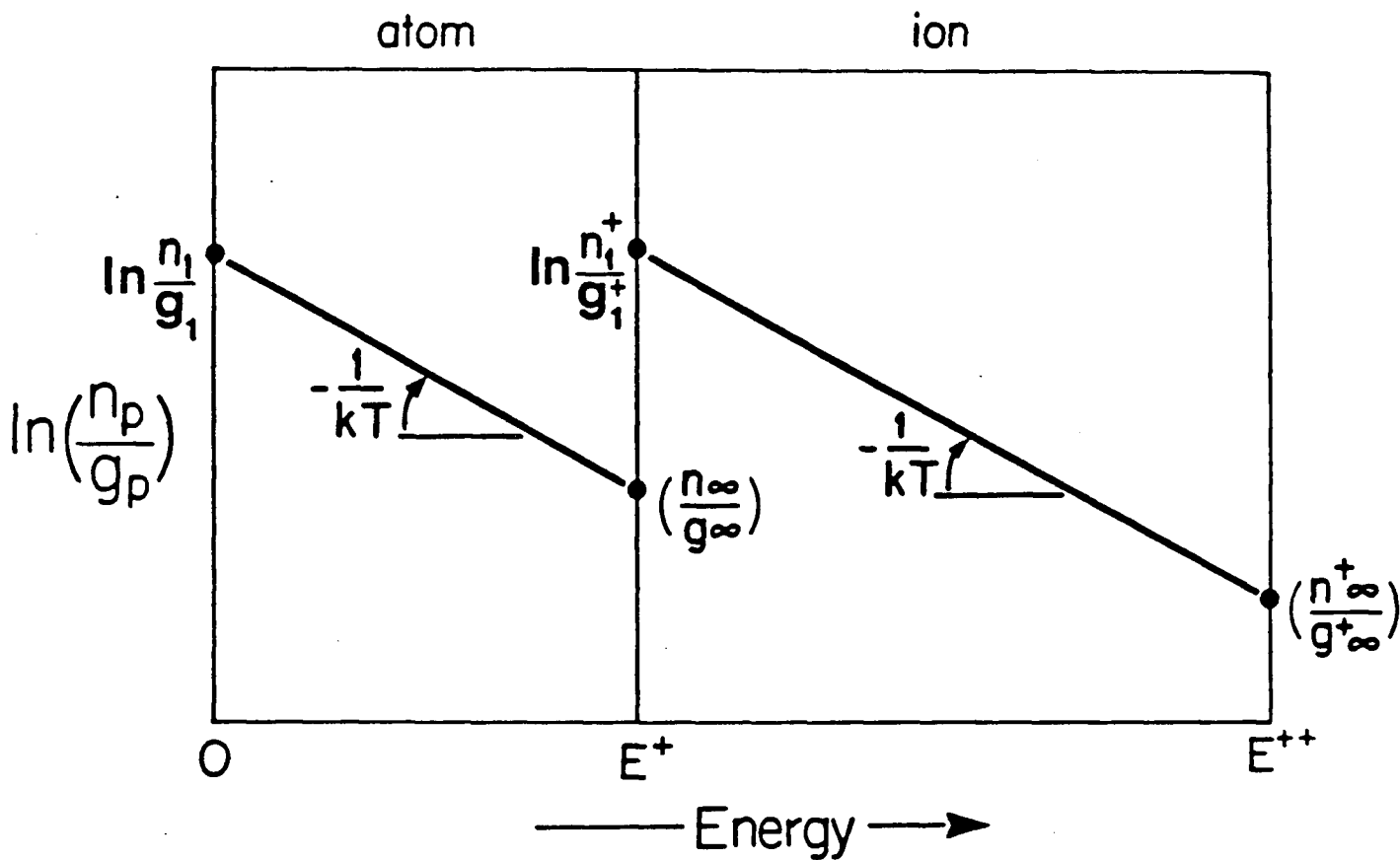


Figure 12. A Saha-Boltzmann LTE plot of the logarithm of level populations as a function of energy. E^+ and E^{++} are the ionization energies of atomic and ionic species respectively. The level populations are represented by a single temperature given by the slope of the Saha-Boltzmann lines ($-1/kT$).

spectral lines covering as wide an excitation range as possible;

(2) Availability of reliable transition probabilities for the emission lines of the particular analyte;

(3) The analytes should have differing ionization potentials, although the ionization potentials should not be very low nor very high.

The third criterion was considered important in case analyte excitation and ionization behaviour is dependent upon ionization potential. Analytes with very low or very high ionization potentials could not be considered as this would lead to extremely low atom populations in the case of low ionization potentials and extremely low ion populations in the case of high ionization potentials. The most important limiting criterion in selecting analytes was the lack of reliable transition probability data. Fe is one of the most frequently spectroscopically studied metals and as a result has some of the most reliable transition probabilities. Because of this, Fe was more extensively studied than either Ba or Cr, which had considerably poorer transition probabilities.

The Fe, Ba, and Cr intensities were measured at various spatial positions and rf input powers. For each of the three analytes, the natural log of the populations have been plotted against excitation energy for both atom and ion species. Representative error bars have been included in one population plot of each of the three analytes (figures 23,27 and 29).

These error bars include an estimated 10 % error in the measured intensity and the appropriate error in gA values provided in Tables II,III and IV. The application of the LPDA spectrometer provided a very effective method of data collection resulting in population plots containing upwards of 48 data points.

In order to facilitate the interpretation of the population plots, LTE curves have been drawn in. The LTE curves were determined by first selecting the appropriate electron density and electron temperature from previously measured data [54] corresponding to the particular spatial position and rf input power being considered. The electron density and electron temperature values are listed in Table I. The choice of electron temperature for an LTE temperature is consistent with the approach taken by other authors in formulating an LTE model [50,55]. A line, with a slope corresponding to the LTE temperature, was fitted to the upper energy atom levels. It would be preferable to place the LTE line through the ground state ion population, as it is believed that the ground state ion and low energy ion levels will be in or very close to LTE [7]. However ground state populations can not be measured in emission studies and the lowest ion excited state has an energy considerably above the ground state, especially for Fe and Cr. As a result, the LTE line was placed such that it passed through the upper energy atom levels. This is consistent with the views of other authors in that upper energy atom levels will be in LTE

TABLE I

LTE Temperatures Corresponding to Measured Electron Densities

<u>Electron Density (cm^{-3})</u>	<u>LTE Temperature (K)</u>
5×10^{14}	7317
1.5×10^{15}	7981
2.5×10^{15}	8370
3.5×10^{15}	8639

with the ground state ion population even if small deviations in the lower energy atom levels exists [7,55]. The LTE line passing through the ion levels was then calculated via the Saha equation using the LTE ground state atom population, given by intercept of the LTE line drawn through the atom levels with the population axis, and the appropriate electron density and LTE temperature.

3.3 FE RESULTS

Spatially resolved emission intensities were measured for 22 atom lines and 26 ion lines from two spectral windows, one covering the wavelength range 243 nm to 291 nm, the second from 343 nm to 391 nm. The intensities were collected at two rf input powers, 1.25 and 1.75 kW, and at two vertical heights, 8 and 16 mm above the load coil. Population plots were constructed by calculating the logarithm of level populations, $\ln(mI)$, ($m = \lambda/gA$), and plotting them against excitation energy. The wave lengths of the lines chosen, along with their gA values are given in Table II. The emission spectra from these two spectral windows, including identification of the lines chosen, are provided in Appendix B.

3.3.1 FE LEVEL POPULATIONS AT 8 MM ABOVE THE LOAD COIL

Radial dependence of FeI level populations at 8 mm above the

TABLE II

FeI lines

<u>Wavelength (nm)</u>	<u>Excitation</u>		<u>% Error*</u>	<u>Reference</u>
	<u>Energy (eV)</u>	<u>gA ($\times 10^8$)</u>		
388.85	4.80	1.43	b	[57]
388.63	3.24	0.376	b	[57]
385.99	3.21	0.796	b	[57]
382.78	4.80	6.00	a	[57]
382.59	4.15	4.56	a	[57]
382.04	4.10	6.16	a	[57]
381.58	4.73	8.15	a	[57]
376.55	6.53	5.9	a	[57]
374.95	4.22	7.02	a	[57]
373.71	3.37	1.29	a	[57]
373.49	4.18	9.76	a	[57]
371.99	3.33	1.79	a	[57]
368.22	6.91	9.37	a	[57]
365.15	6.15	6.15	a	[57]
361.88	4.42	5.09	a	[57]
360.89	4.45	4.16	a	[57]
360.67	6.13	11.7	a	[57]
360.55	6.17	6.31	b	[57]
358.12	4.32	12.5	a	[57]
357.01	4.39	7.56	b	[57]
356.54	4.44	3.71	a	[57]
355.37	7.06	7.99	b	[57]

TABLE II: continued

FeII lines

<u>Wavelength (nm)</u>	<u>Excitation</u>		<u>% Error*</u>	<u>Reference</u>
	<u>Energy (eV)</u>	<u>gA ($\times 10^8$)</u>		
276.18	5.59	0.459	a	[58]
275.57	5.48	21.1	a	[58]
275.33	7.77	24.8	c	[59]
274.65	5.59	11.7	a	[58]
274.32	5.62	7.20	a	[58]
273.96	5.51	15.4	a	[58]
273.07	5.62	1.00	a	[58]
272.75	5.59	3.41	b	[58]
271.44	5.55	3.86	c	[59]
266.66	8.07	24.1	c	[59]
266.47	8.04	26.5	c	[59]
262.83	4.84	3.43	a	[58]
262.57	4.77	3.35	a	[58]
262.17	4.85	0.97	a	[58]
261.76	4.82	2.62	a	[58]
261.38	4.85	3.98	a	[58]
261.19	4.79	8.71	a	[58]
260.71	4.84	6.63	a	[58]
259.94	4.77	22.1	a	[58]
259.84	4.82	7.85	a	[58]
259.15	5.82	4.07	c	[58]
258.59	4.79	6.44	a	[58]
258.26	5.88	3.09	a	[58]
256.69	5.91	2.60	c	[59]
256.35	5.88	5.21	a	[58]
256.25	5.82	12.8	c	[59]

* Estimated % error is : a = +/-10% ; b = +/-15% ; c = +/-25%

load coil was examined by plotting $\ln (mI)$ versus excitation energy for two radial positions, 0.0 mm (squares) and 1.5 mm (circles), taken at 1.25 kW rf input power as shown in figure 13. The relative magnitudes of $\ln (mI)$ at the two radial positions are indicative of the shape of the spatial population profile; the smaller the difference between the two $\ln (mI)$ values, the broader the radial population profile. From the data presented in this plot, the shape of the spatial population profile is dependent upon excitation energy, being broader for higher energy lines. The overall lower level populations encountered at the off axis position relative to 0.0 mm, indicates the highest concentration of FeI species occurs at the center of the plasma. The most outstanding feature of the level populations in figure 13 is their non-linearity with respect to excitation energy. The degree of curvature can best be emphasized by calculating the level dependent temperatures as a function of excitation energy for 0.0 mm radial position using the method outlined by Kornblum and Smeyers-Verbeke [52]. These level dependent temperatures have been calculated and plotted in figure 14. From this plot it is observed that excitation temperatures can vary from approximately 4500 to 7000 K. Due to problems associated with using a second order polynomial to fit the data, the plot suggests that the temperature continues to increase at the higher excitation energy where in fact it should begin to level off. The non-linear level populations and level

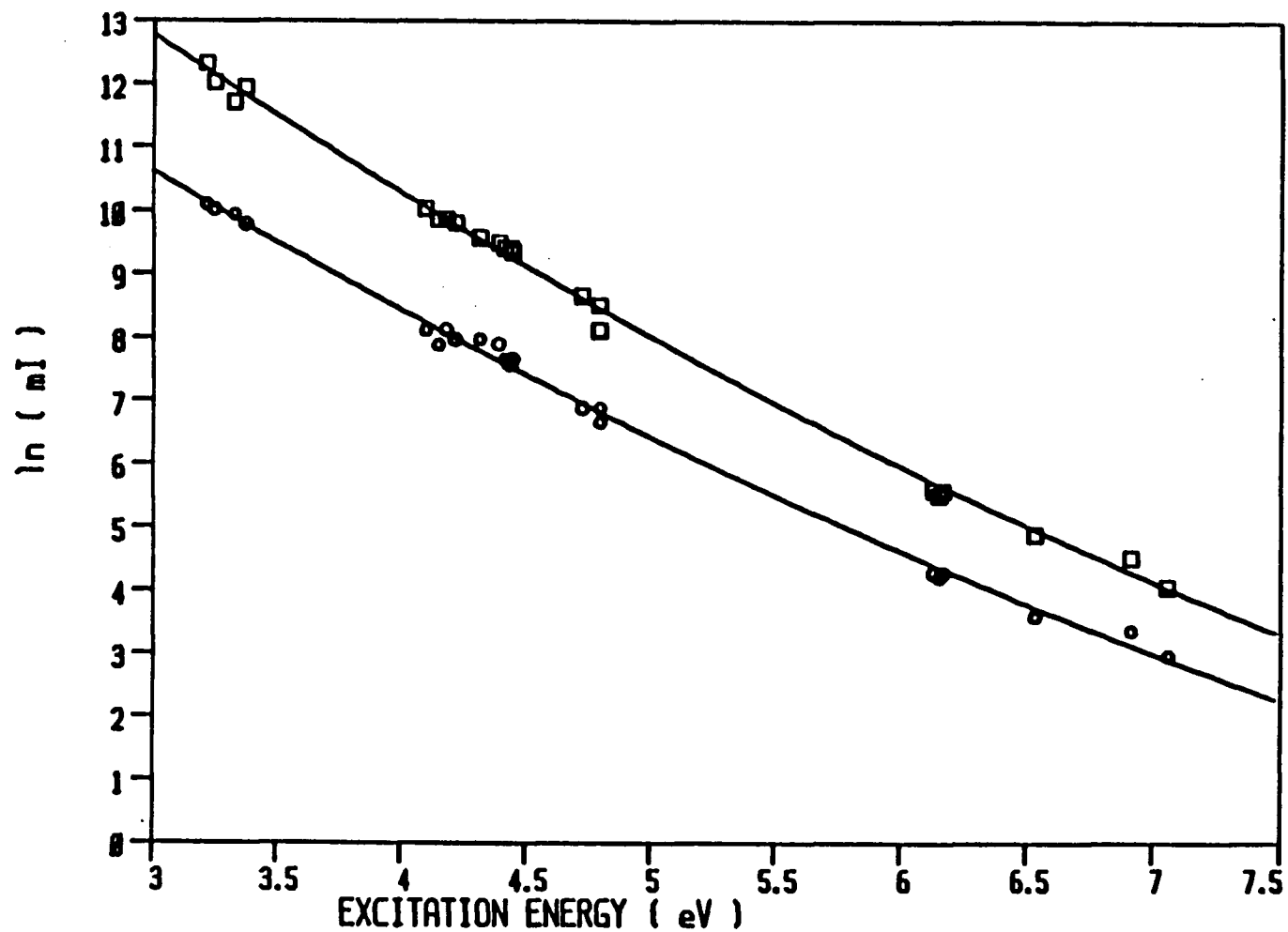


Figure 13. A plot of the logarithm of FeI level populations determined at 8 mm above the load coil and at 1.25 kW rf input power as a function of energy. Radial position; (\square) 0 mm, (\circ) 1.5 mm.

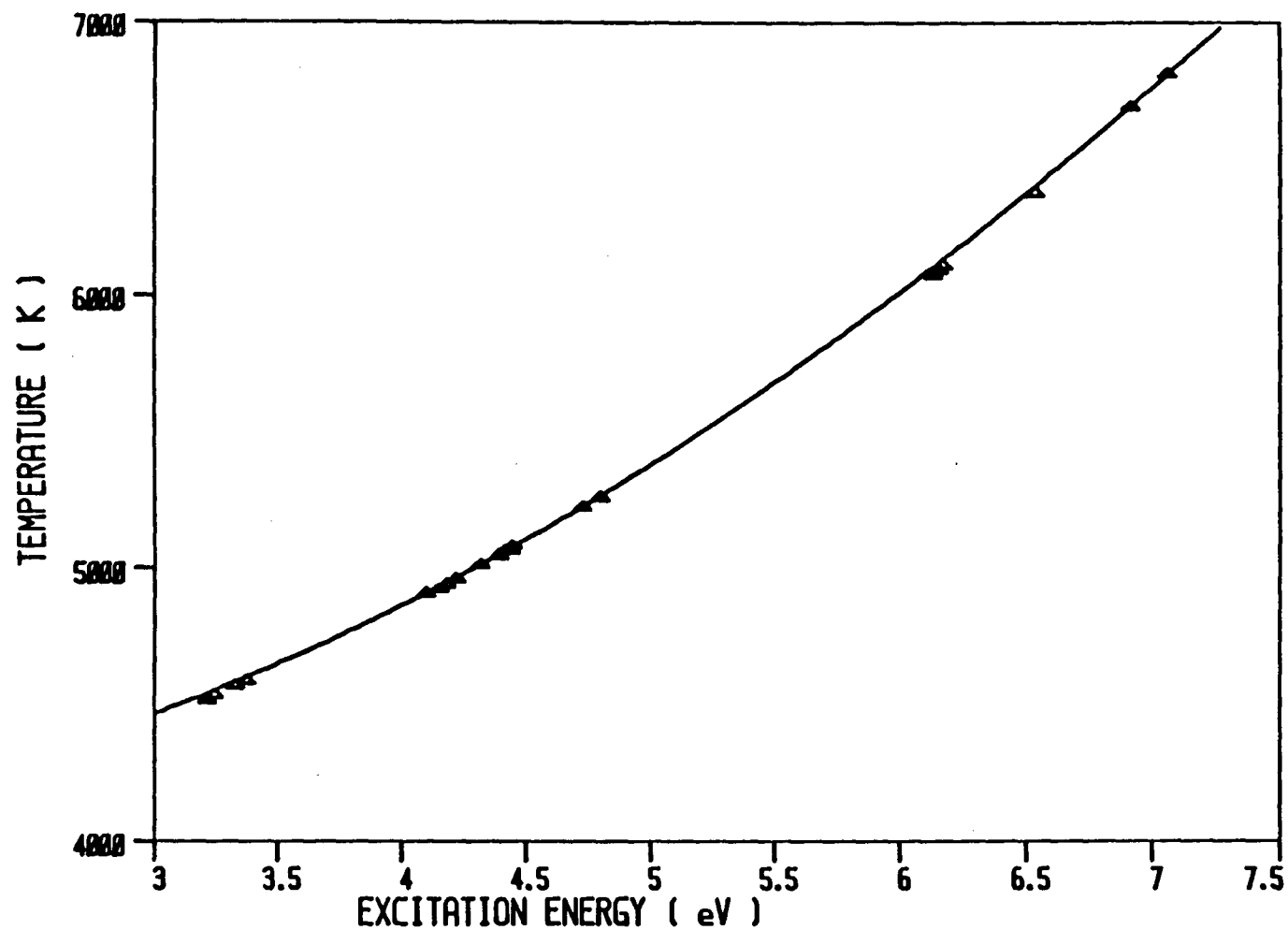


Figure 14. FeI level dependent temperatures calculated from FeI level populations determined at 8 mm above the load coil, at an rf input power of 1.25 kW and at a radial position of 0 mm.

dependent temperatures are consistent with previous findings in studies on FeI level populations [51,52].

Figure 15 contains a plot of FeII level populations as a function of excitation energy at 1.25 kW. Once again two radial positions were examined, 0.0 mm (squares) and 1.5 mm (circles). In contrast to the non-linearity observed with the FeI level populations, the FeII levels do appear to vary linearly with excitation energy, suggesting the existence of Boltzmann equilibrium between the FeII levels. The excitation, or Boltzmann, temperature evaluated from the slope ($-1/kT$) was found to be 8200 K at both radial positions of 0.0 mm and 1.5 mm.

The population plots in figure 15 also provide evidence against the importance of asymmetric charge transfer as a possible analyte excitation/ionization mechanism. The three uppermost FeII levels have total energies of 15.64, 15.91 and 15.94 eV, with respect to the ground state atom, which are sufficiently close to the ionization potential of Ar (15.75 eV) to yield small energy defects of between 0.11 and 0.19 eV for the reaction. The fact that these levels appear to be in Boltzmann equilibrium with the lower levels argues against asymmetric charge transfer as being a significant excitation and ionization mechanism.

Upon comparison of figures 13 and 15, a similarity is observed in the population spacing between 0.0 mm and 1.5 mm for all FeII levels and for the high energy FeI levels. This

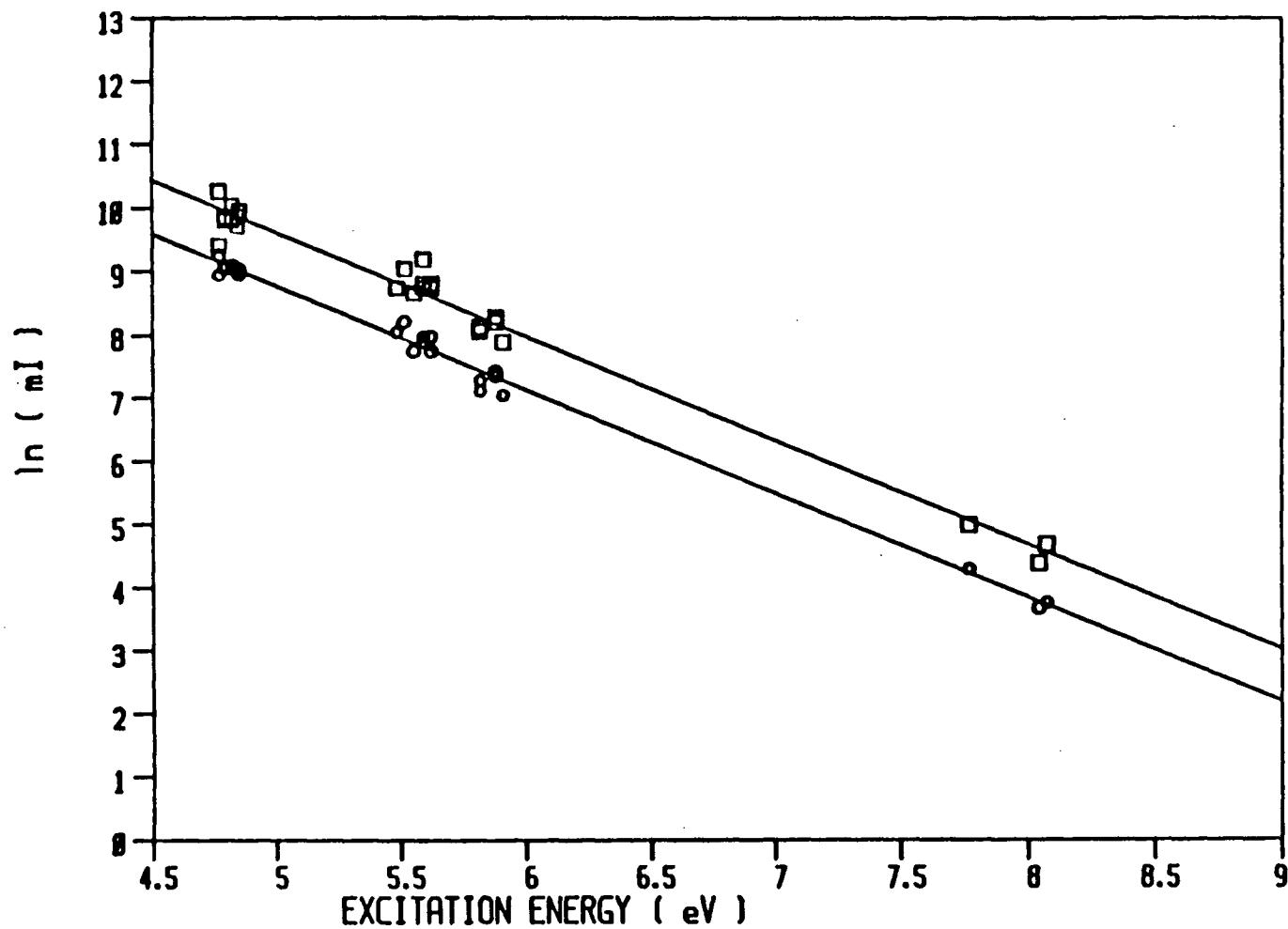


Figure 15. A plot of the logarithm of FeII level populations determined at 8 mm above the load coil and at 1.25 kW rf input power as a function of energy. Radial position; (\square) 0 mm, (\circ) 1.5 mm.

suggests a close coupling (Saha equilibrium) between the upper levels of the atom and the excited ion levels through the ion ground state. Further evidence of this coupling is apparent in the similar excitation temperatures determined from the upper FeI levels (7500 K) and the FeII levels (8200 K) at 0.0 mm.

FeI level populations measured at 1.75 kW and 8 mm above the load coil are provided in figure 16. Once again non-linearity is observed in the level populations corresponding to a radial position of 0.0 mm. However at a radial position of 1.5 mm, the population points can best be approximated by a straight line. The lack of curvature in this data collected at 1.5 mm may be a result of the high electron density encountered off axis at 1.75 kW. Previous measurements in our lab indicate the electron density changes from between 2.0 to $2.5 \times 10^{15} \text{ cm}^{-3}$ to 3.5 to $4.0 \times 10^{15} \text{ cm}^{-3}$ as one moves from the center of the plasma to a radial position of 1.5 mm off axis at a vertical height of 8 mm above the load coil [54]. The excitation temperature derived for the 1.5 mm line is 8400 K. This value corresponds quite closely to an electron temperature of approximately 8600 K derived from an electron density of $3.5 - 4.0 \times 10^{15} \text{ cm}^{-3}$, suggesting a close coupling between the two distributions.

The FeII level populations measured at 1.75 kW and at two radial positions, 0.0 mm (squares) and 1.5 mm (circles), are presented in figure 17. As was the case with the FeII level populations at 1.25 kW, the FeII level populations at 1.75 kW

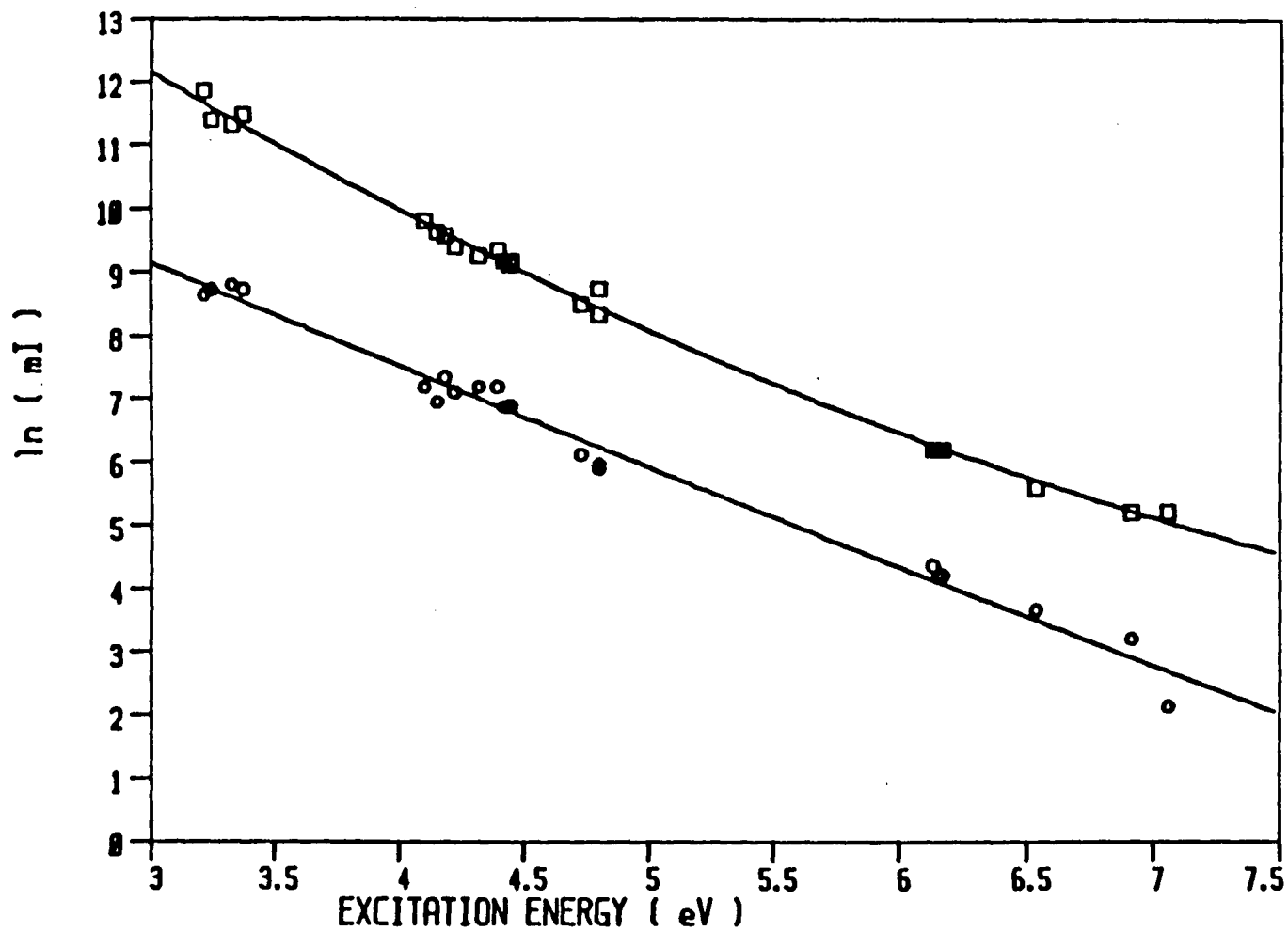


Figure 16. A plot of the logarithm of FeI level populations determined at 8 mm above the load coil and at 1.75 kW rf input power as a function of energy. Radial position; (\square) 0 mm, (\circ) 1.5 mm.

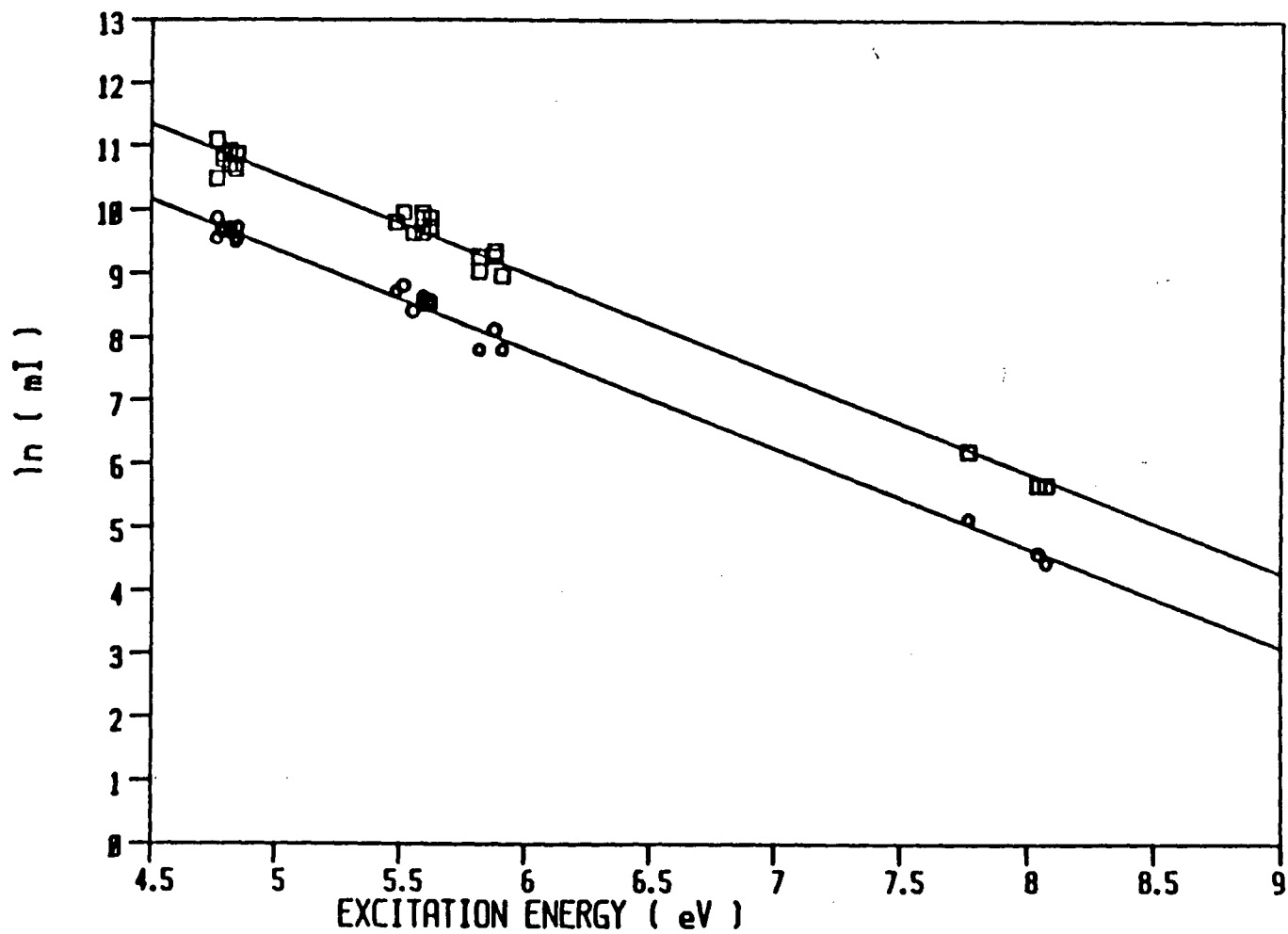


Figure 17. A plot of the logarithm of FeII level populations determined at 8 mm above the load coil and at 1.75 kW rf input power as a function of energy. Radial position; (□) 0 mm, (○) 1.5 mm.

appear to vary linearly with respect to excitation energy. The excitation temperatures derived from the two lines in figure 17 are 8700 K for 0.0 mm and 8600 K for 1.5 mm.

3.3.2 FE LEVEL POPULATIONS AT 16 MM ABOVE THE LOAD COIL

Level population plots for FeI and FeII at 16 mm above the load coil and at an rf input power of 1.25 kW are presented in figures 18 and 19 respectively. The FeI populations appear to be curved and the FeII populations are best represented by straight lines, which is essentially the same as the findings at 8 mm above the load coil for the same rf input power. The linearity in the FeII levels once again suggests the existence of Boltzmann equilibrium between these levels. The excitation temperature derived from the two FeII population plots was approximately 7400 K. The relatively small separation between the population plots at 0.0 mm and 1.5 mm for both FeI and FeII species is indicative of broad radial population profiles. This is consistent with the relatively uniform excitation conditions (temperature [56] and electron density [54]) as a function of radial position that are encountered at this vertical height.

Level-dependent temperatures were determined from the FeI population plot at a radial position of 0.0 mm and are presented as a function of excitation energy in figure 20. The temperatures range from approximately 5200 K for the levels

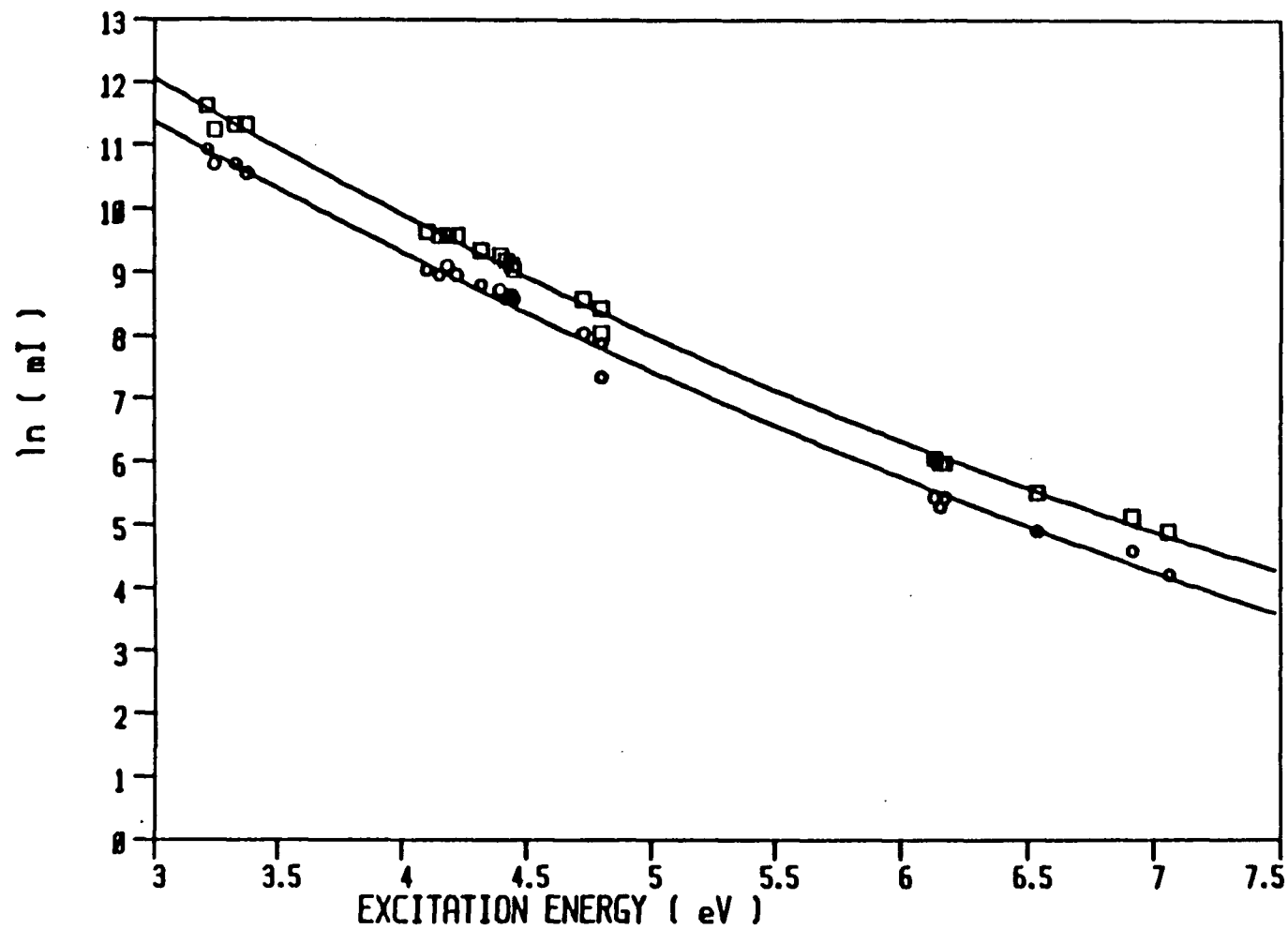


Figure 18. A plot of the logarithm of FeI level populations determined at 16 mm above the load coil and at 1.25 kW rf input power as a function of energy. Radial position; (\square) 0 mm, (\circ) 1.5 mm.

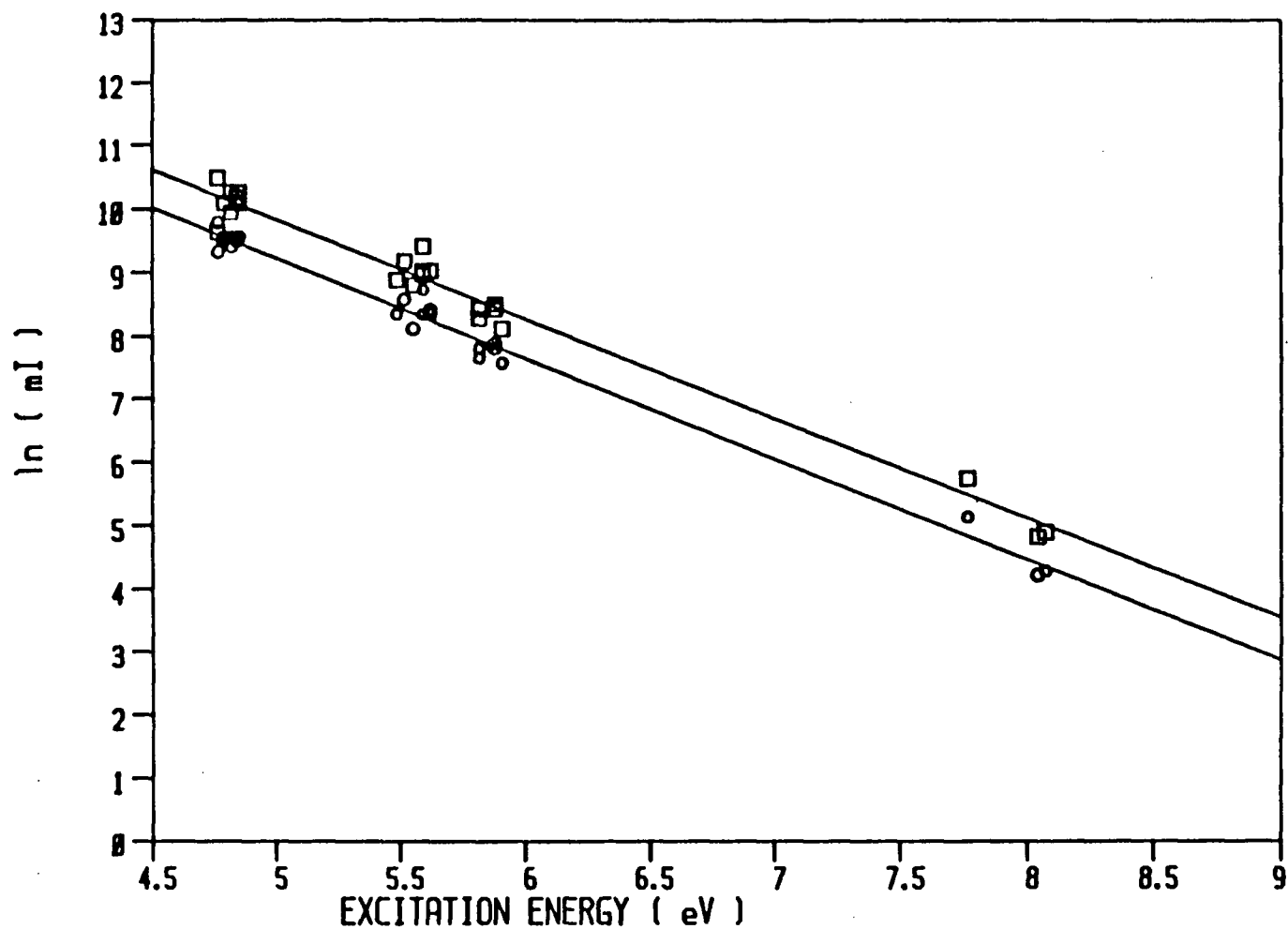


Figure 19. A plot of the logarithm of FeII level populations determined at 16 mm above the load coil and at 1.25 kW rf input power as a function of energy. Radial position; (\square) 0 mm, (\circ) 1.5 mm.

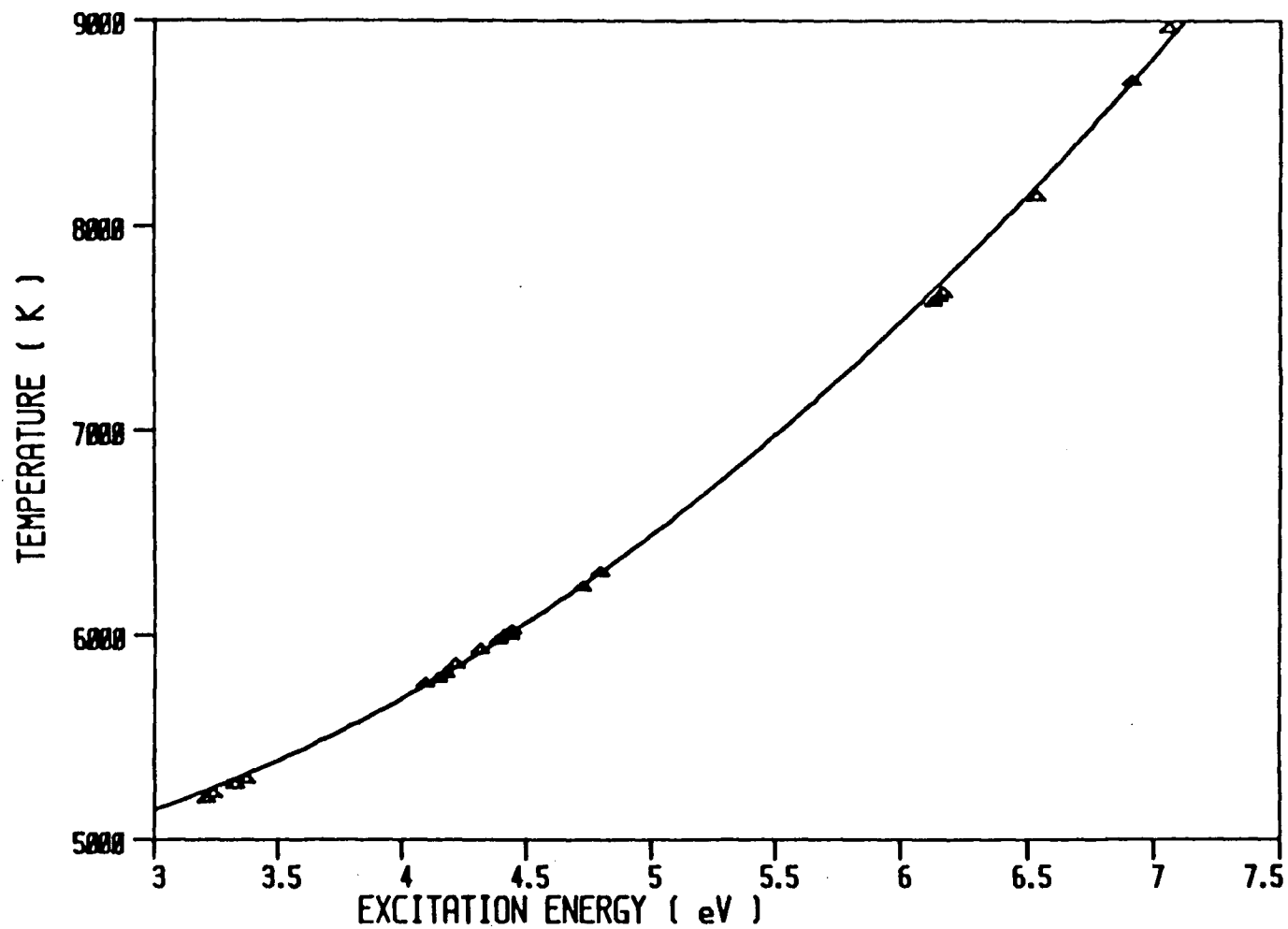


Figure 20. FeI level dependent temperatures calculated from FeI level populations determined at 16 mm above the load coil, at an rf input power of 1.25 kW and at a radial position of 0 mm.

between 3.2 and 3.4 eV to 8700 K for the levels between 6.5 and 7.1 eV. Once again the temperatures obtained at high excitation energies suggest a continual increase where in fact the temperatures should begin to level off.

An interesting point is observed if excitation temperatures are compared for FeI and FeII at the two vertical heights of 8 mm and 16 mm above the load coil, and at 1.25 kW rf input power. The excitation temperature for the FeI levels with excitation energies of between 3.2 and 3.4 eV are found to increase from 4500 K at 8 mm to 5200 K at 16 mm. This spatial dependence in temperature is consistent with findings of FeI temperature studies undertaken by Faires et al. [53] and Blades and Caughlin [56]; that is, the FeI temperature increases with height from 8 mm to 16 mm above the load coil. In contrast to this increase in FeI excitation temperatures at 1.25 kW, the FeII excitation temperature decreases from 8200 K at 8 mm to 7700 K at 16 mm above the load coil.

FeI and FeII level populations determined at 16 mm above the load coil and at an rf input power of 1.75 kW are provided in figures 21 and 22 respectively. The FeI population plots at 0.0 mm and 1.5 mm both contain curvature, although the degree of curvature is somewhat reduced from that observed in the analogous plot at 1.25 kW. The FeII levels appear to vary linearly with excitation energy and yield an excitation energy of approximately 8000 K for both radial positions.

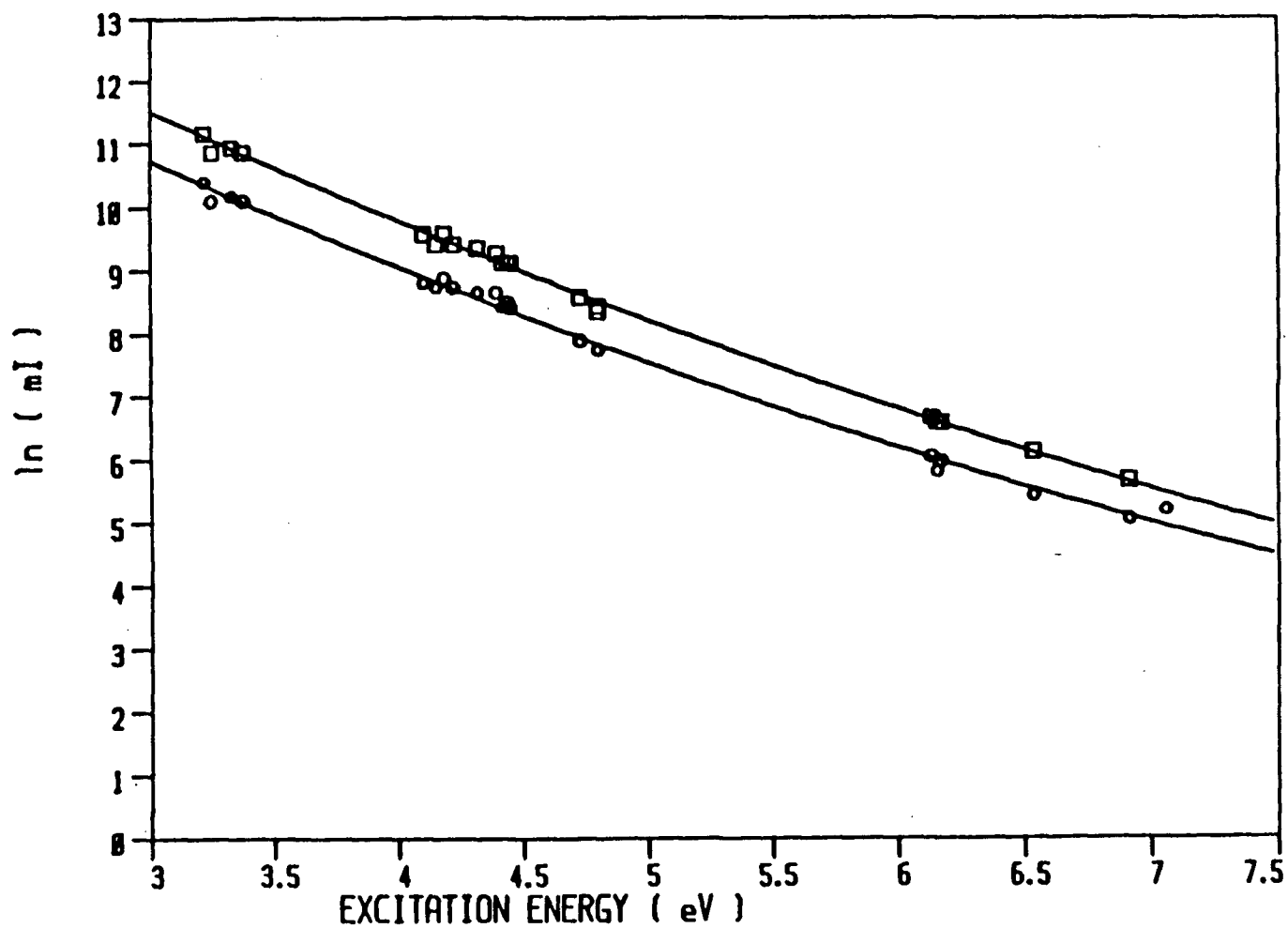


Figure 21. A plot of the logarithm of FeI level populations determined at 16 mm above the load coil and at 1.75 kW rf input power as a function of energy. Radial position; (\square) 0 mm, (\circ) 1.5 mm.

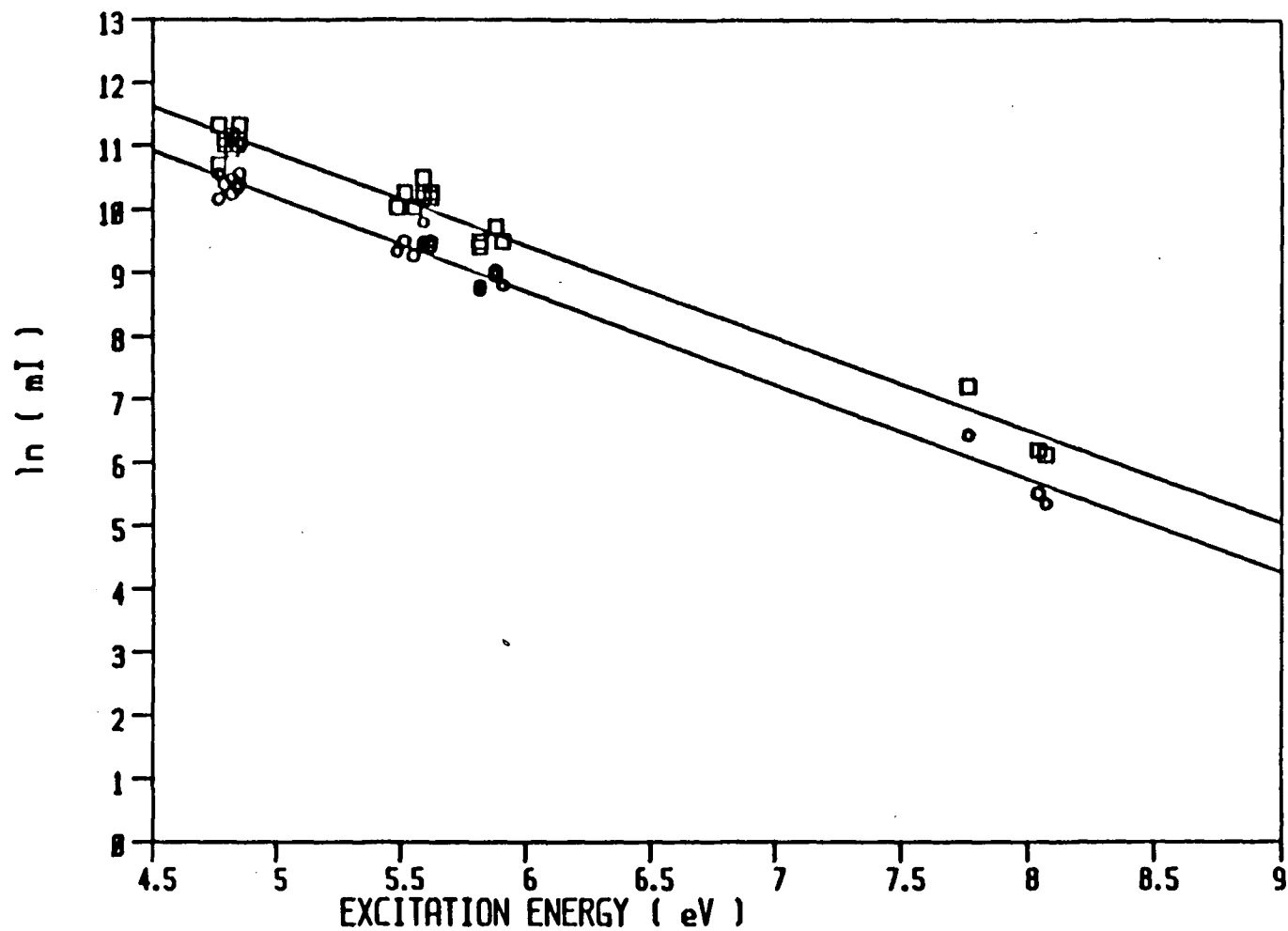


Figure 22. A plot of the logarithm of FeII level populations determined at 16 mm above the load coil and at 1.75 kW rf input power as a function of energy. Radial position; (□) 0 mm, (○) 1.5 mm.

3.3.3 FE EXCITED STATE LEVEL POPULATIONS

In order to investigate overall trends in the Fe level populations at the two powers and two vertical positions, population plots have been constructed which include both FeI and FeII levels on the same plot. Figures 23 and 24 contain data collected at 8 mm above the load coil and at the two rf powers of 1.25 and 1.75 kw respectively. Figures 25 and 26 contain data collected at 16 mm above the load coil and at 1.25 and 1.75 kw respectively. The vertical line drawn in on these plots corresponds to an ionization potential of Fe of 7.87 eV. The excitation energies on the abscissa are relative to the atom ground state. The solid lines in these plots represent LTE lines which have been determined according to the procedure outlined in section 3.1.

The most striking observation to be made from the four population plots is the overpopulation of the low energy atom levels and the underpopulation of the ion levels with respect to the LTE curves. It is also important to notice that the degree of overpopulation of the FeI levels and underpopulation of the FeII levels decreases upon going from an rf input power of 1.25 kW, figure 23 and 25, to 1.75 kW, figure 24 and 26. An overpopulation of FeI levels is consistent with the underpopulation of FeII levels as the excess atom population must come from a depletion of ionic levels. Also the degree of

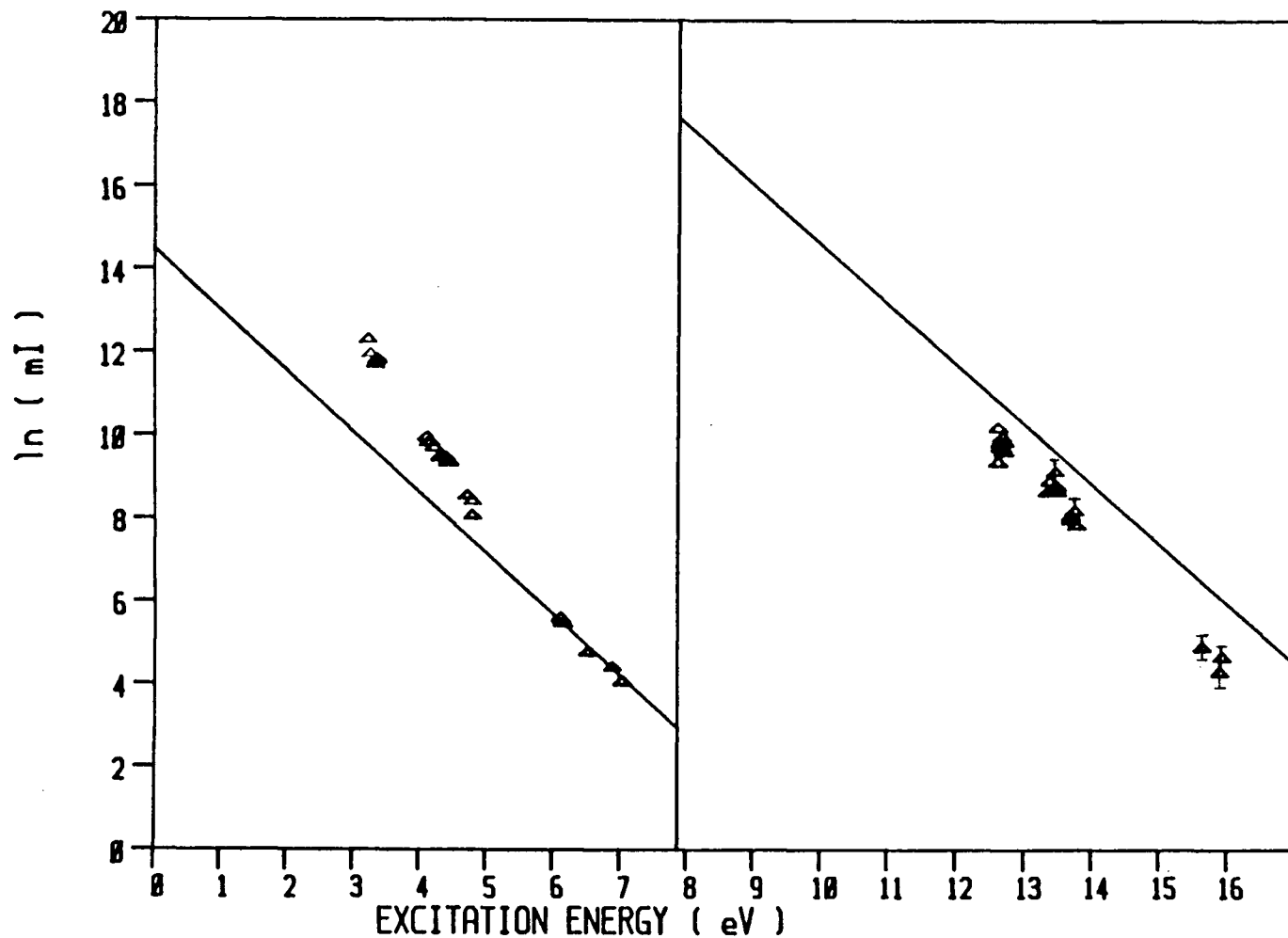


Figure 23. A plot of the logarithm of FeI and FeII level populations determined at 8 mm above the load coil, at a radial position of 0 mm and at an rf input power of 1.25 kW. The solid lines represent LTE calculated populations.

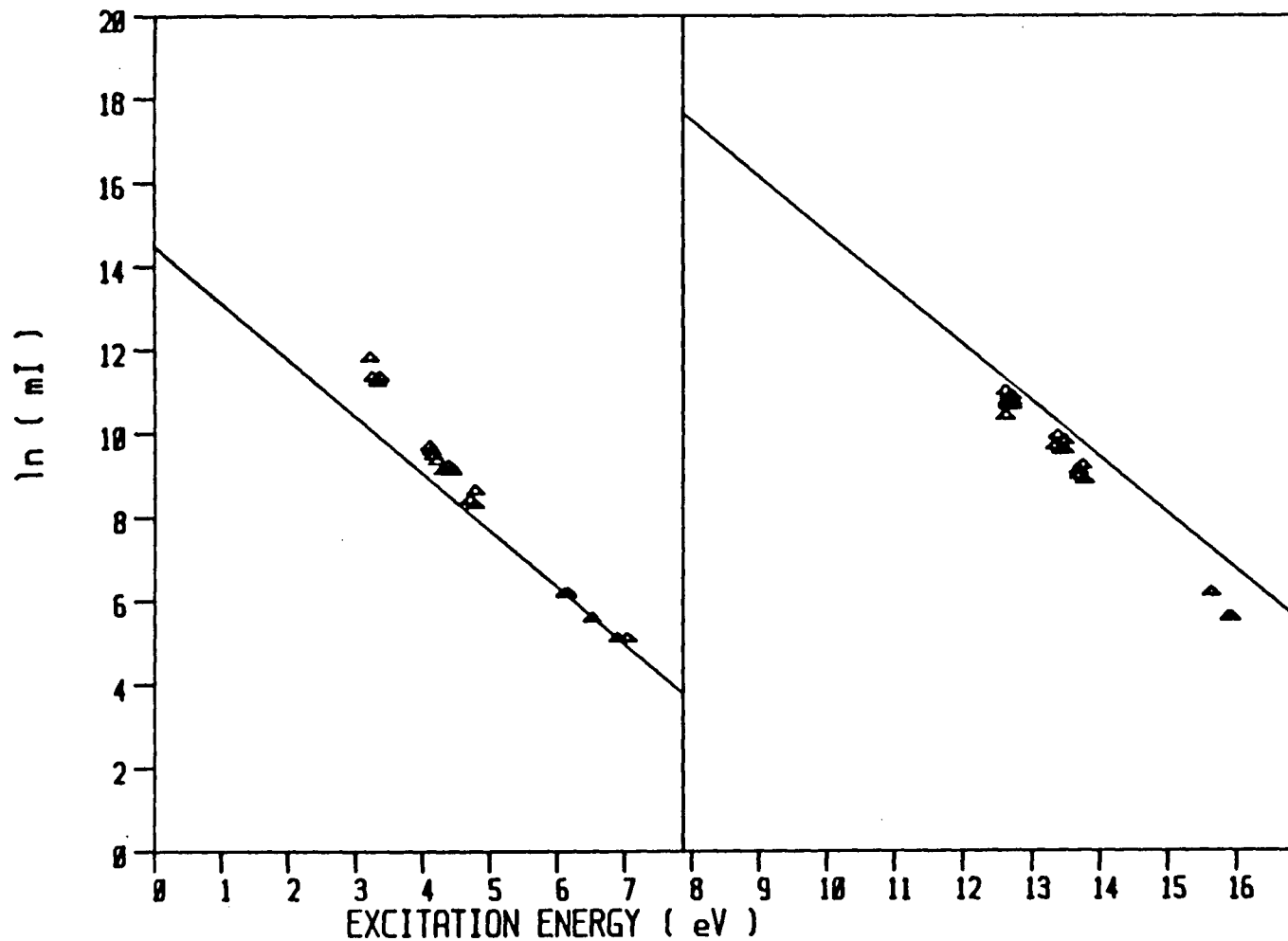


Figure 24. A plot of the logarithm of FeI and FeII level populations determined at 8 mm above the load coil, at a radial position of 0 mm and at an rf input power of 1.75 kW. The solid lines represent LTE calculated populations.

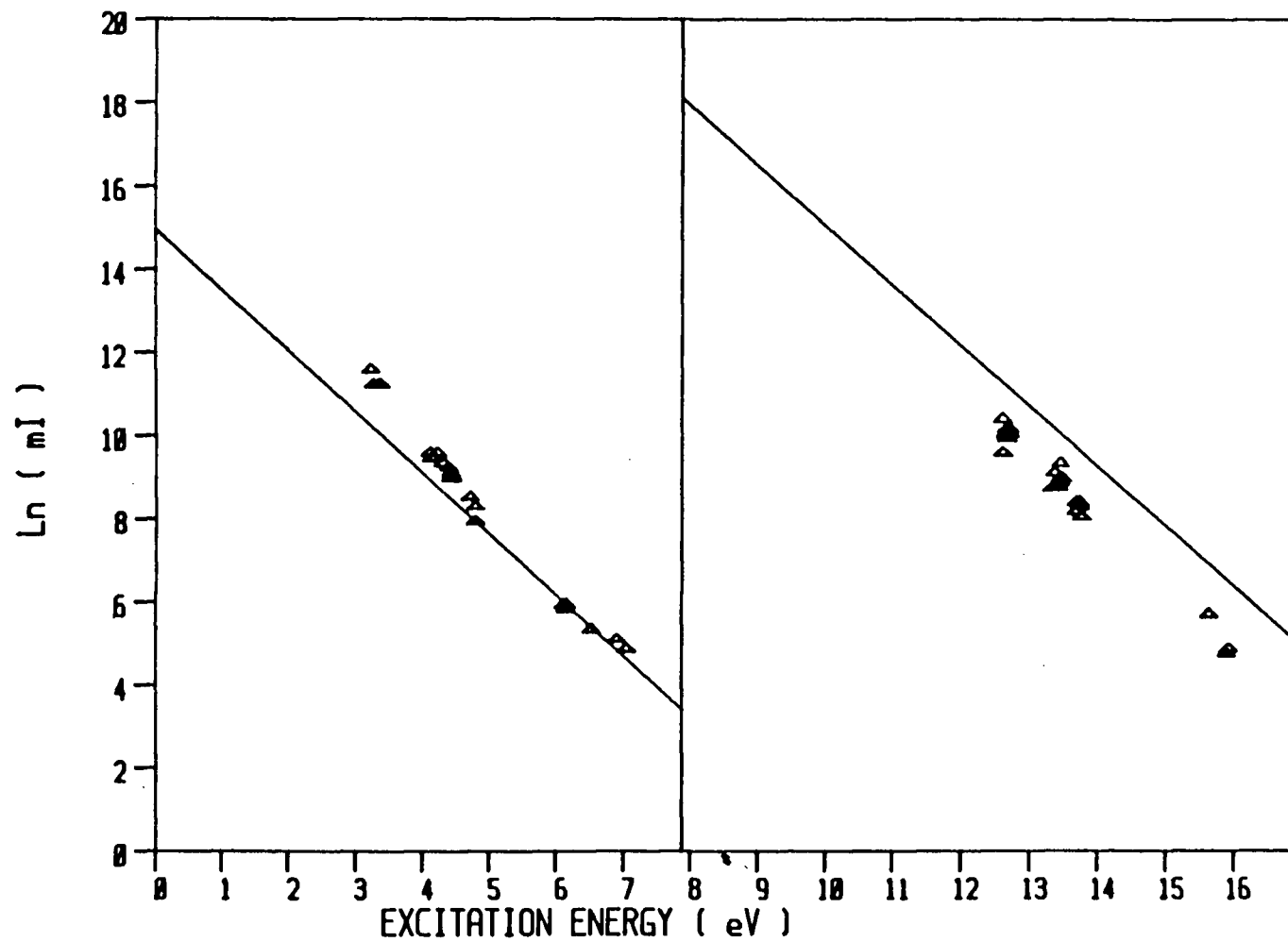


Figure 25. A plot of the logarithm of FeI and FeII level populations determined at 16 mm above the load coil, at a radial position of 0 mm and at an rf input power of 1.25 kW. The solid lines represent LTE calculated populations.

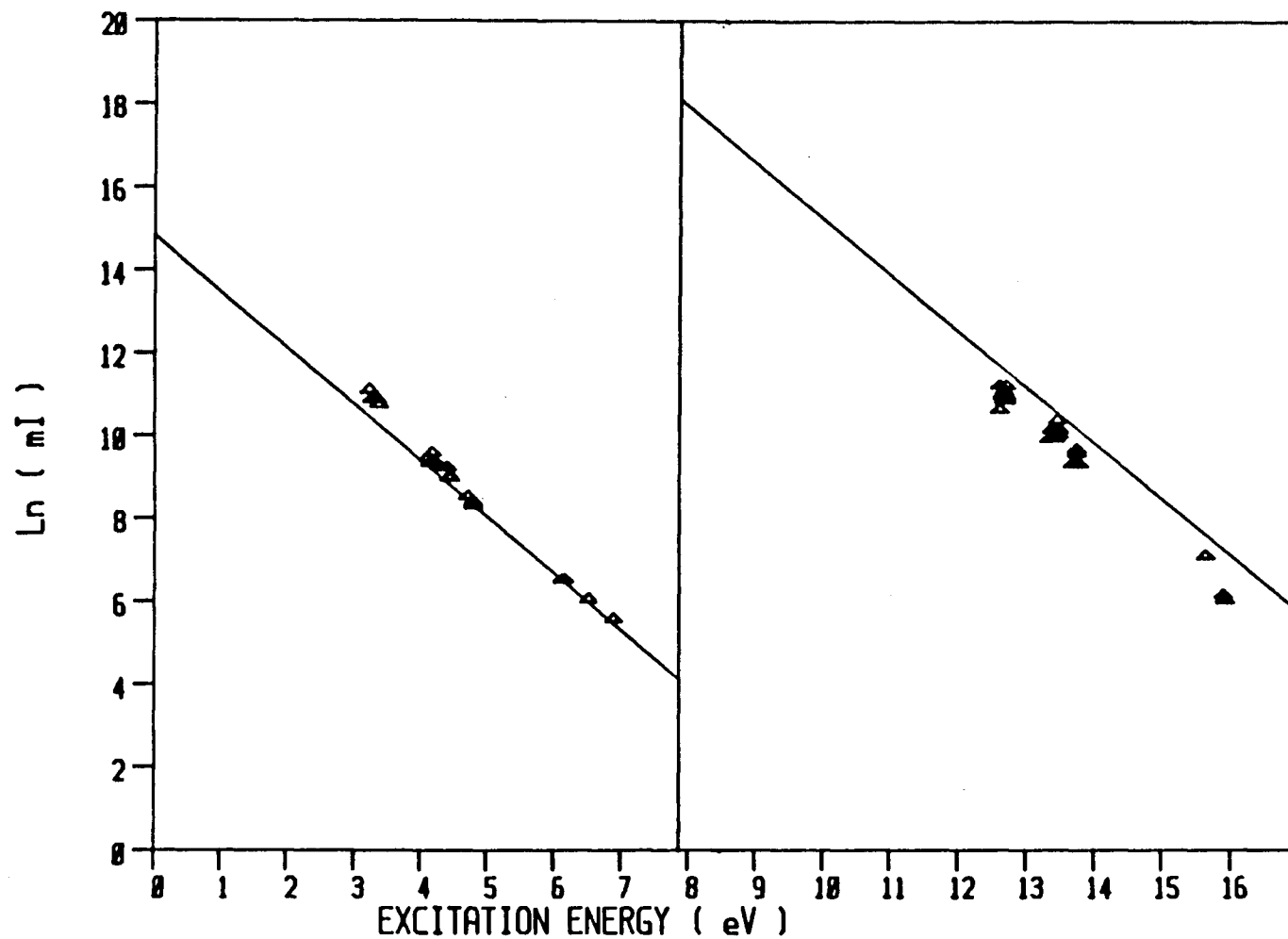


Figure 26. A plot of the logarithm of FeI and FeII level populations determined at 16 mm above the load coil, at a radial position of 0 mm and at an rf input power of 1.75 kW. The solid lines represent LTE calculated populations.

overpopulation of FeI levels decreases with increasing excitation energy, until the upper most levels fall on the LTE curve.

3.4 BA RESULTS

Spatially resolved emission intensities were measured for 8 atom lines and 9 ion lines from four spectral windows, centered at 273 nm, 410 nm, 470 nm and 573 nm. The intensities were collected at two rf input powers, 1.25 and 1.75 kW, and at one vertical height of 16 mm above the load coil. The wavelength of the lines chosen, along with their gA values are given in Table III. The emission spectra from these four spectral windows, including identification of the lines chosen, are provided in Appendix C.

3.4.1 BA EXCITED STATE LEVEL POPULATIONS

Excited state level populations of Ba, including both atom and ion levels, have been constructed for data collected at rf input powers of 1.25 kW and 1.75 kW and are presented in figures 27 and 28 respectively. LTE lines have once again been determined from the appropriate electron densities and electron temperatures given in Table I.

The BaII level populations in figure 27, which were collected at an rf power of 1.25 kW, show a very close correlation to the

TABLE III

BaI lines

<u>Wavelength (nm)</u>	<u>Excitation</u>		<u>% Error</u> *	<u>Reference</u>
	<u>Energy (eV)</u>	<u>gA ($\times 10^8$)</u>		
597.17	3.22	1.45	d	[60]
590.76	3.22	0.18	d	[60]
582.63	3.54	1.68	d	[60]
577.76	3.82	4.48	d	[60]
435.03	4.42	3.00	d	[60]
428.31	4.31	4.48	d	[60]
399.34	4.29	4.95	d	[60]
393.57	4.29	3.29	d	[60]

BaII lines

<u>Wavelength (nm)</u>	<u>Excitation</u>		<u>% Error</u> *	<u>Reference</u>
	<u>Energy (eV)</u>	<u>gA ($\times 10^8$)</u>		
585.37	2.72	0.192	b	[60]
493.41	2.51	1.91	b	[60]
490.00	5.25	1.55	b	[60]
455.40	2.72	4.68	a	[60]
452.49	5.25	1.44	d	[60]
416.60	5.70	1.48	d	[60]
413.07	5.72	10.8	b	[60]
389.18	5.70	6.68	b	[60]
277.14	7.19	0.80	d	[60]
263.48	7.43	4.56	d	[60]

* Estimated % error is : a = +/-10% ; b = +/-15% ; c = +/-25% ;
d = +/-50%

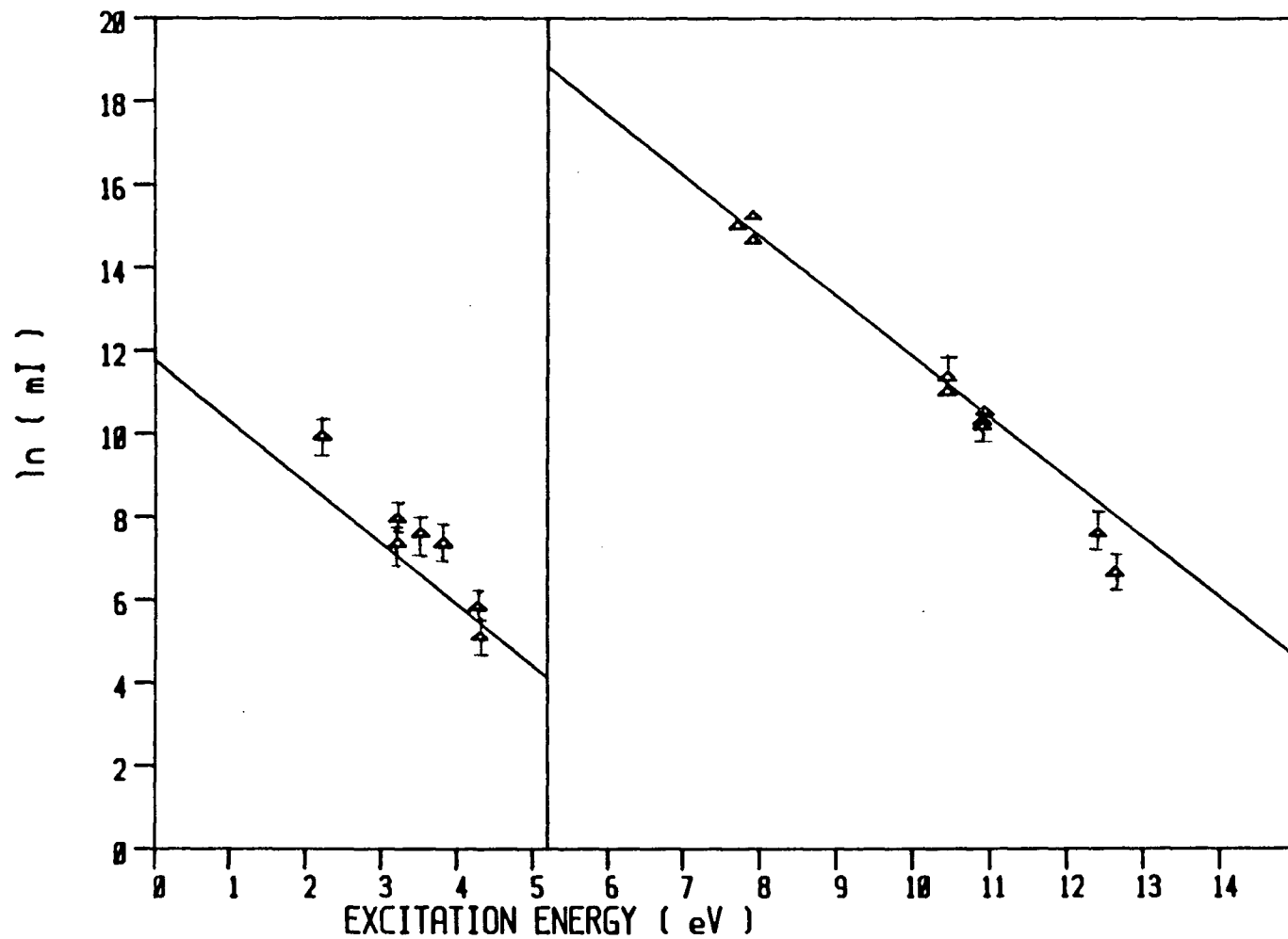


Figure 27. A plot of the logarithm of BaI and BaII level populations determined at 16 mm above the load coil, at a radial position of 0 mm and at an rf input power of 1.25 kW. The solid lines represent LTE calculated populations.

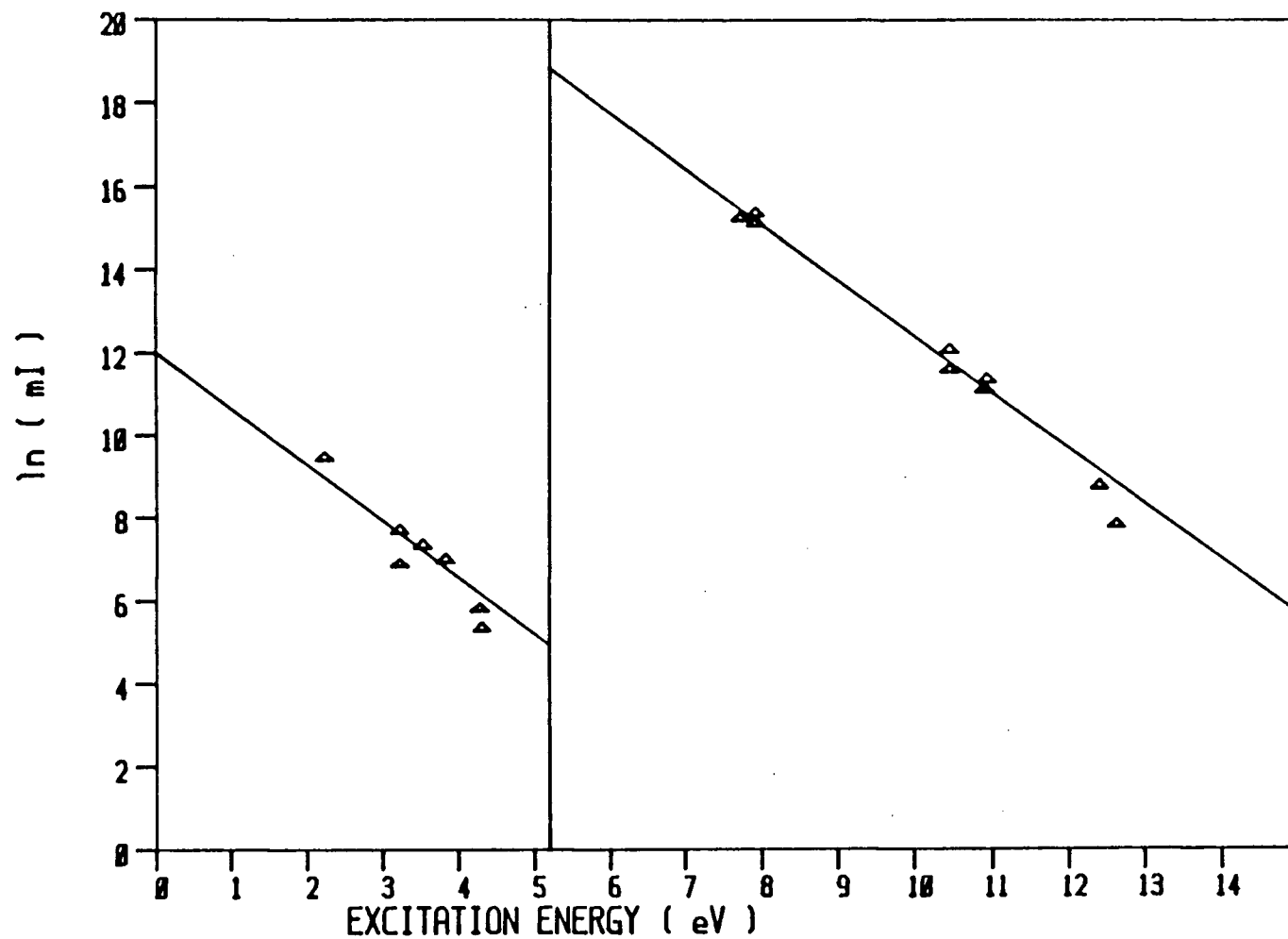


Figure 28. A plot of the logarithm of BaI and BaII level populations determined at 16 mm above the load coil, at a radial position of 0 mm and at an rf input power of 1.75 kW. The solid lines represent LTE calculated populations.

LTE line. The upper two levels appear to be underpopulated, although their deviation from the LTE curve is more likely to result from faulty gA values. The lower energy atom lines in figure 27 appear to be overpopulated with respect to the LTE curve. This behaviour is consistent with the findings in the FeI data. The fact that an underpopulation of BaII levels is not observed is not surprising upon realizing the degree of ionization of Ba. At 1.25 kW, and at an electron density and temperature of 1.5×10^{15} and 8000 K respectively, less than 1% of the Ba exists as atomic species due to its relatively low ionization potential of 5.21 eV. Thus a significant increase in atom population will not necessarily be paralleled by a significant decrease in ion population.

Figure 28 presents Ba level populations collected at an rf input power of 1.75 kW. Once again the BaII levels show a close correlation to the LTE curve. The BaI levels are overpopulated with respect to the LTE curve, although the degree of overpopulation is somewhat reduced from that observed at 1.25 kW. This type of behaviour is consistent with the findings in the Fe results.

3.5 CR RESULTS

Due to low intensities of many of the higher energy Cr emission lines, measurement of spatially resolved intensities

was not possible. However, 16 CrI and 16 CrII line intensities were measured at 16 mm above the load coil, and at a lateral position corresponding to the center of the plasma, from three spectral windows centered at 268 nm, 307 nm and 419 nm. In order to examine the possible introduction of significant error by using lateral intensities to calculate level populations instead of radially resolved intensities, the following comparison was made. Ratios of lateral Fe intensities to the corresponding radially resolved intensities were calculated from data collected at 16 mm above the load coil. Ratios were determined for both low energy and high energy lines. The result of this comparison revealed a difference of only 5% was encountered between ratios calculated from high energy lines and those from low energy lines. This small difference would indicate that laterally collected intensities accurately reflect the spatial intensities encountered at the center of the plasma at a vertical height of 16 mm. The wavelengths of the lines, along with their gA values, are given in Table IV. The emission spectra from these three spectral windows, including identification of the lines chosen, are provided in Appendix D.

3.5.1 CR EXCITED STATE LEVEL POPULATIONS

Figures 29, 30, 31, 32 and 33 provide Cr level population plots determined from intensities collected at five rf input

TABLE IV

CrI lines

<u>Wavelength (nm)</u>	<u>Excitation</u>		<u>% Error*</u>	<u>Reference</u>
	<u>Energy (eV)</u>	<u>gA ($\times 10^8$)</u>		
435.18	3.88	1.32	c	[60]
434.45	3.86	0.99	c	[60]
428.97	2.89	1.57	b	[60]
427.48	2.90	2.14	b	[60]
425.44	2.91	2.84	b	[60]
305.39	5.09	8.40	c	[60]
302.44	5.08	11.5	c	[60]
302.16	5.13	35.2	c	[60]
300.51	5.15	6.44	c	[60]
300.09	5.13	8.0	c	[60]
299.66	5.12	6.0	c	[60]
297.55	5.13	4.45	c	[60]
290.91	5.24	2.04	c	[60]
276.99	5.48	5.5	c	[60]
273.19	5.48	3.9	c	[60]
272.65	5.49	5.25	c	[60]

TABLE IV: continued

CrII lines

<u>Wavelength (nm)</u>	<u>Excitation</u>		<u>% Error</u> *	<u>Reference</u>
	<u>Energy (eV)</u>	<u>gA ($\times 10^8$)</u>		
323.41	8.13	7.36	d	[60]
318.07	6.44	7.0	d	[60]
312.04	6.41	9.0	d	[60]
311.87	6.40	6.8	d	[60]
305.01	8.38	25.2	d	[60]
304.09	8.37	57.6	d	[60]
297.97	7.92	21.6	d	[60]
297.19	7.94	28.0	d	[60]
292.71	9.02	28.0	d	[60]
287.04	6.77	7.8	d	[60]
286.26	5.86	5.04	d	[60]
284.98	5.86	7.36	d	[60]
277.81	9.40	32.0	d	[60]
266.60	6.16	4.72	d	[60]
265.86	6.15	2.32	d	[60]
265.36	6.16	2.10	d	[60]

* Estimated % error is : a = +/-10% ; b = +/-15% ; c = +/-25% ;
d = +/-50%

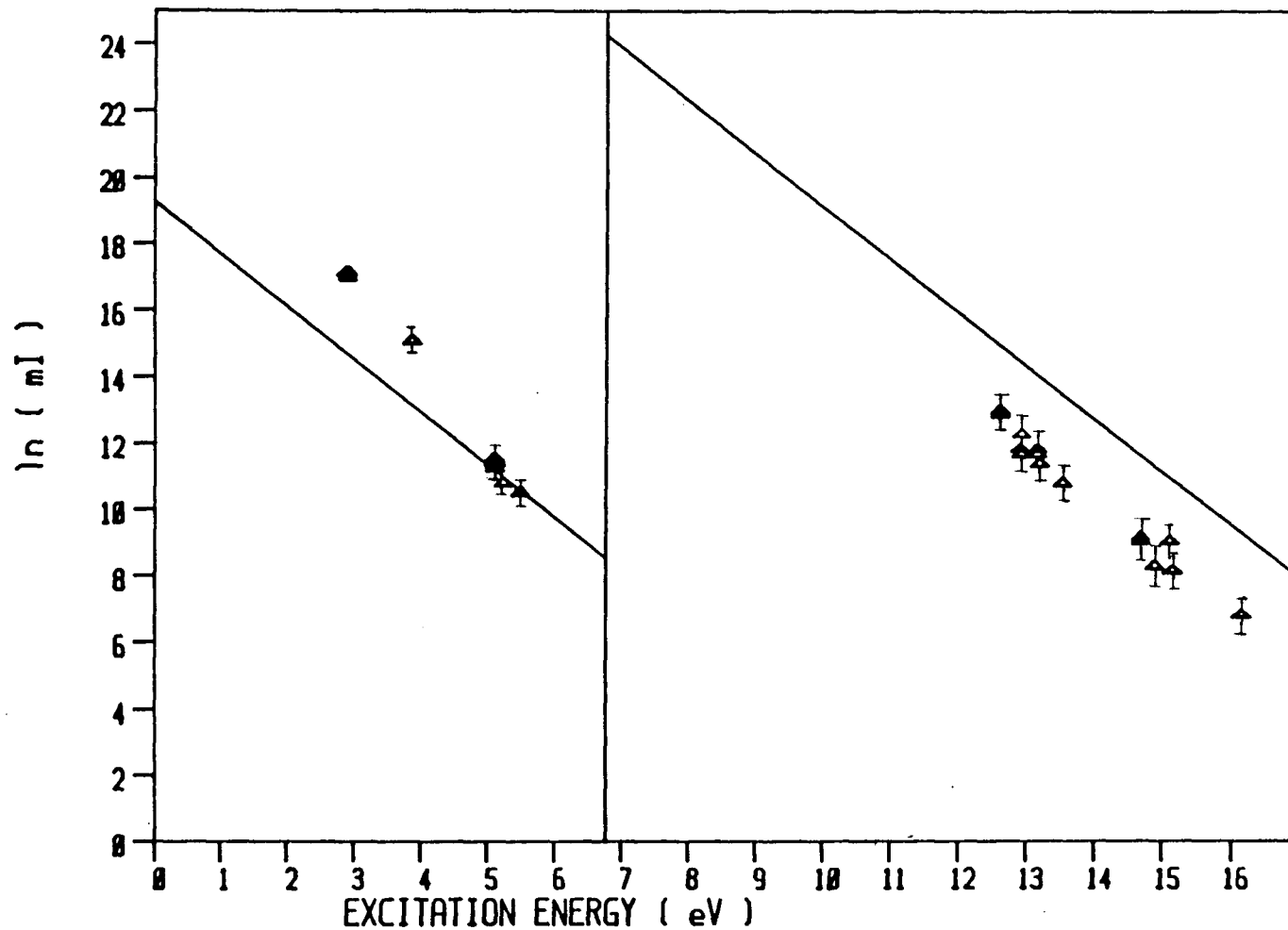


Figure 29. A plot of the logarithm of CrI and CrII level populations determined at 16 mm above the load coil, at a radial position of 0 mm and at an rf input power of 0.75 kW. The solid lines represent LTE calculated populations.

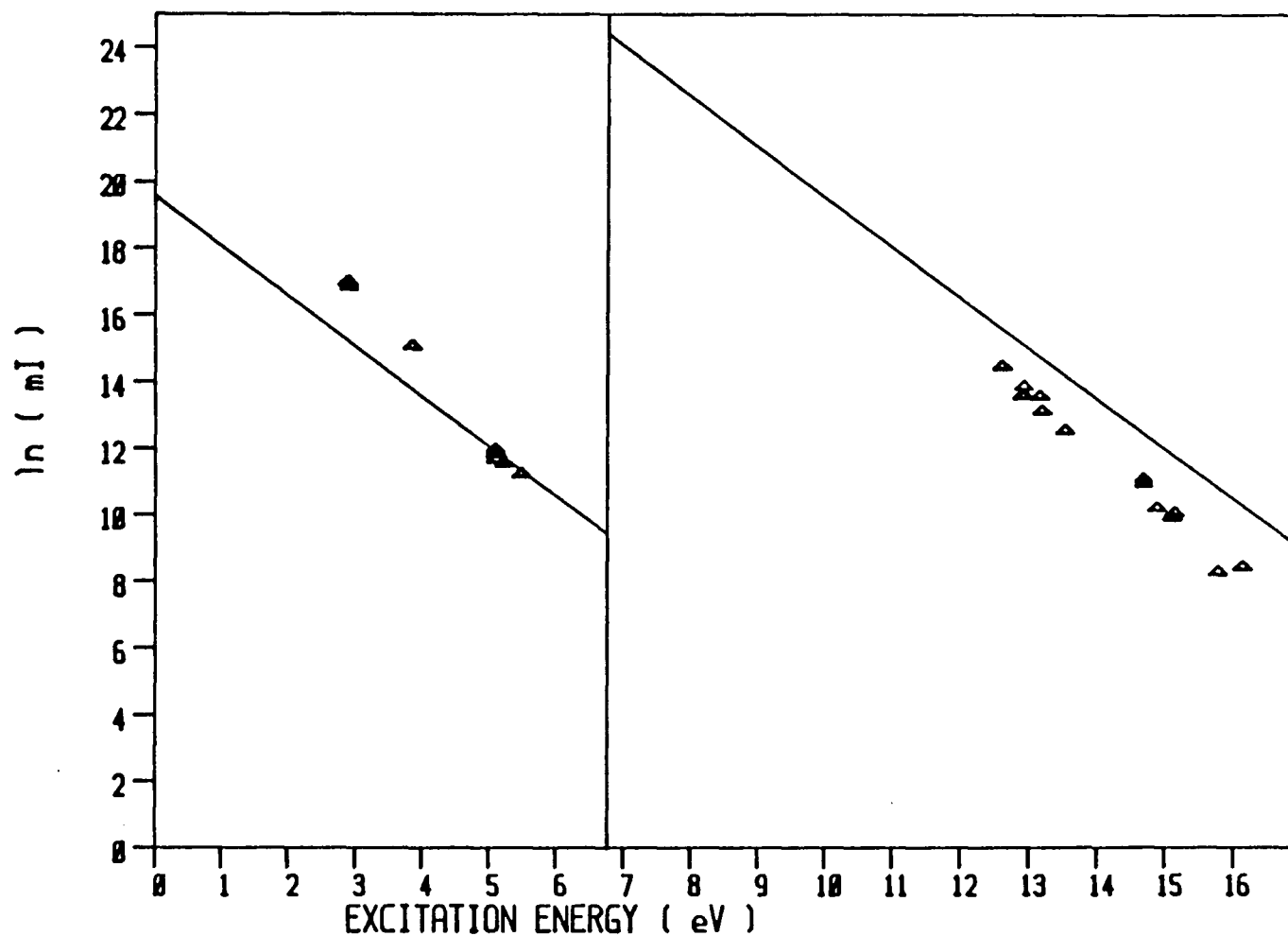


Figure 30. A plot of the logarithm of CrI and CrII level populations determined at 16 mm above the load coil, at a radial position of 0 mm and at an rf input power of 1.00 kW. The solid lines represent LTE calculated populations.

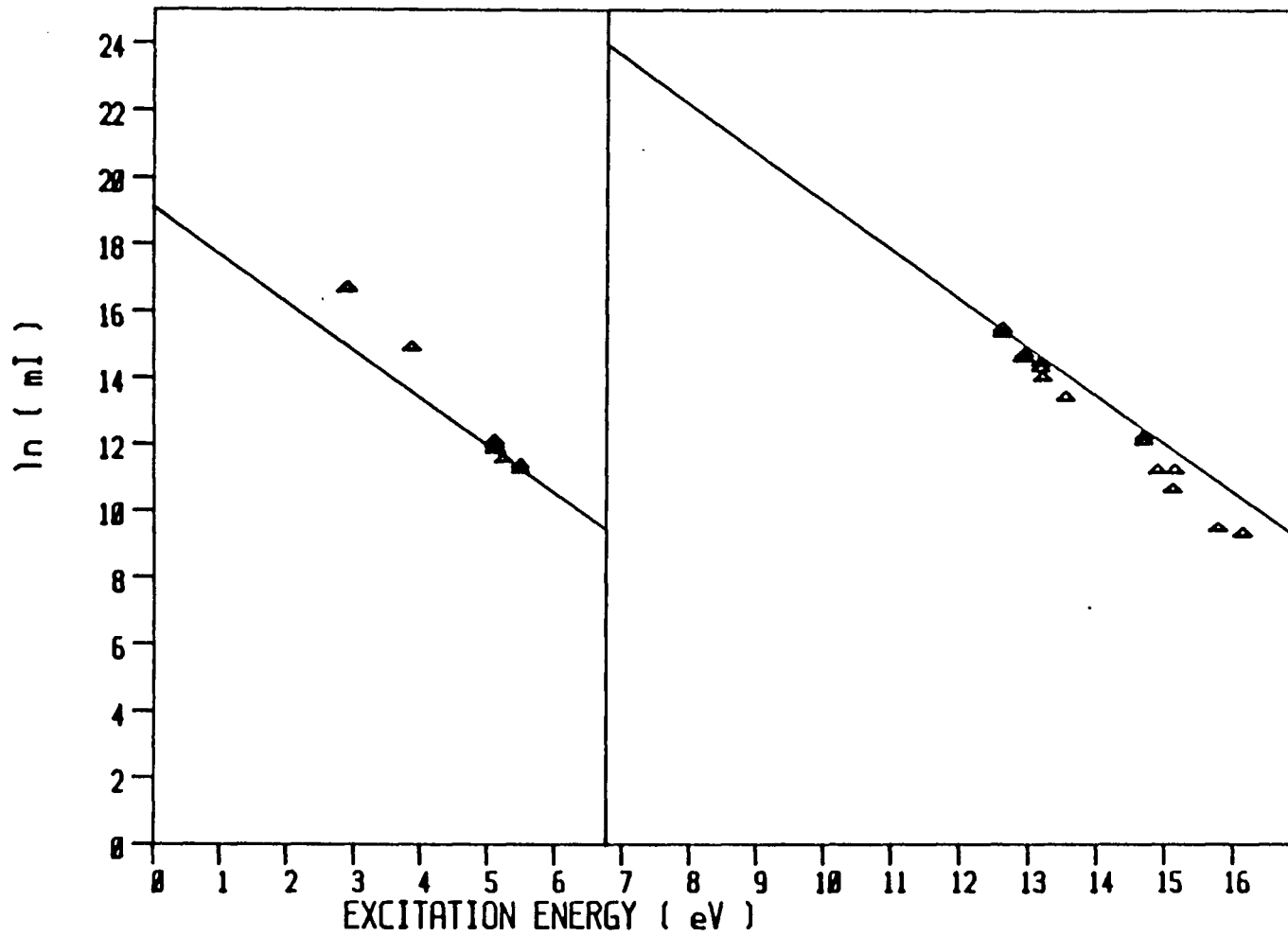


Figure 31. A plot of the logarithm of CrI and CrII level populations determined at 16 mm above the load coil, at a radial position of 0 mm and at an rf input power of 1.25 kW. The solid lines represent LTE calculated populations.

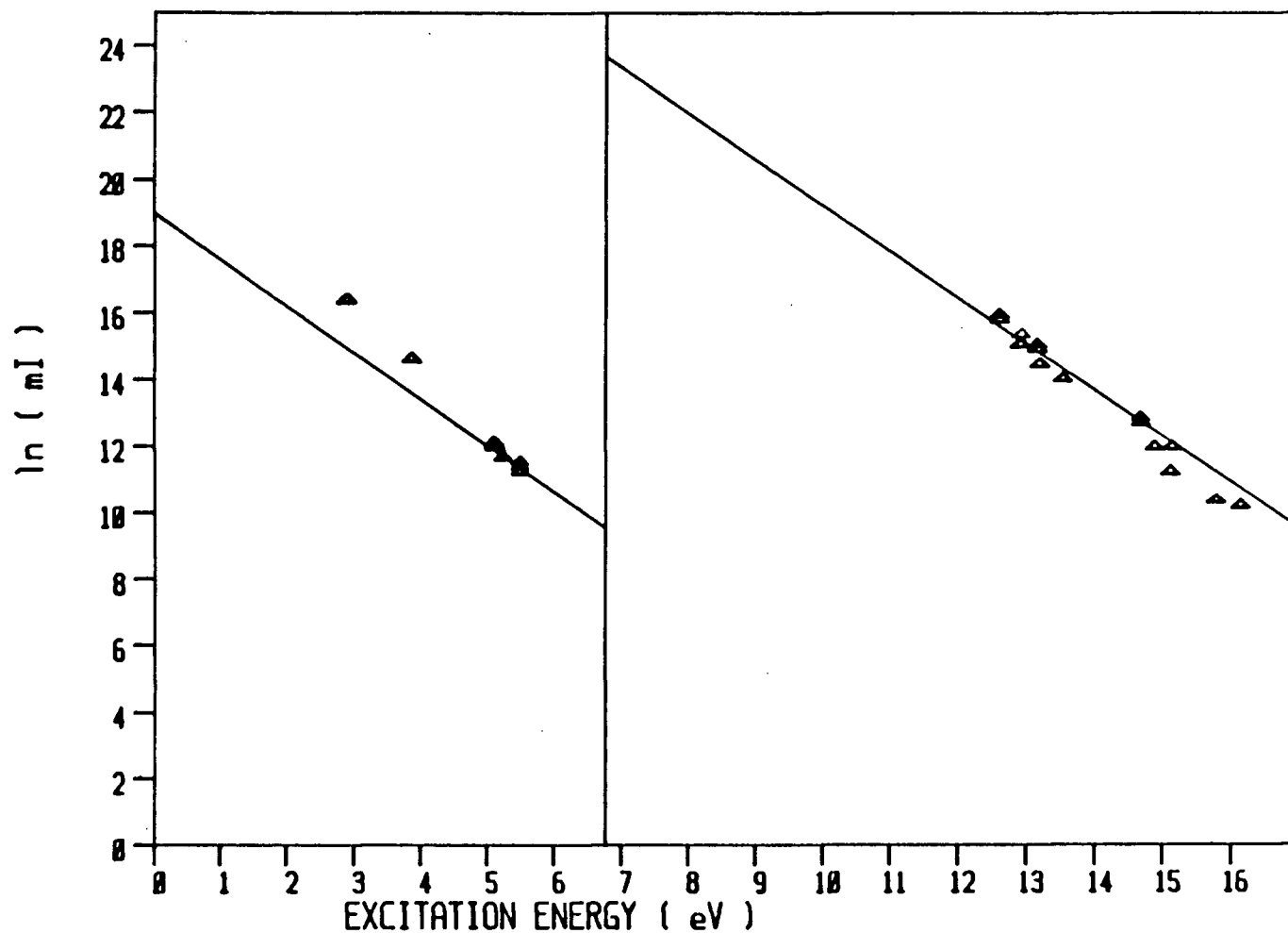


Figure 32. A plot of the logarithm of CrI and CrII level populations determined at 16 mm above the load coil, at a radial position of 0 mm and at an rf input power of 1.50 kW. The solid lines represent LTE calculated populations.

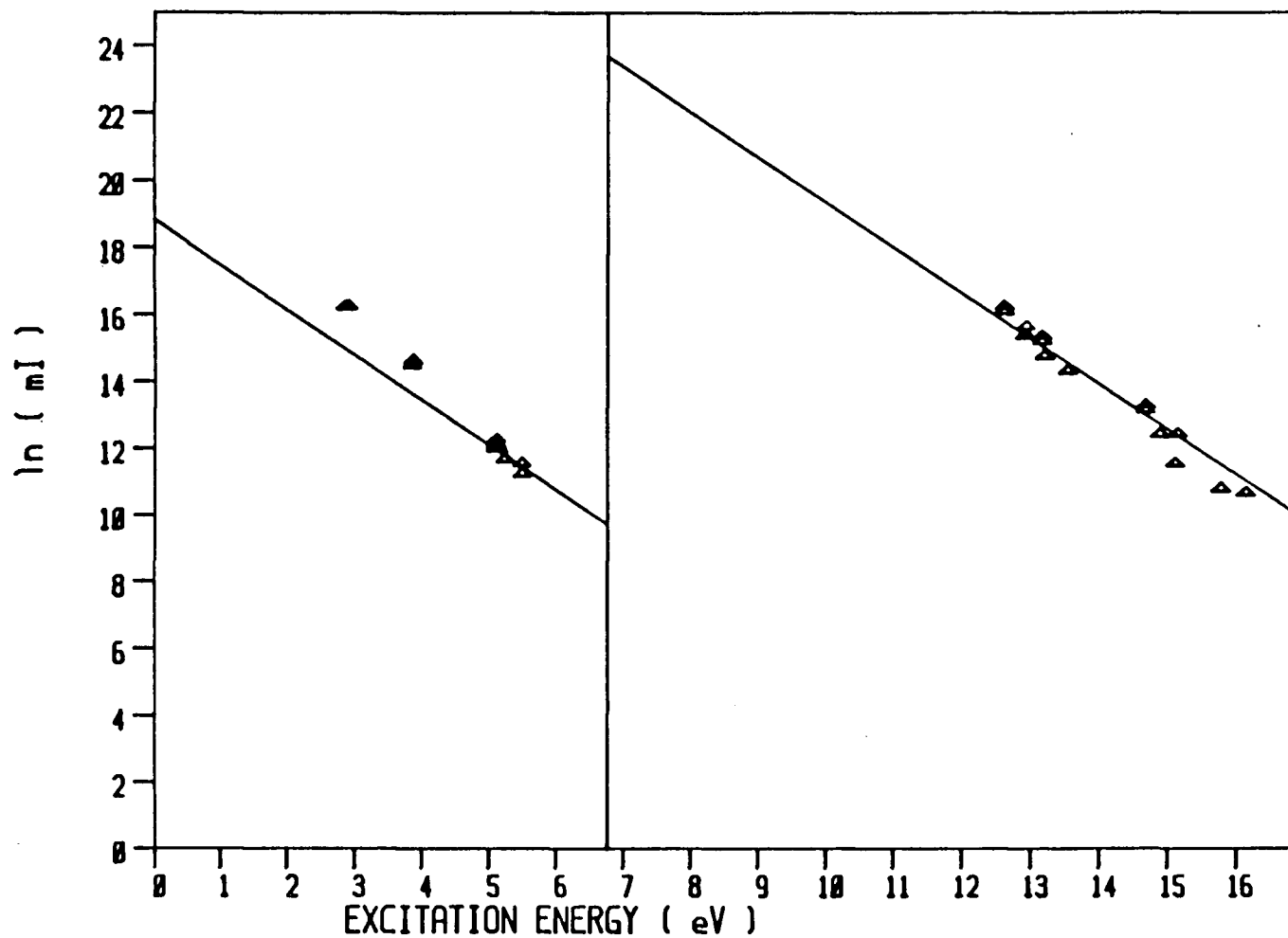


Figure 33. A plot of the logarithm of CrI and CrII level populations determined at 16 mm above the load coil, at a radial position of 0 mm and at an rf input power of 1.75 kW. The solid lines represent LTE calculated populations.

powers, 0.75 kW, 1.00 kW, 1.25 kW, 1.50 kW and 1.75 kW respectively. LTE curves have been determined from the electron densities and temperatures presented in Table I, for population plots at all rf input powers.

Problems in interpreting the Cr population plot arise from the rather large errors associated with the gA values, most values were reported in the literature with errors of $\pm 50\%$ (see Table IV). Upon examining figures 29, 30, 31, 32 and 33, the atom populations appear overpopulated with respect to the LTE curves and the ion populations underpopulated. There also appears to be a slight decrease in the degree of overpopulation and underpopulation upon going to higher rf input powers. Due to the linear appearance of the atom populations with respect to excitation energy, it was possible to determine excitation temperatures for both atom and ion levels and these temperatures are presented in Table IV. In order to compare these temperatures, LTE temperatures determined from measured electron densities have also been included. Both CrI and CrII excitation temperatures show a general trend of increasing magnitude with increasing rf input power, which is consistent with the trend in LTE temperatures. CrII excitation temperatures also tend to show more agreement with the LTE temperatures than CrI excitation temperatures, suggesting a closer coupling of ion levels to the distribution of electron energies than atom levels.

TABLE V

Cr(I) and Cr(II) Excitation Temperatures and LTE Temperatures in K

RF Input Power	$T_{\text{exc}} \text{ Cr(I)}^*$	$T_{\text{exc}} \text{ Cr(II)}^*$	T_{LTE}
0.75	4400	7000	7317
1.00	5100	6600	7736
1.25	5500	6800	7981
1.50	5900	7300	8370
1.75	6000	7500	8639

* Estimated Error in Temperature is +/- 150 K

3.6 DISCUSSION

From examining the population plots presented in the previous sections, a convenient framework for a discussion on these plots would appear to be in terms of partial local thermodynamic equilibrium (p-LTE) [55]. p-LTE is a frequently occurring deviation from LTE which is characterized by the existence of Saha equilibrium between excited atom levels and the ion ground state level. The atom ground state on the other hand deviates from the Saha equilibrium and from the Boltzmann equilibrium with higher energy atom levels. The reason for these deviations in the lower energy atom levels are primarily due to radiative contributions to excited state de-population in which the radiative de-excitation rate becomes comparable to the collisional de-excitation rate for the lower energy levels. p-LTE can also be caused by significant transport contributions which give rise to convection and diffusion of plasma and analyte species [55].

Raaijmakers et al. [55] have suggested two approaches in describing the regime of p-LTE, one in context with spectrochemical work, the second in context with plasma physical work. In spectrochemical work the plasma system can be described in terms of two temperatures, the excitation temperature and the ionization temperature. The more useful approach in discussing p-LTE with respect to this thesis is the plasma physical approach

which describes the system in terms of electron density, or electron temperature, and an additional parameter b_p , [49,55,7], which is defined as the ratio of the experimentally measured atomic level population, n_p , and the atomic level population calculated from the Saha equation, $n_{p,s}$, viz

$$b_p = n_p/n_{p,s}. \quad (30)$$

The parameter b_p is used to describe an overpopulation of the atomic level, ($b_p > 1$), or an underpopulation of the atomic level, ($b_p < 1$).

Keeping the parameter b_p in mind, the following conclusions can be made from the Fe, Ba and Cr level population plots. These are:

(1) high energy atom levels appear to be in Saha equilibrium with the ion ground state. This is observed as an overlap of experimentally measured level populations with the calculated LTE curve. Since electron density was used to determine the LTE curve, this suggests the equilibrium is maintained primarily by electron collisions;

(2) lower atom levels appear to be overpopulated with respect to the LTE curve. This translates to values of $b_p > 1$. Furthermore the degree of overpopulation is dependent on excitation energy, being greater for lower energy levels. At high excitation energies, b_p approaches unity;

(3) the degree of overpopulation of low energy atom levels decreases with an increase in rf input power.

These findings help to elucidate some of the observations made in the atom-ion intensity ratio studies discussed in the introduction of this chapter [49,50]. The $(I_i/I_a)_{\text{EXP}}$ values, determined from low energy atom and ion emission lines, were found to be less than the $(I_i/I_a)_{\text{LTE}}$ values, thus yielding b_r values < 1 . In the population plots presented in this chapter, this behaviour was observed as an overpopulation of low energy atom levels and underpopulation of ion levels. It was also observed that b_r increased with increasing rf input power, which has been paralleled in the level population plots by a decrease in the degree of over and underpopulation with an increase in the rf input power. The under-ionization of analyte observed in the ion-atom intensity studies can be explained by the overpopulation of low energy atom levels and underpopulation of ion levels.

It is also possible to compare the excitation temperatures determined from the atom and ion excited state level populations of the three analytes, Fe, Ba, Cr. In the case of Fe(II), Ba(I), Ba(II), Cr(I), and Cr(II), excitation temperatures were determined from the slope of a linear regression fit performed on each set of ion and atom populations. An excitation temperature for the Fe(I) levels, which yielded a non-linear relationship with excitation energy, was determined from the level dependent temperatures calculated for levels of intermediate excitation

energy, in the range of 3.5 to 4 eV. These excitation temperatures calculated from data collected at 16 mm above the load coil and corresponding to a radial position of 0 mm off axis are provided in Table VI. LTE temperatures corresponding to the electron densities encountered at the same spatial position and at the two rf input powers are also provided. Two trends in the temperatures can be observed. The first is that each of the excitation temperatures determined from Fe(I), Ba(I) and Cr(I) are considerably less than the corresponding excitation temperature determined from the ion species, namely Fe(II), Ba(II) and Cr(II). Both atom and ion excitation temperatures are less than the LTE value, although the degree of departure is less for the ion temperatures, indicating a closer coupling of the ion levels to the electron distribution. The second is the increase in both atom and ion excitation temperatures upon going from an rf input power of 1.25 to 1.75 kW. This trend is consistent with the behaviour in the LTE temperatures.

The systems studied do appear for the most part to be collisionally dominated, that is excitation and ionization due to inelastic electron collisions. This type of system has been referred to as an EEK plasma, where EEK refers to electron excitation kinetics [61]. The contribution of radiative de-excitation as a possible de-excitation pathway becomes significant only for the lower energy atom levels. Unlike the ion ground state, which has a number of de-excitation pathways to

TABLE VI

Fe, Ba, and Cr Excitation Temperatures* at 1.25 kW and 1.75 kW

<u>1.25 kW RF Input Power</u>		$T_{\text{LTE}} = 7981 \text{ K}$		
		<u>Fe</u>	<u>Ba</u>	<u>Cr</u>
T_{exc}	from atom levels	5700 K	5700 K	5500 K
T_{exc}	from ion levels	7400 K	7100 K	6800 K

<u>1.75 kW RF Input Power</u>		$T_{\text{LTE}} = 8639 \text{ K}$		
		<u>Fe</u>	<u>Ba</u>	<u>Cr</u>
T_{exc}	from atom levels	7000 K	6700 K	6000 K
T_{exc}	from ion levels	8000 K	8100 K	7500 K

* Estimated Error in Experimentally Determined T is +/- 300 K

lower energy atom levels and thus preventing a build up of the ground state population, the atom ground state does not and becomes a bottleneck into which the lower energy levels begin to overpopulated. An increase in rf input power produces a higher electron density, which encourages collisional de-excitation, thus decreasing the significance of radiative de-excitation processes. This is observed as a decrease in the degree of overpopulation at higher rf input powers.

Deviations between electron temperatures and excitation and ionization temperatures may result from shifts in the distribution of electron energies. The Maxwellian distribution of electron energies at a temperature of 8000 K has been plotted and is provided in figure 34. From such a plot it is possible to divide the electrons into one of two groups; a bulk group containing the majority of electrons with relatively low energies, and a tail group which contains a small number of higher energy electrons. In fact, if the Maxwell distribution function given in equation (15) is integrated over the energy range from 0 to 3.0 eV, it can be shown that at 8000 K, 97% of all electrons have energies in this range. The result of this is that relatively few electrons are available to induce excitation and ionization of analyte. When a tail-electron gives rise to excitation or ionization, it loses an amount of energy corresponding to the energy required to excite and / or ionize the analyte and is removed from this tail section. In order to

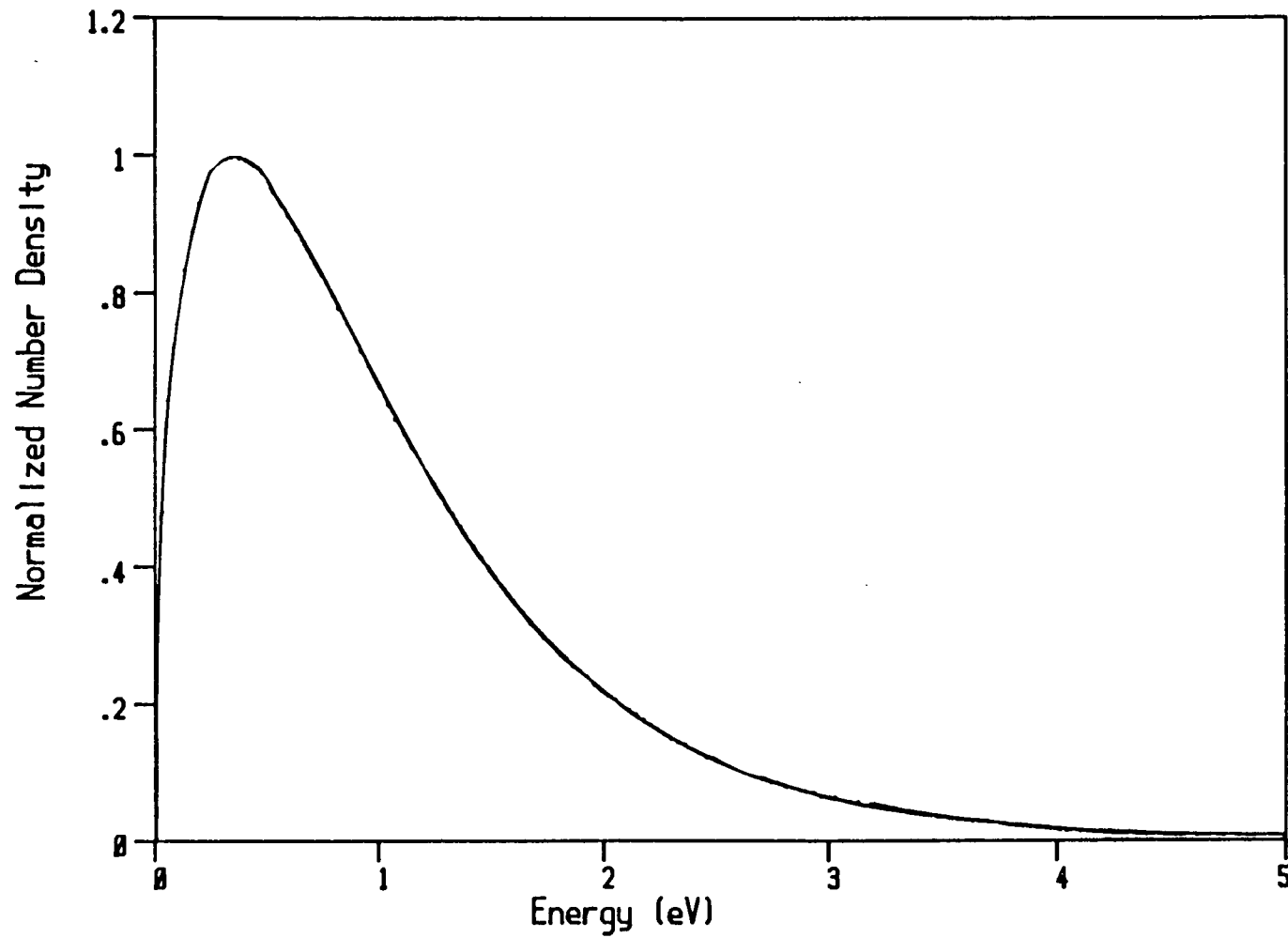


Figure 34. Maxwell distribution of electron energies corresponding to an equilibrium temperature of 8000 K.

maintain the Maxwell distribution of electrons, some electrons from the bulk group must increase their energies through electron-electron collisions, thus balancing loss of tail-electrons. If the rate of loss of electrons from the tail section is greater than the rate of input from the bulk, deviations in the Maxwell distribution can be expected. Due to the relatively small number of tail-electrons, a shift in the energy distribution of these electrons will not be paralleled by a shift in the average electron kinetic energy or electron temperature and as a result will go undetected. Thus analyte being excited and ionized will see a different temperature from the bulk electron temperature.

CHAPTER 4

SUMMARY

In an effort to elucidate some of the mysteries surrounding analyte excitation and ionization in the ICP, excited state level populations for both atom and ion species have been determined for three analytes, Fe, Ba and Cr. Population plots were constructed from measured emission line intensity collected at various spatial positions and rf input powers. All laterally collected line intensity profiles were Abel inverted resulting in radially resolved intensities. The task of measuring emission line intensities was simplified with the application of a linear photodiode array spectrometer, which permitted the simultaneous measurement of line intensities from a 50 nm wide window.

Excited state level populations were determined from FeI and FeII radially resolved line intensities collected at two vertical positions, 8 mm and 16 mm above the load coil, and at two rf input powers, 1.25 kW and 1.75 kW. The FeI levels showed a non-linear variation with excitation energy, while the FeII levels appeared to vary linearly. Generally speaking the FeI lower energy levels appeared overpopulated and the ion levels underpopulated when compared to LTE lines calculated from the appropriate electron densities and temperatures. A direct correlation was observed between the degree of departure

from LTE and the electron density, the departure decreasing with increasing electron density. Due to the non-linear behaviour of the FeI levels, level dependent temperatures were calculated for each FeI level, showing a variation of several thousand degrees over the excitation energy range of the lines. The level dependent temperatures determined from the higher energy FeI levels were similar to the excitation slope temperatures determined from the FeII levels, suggesting a coupling between high energy atom levels and the ground state ion.

Excited state level populations were also determined from BaI and BaII emission line intensities collected at 16 mm above the load coil and at two rf input powers, 1.25 kW and 1.75 kW. Both BaI and BaII populations appeared to vary linearly with excitation energy. When these populations were compared to the LTE lines, the atom levels appeared overpopulated and the ion levels underpopulated, showing consistency with the results obtained from the Fe data. Excitation temperatures were determined from both BaI and BaII levels and at the two rf input powers.

CrI and CrII emission line intensities were measured at the on axis lateral position at a vertical height of 16 mm above the load coil and at five rf input powers, 0.75 kW, 1.00 kW, 1.25 kW, 1.50 kW and 1.75 kW. The corresponding population plots were then constructed. Both CrI and CrII level populations appeared to vary linearly with excitation energy. Once again the atom

levels appeared overpopulated and the ion levels underpopulated. Comparison of the excitation slope temperatures for both CrI and CrII at all five powers revealed two trends: firstly, an increase in excitation temperature determined from both CrI and CrII populations with an increase in rf input power and secondly, a higher temperature determined from CrII levels than from CrI levels.

Comparison of the excitation temperatures determined from all three analytes, Fe, Ba and Cr, at a vertical height of 16 mm above the load coil and at two rf input powers of 1.25 kW and 1.75 kW revealed similar trends among the three analytes. Excitation temperatures determined from atom excited levels are consistently lower than those determined from ion excited levels. Secondly, excitation temperatures determined from both atom and ion excited state levels increased upon going from 1.25 kW to 1.75 kW rf input power.

Conclusions drawn from the results indicate analyte excitation and ionization in the ICP appear, for the most part, to be collisionally dominated. Low energy atom level populations are overpopulated with respect to LTE, most likely a result of contributions of radiative de-excitation as a possible de-excitation pathway. The degree of overpopulation of low energy atom levels decreases with an increase in electron density, which encourages collisional rather than radiative de-excitation. High energy atom levels seem to be in Saha

equilibrium with the ground state ion, which is thought to be maintained through electron collisions.

REFERENCES

1. B.L. Caughlin and M.W. Blades, *Spectrochim. Acta.*, 39B, 1583 (1984).
2. N. Furuta, *Spectrochim. Acta.*, 40B, 1013 (1985).
3. J. Jarosz, J.M. Mermet and J.P. Robin, *Spectrochim. Acta.*, 33B, 55 (1978).
4. J.M. Mermet, *Spectrochim. Acta.*, 30B, 383 (1975).
5. P.W.J.M. Boumans and F.J. De Boer, *Spectrochim. Acta.*, 32B, 365 (1977).
6. M.W. Blades and G.M. Hieftje, *Spectrochim. Acta.*, 37B, 191 (1982).
7. R.J. Lovett, *Spectrochim. Acta.*, 37B, 969 (1982).
8. F. Aeschbach, *Spectrochim. Acta.*, 37B, 987 (1982).
9. G.I. Babat, *J. Inst. Elec. Engrs.*, 94, 27 (1947).
10. T. Reed, *J. Appl. Phys.*, 32, 821 (1961).
11. T. Reed, *J. Appl. Phys.*, 32, 2534 (1961).
12. S. Greenfield, I.L. Jones, and C.T. Berry, *Analyst*, 89, 713 (1964).
13. R.H. Wendt and V.A. Fassel, *Anal. Chem.*, 37, 920 (1965).
14. C. Veillon and M. Margoshes, *Spectrochim. Acta.*, 23B, 503 (1968).
15. S. Greenfield, H. McD. Mcgeachin and P.B. Smith, *Talanta*, 23, 1 (1976).

16. G.W. Dickenson and V.A. Fassel, Anal. Chem., 41, 1021 (1969).
17. M. Borsier and M. Garcia, Spectrochim. Acta., 38B, 123 (1983).
18. A. Bolton, J. Hwang and A.V. Voet, Spectrochim. Acta., 38B, 165 (1983).
19. R.J. Brown, Spectrochim. Acta., 38B, 283 (1983).
20. Z. Mianzhi and R.M. Barnes, Spectrochim. Acta., 38B, 259 (1983).
21. R.M. Barnes, R.P. Khosah and H.S. Mahanti, Spectrochim. Acta., 38B, 291 (1983).
22. A.A. Verbeek, Spectrochim. Acta., 39B, 599 (1984).
23. K.A. Wolnik, F.L. Fricke and C.M. Gaston, Spectrochim. Acta., 39B, 64 (1984).
24. N.R. McQuaker and D.F. Brown, Developements in Atomic Plasma Spectrochemical Analysis, editor R.M. Barnes, Heyden (1981).
25. K.J. Irgolic, R.A. Stockton and D. Chakrabarti, Spectrochim. Acta., 38B, 437 (1983).
26. N. Omenetto and H.G.C. Human, Spectrochim. Acta., 39B, 1333 (1984).
27. A.R. Gray and A.L. Date, Analyst, 106, 1255 (1981).
28. R.M. Barnes, Phil. Trans. R. Soc. Lond. A, 305, 499 (1982).
29. S. Greenfield, Analyst, 105, 1032 (1980).
30. V.A. Fassel, Anal. Chem., 51, 1290A (1979).
31. V.A. Fassel, Science, 202, 183 (1978).

32. Webster's Third New International Dictionary, G.&C. Merriam Company, Springfield (1976).
33. R.M. Dagnell, D.J. Smith, T.S. West and S. Greenfield, Anal. Chim. Acta., 54, 397 (1971).
34. H.C. Hoare and R.A. Mostyn, Anal. Chem., 39, 1153 (1967).
35. A. Aziz, J.A.C. Broekaert, K. Laqua and F. Leis, Spectrochim. Acta., 39B, 1091 (1984).
36. D.R. Hull and G. Horlick, Spectrochim. Acta., 39B, 843 (1984).
37. T. Ishizuka and Y. Uwamino, Spectrochim. Acta., 38B, 519 (1983).
38. M. Blades, "Excitation Mechanisms and Discharge Characteristics: Recent Developments", in ICP Emission Spectrometry, Vol. 2, P.W.J.M. Boumans, ed. (in press).
39. G.H. Hieftje, G.D. Rayson and J.W. Olesik, Spectrochim. Acta., 40B, 167 (1985).
40. L. De Galan, Spectrochim. Acta., 39B, 537 (1984).
41. L. De Galan, R. Smith and J.D. Winefordner, Spectrochim. Acta., 23B, 521 (1968).
42. H.W. Darwin, High Pressure - High Temperatures, 2, 359 (1970).
43. Horlick and W.K. Yuen, Anal. Chem., 48, 1643 (1976).
44. Handbook of Chemistry and Physics 61st Edition, CRC Press, Inc., E-393 (1980).
45. A. Savitzky and M.J.E. Golay, Anal. Chem., 38, 1627 (1964).

46. M.W. Blades, Appl. Spectrosc., 37, 371 (1983).
47. R. Stair, W.E. Schneider and J.K. Jackson, Appl. Optics, 2, 1151 (1963).
48. D.J. Kalnicky, V.A. Fassel and R.N. Kniseley, Appl. Spect., 31, 137 (1977).
49. B.L. Caughlin and M.W. Blades, Spectrochim. Acta., 39B, 1583 (1984).
50. B.L. Caughlin and M.W. Blades, Spectrochim. Acta., 40B, 1539 (1985).
51. J.F. Alder, R.M. Bombelka and G.F. Kirkbright, Spectrochim. Acta., 35B, 163 (1980).
52. G.R. Kornblum and J. Smeyers-Verbeke, Spectrochim. Acta., 37B, 83 (1982).
53. L.M. Faires, B.A. Palmer and R. Engleman, Jr., Spectrochim. Acta., 39B, 819 (1984).
54. B.L. Caughlin and M.W. Blades, Spectrochim. Acta., 40B, 987 (1985).
55. I.J.M.M. Raaijmakers, P.W.J.M. Boumans, B. van der Sude, D.C. Schram, Spectrochim. Acta., 38B, 697 (1983).
56. M.W. Blades and B.L. Caughlin, Spectrochim. Acta., 40B, 579 (1985).
57. J.M. Bridges and R.L. Kornblith, Astrophys., 192, 793 (1974).
58. W. Whaling, Technical Report #84A, Kellog Radiation Laboratory, California Institute of Technology, 1985.

59. J.Moity, Astron. Astrophys. Suppl., Ser. 52, 37 (1983).
60. W.L. Wiese and G.A. Martin, NBS Monograph 68, U.S. Government Printing Office, Washington, D.C. (1980).
61. J.J.A.M. van der Muellen, Ph.D. Dissertation, De Technische Hogeshool Eindhoven, (1986).

APPENDIX A

68000 assembly language program employed to control the transfer of data between the LPDA and the microcomputer.

```

        lobyte=$ff002f
        histat=$ff002d
        busy=$ff0023
        k_cr=13
        k_lf=10
        .globl PD496A
PD496A: movem.l d0-d7/a0-a6,temp
        move.l (a7)+,d4      *save ret addr in d4
        move.l (a7)+,a5      *save addr of # scans in a5
        move.l (a7)+,a3      *get addr of # points in a3
        move.l (a7),d6       *get address of array storage
        move.l #lobyte,a0     *address of lobyte in a0
        move.l #histat,a1     *address of hobyte/status in a1
        move.l #0,d1         *mask for busy
        move.l #busy,a4       *address of busy signal
        move.w (a3),d0        *points counter to d0
        move.l d6,a2          *array address to a2
zero:   move.l #0,(a2)+       *load 0's into array
        subq    #1,d0
        brie    zero
        move.l #schrnum,a6
        move.w (a5),d5        *get # of scans in d5
acquir: move.l d6,a2          *get address of array in a2
        move.b #$f0,(a1)      *acquire mode
        move.b #$b0,(a1)
        nop
        nop
        nop
        move.b #$f0,(a1)      *send pulse to enable
ready:  btst    d1,(a4)
        beq     ready
x1:     btst    d1,(a4)
        brie    x1
done:   move.b #$d0,(a1)      *transfer mode
        move.b #$90,(a1)      *enable
        nop
        nop
        nop
        move.b #$d0,(a1)
        move.w (a3),d0

```

```

get:      clr      d2          *clear space
          clr      d3          *clear space
          move.b   (a0),d2     *get lobyte
          move.b   (a1),d3     *get hbyte
          andi     #$0f,d3     *erase upper 4 bits
          mulu     #256,d3     *shift 8 bits left
          add.w    d2,d3       *generate the 16 bit number
          add.l    d3,(a2)+    *add current number to previous
          subq     #1,d0       *done?
          beq      next       *if yes exit loop
          move.b   #$c0,(a1)   *send pulse to
          nop
          nop
          move.b   #$d0,(a1)   *increment address
          bra      get
next:     subq     #1,d5        *all scans complete?
          beq      over        *if no go back and get more
entout:   move.b   #$2,d0
          move.b   (a6)+,d1
          trap     #2
          move.b   #2,d0
          move.b   (a6)+,d1
          trap     #2
          move.b   #2,d0
          move.b   (a6)+,d1
          trap     #2
          move.b   #$2,d0
          move.b   #13,d1
          trap     #2
          move.b   #2,d0
          move.b   #10,d1
          trap     #2
          move.l   #0,d1
          bra      acquir
over:     move.l   d4,(a7)      *otherwise restore sp
          movem.l  temp,d0-d7/a0-a6
          rts
          .even
          .bss
temp:     ds.l     15
          .even
          .data
scrnum:   dc.b     '001002003004005006007'
          dc.b     '008009010011012013014015016017018019020021022023024025'
          dc.b     '026027028029030031032033034035036037038039040041042043044'
          dc.b     '045046047048049050051052053054055056057058059060061062063064'
          dc.b     '065066067068069070071072073074075076077078079080081082083084'
          dc.b     '08508708808909009109209309409509609709809910010102103104105'
          dc.b     '106107108109110111112113114115116117118119120121122123124125'
          dc.b     '126127128129130131132133134135136137138139140141142143144145'
          dc.b     '146147148149150151152153154155156157158159160161162163164165'
          .enc

```

Fortran-77 language Program used to collect lateral emission
line intensities.

```
*****
*
*                               MULTI-PROFILE
*
*                               BY
*
*                               ZANE WALKER
*
*   THIS PROGRAM IS TO BE USED TO COLLECT DATA FROM A 4096
*   DIODE ARRAY.  ALSO DOES PEAK SEARCH.
*
*   USE SUBMIT PROGRAM MPDA.SUB; MUST HAVE ACCESS TO THIS
*   PROGRAM AS WELL AS MACHINE LANGUAGE PROGRAM PDA7.0 & STATUS.0
*
*   NOTE:  THIS PROGRAM IS OPERATING SYSTEM DEPENDANT!
*          IN ORDER FOR VARIOUS OUTPUT DEVICES TO BE ASSIGNED
*          AS 'LST:' THE NUMBER OF THE THE DEVICE MUST BE PLACED
*          IN THE TWO ALLOCATED MEMORY BYTES (PRESENTLY $F9CDB
*          AND $F9D0F).
*
*   LAST REVISION JUNE 11, 1985
*
*****
```

```
PROGRAM MAIN
REAL FORE(0:50,0:150),BACK(0:50,0:150),FMB(0:50,0:150)
INTEGER*4 IADDR
INTEGER*2 IDIO,IDIOF
INTEGER*2 IDN(S1),IDIOD,ISTEP,ISCN,IPULSE
INTEGER*1 INTT,IVAL
COMMON FORE,BACK,FMB,IDIO,IDIOF,INTT
COMMON /BL1/ IDN,IDIOD,ISTEP,ISCN,IPULSE
IDIO=4095
IDIOF=4096
CALL HOME
INTT=$FE
IADDR=$FF0017
IVAL=$04
CALL POKE(IADDR,IVAL)
IADDR=$FF0012
IVAL=$FE
CALL POKE(IADDR,IVAL)
IADDR=$FF002C
IVAL=$93
CALL POKE(IADDR,IVAL)
IADDR=$FF0020
IVAL=$9B
CALL POKE(IADDR,IVAL)
*   SET TRANSIENT RECORDER IN THE TRANSFER MODE
  IVAL=$F0
  IADDR=$FF00ED
  CALL POKE(IADDR,IVAL)
*
10  PRINT*,'READ FROM DISC (1)'
    PRINT*,'TAKE NEW SPECTRUM (2)'
    PRINT*,'SET INTEGRATION TIME (3)'
    PRINT*,' '
    PRINT*,' '
    WRITE(*,20)
20  FORMAT('WHAT WOULD YOU LIKE TO DO? - '\)
    READ(*,30) M
111
```

```

90      FORMAT(I1)
      CALL HOME
      IF (M.EQ.1) CALL RFDISC
      IF (M.EQ.2) CALL MPROF
      IF (M.EQ.3) CALL INTTIM
      IF (M.GE.4) GO TO 10
      GO TO 100
*****
100     CALL HOME
      PRINT*, 'PLOT(1)'
      PRINT*, 'STORE(3)'
      PRINT*, 'NEW SCAN(4)'
      PRINT*, 'SET INTEGRATION TIME(5)'
      PRINT*, 'TRANS STAGE(6)'
      PRINT*, 'READ FROM DISC(7)'
      PRINT*, ' '
      WRITE(*,110)
110     FORMAT('WHAT WOULD YOU LIKE TO DO ?- '\)
      READ(*,120) M
120     FORMAT(I1)
      CALL HOME
      IF (M.EQ.1) CALL PLOT
      IF (M.EQ.3) CALL STORE
      IF (M.EQ.4) CALL MPROF
      IF (M.EQ.5) CALL INTTIM
      IF (M.EQ.6) CALL TRSTG
      IF (M.EQ.7) CALL RFDISC
      GO TO 100
      STOP
      END
*****
      SUBROUTINE BELL
      INTEGER*4 IADDR, IVAL*1
      IADDR=$FF00FC
      IVAL=$7
      CALL POKE(IADDR, IVAL)
      RETURN
      END
*****
      SUBROUTINE HOME
      INTEGER*4 IADDR, IVAL*1
      IADDR=$FF00FC
      IVAL=$1A
      CALL POKE(IADDR, IVAL)
      RETURN
      END
*****
      SUBROUTINE MPROF
      REAL FORC(0:50,0:150), BACK(0:50,0:150), FMB(0:50,0:150)
      REAL RANGE, PULSE, STEP
      INTEGER*2 IDIO, IDIOR
      INTEGER*2 IDN(S1), IDIOD, ISTEP, ISCN, IPULSE
      INTEGER*1 INTT
      COMMON FORC, BACK, FMB, IDIO, IDIOR, INTT
      COMMON /BL1/ IDN, IDIOD, ISTEP, ISCN, IPULSE
      CHARACTER*1 ANSW, YES
      IX=0
      IY=0
90      CALL HOME
      WRITE(*,100)
100     FORMAT('HOW MANY DIODES WOULD YOU LIKE TO SCAN- '\)
      READ(*,110) IDIOD
110     FORMAT(I4)
      DO 130 J=1, IDIOD
      WRITE(*,120)
120     FORMAT('DIODE- '\)

```



```

      READ(*,110) IDN(J)
130    CONTINUE
      CALL HOME
      DO 140 J=1,IDIOD
      WRITE(*,150) 'DIODE- ',IDN(J)
150    FORMAT(A,I4)
140    CONTINUE
      PRINT*,' '
      PRINT*,' '
      WRITE(*,160)
160    FORMAT('CHANGE THE DIODES SPECIFIED? (Y OR N)- '\)
      READ(*,170) ANSW
170    FORMAT(A)
      YES='Y'
      IF(ANSW.EQ.YES) GO TO 90
      DO 175 J=1,IDIOD
      FORE(J,0)=IDN(J)
      BACK(J,0)=IDN(J)
      FMB(J,0)=IDN(J)
175    CONTINUE
      PRINT*,' '
      PRINT*,' '
      WRITE(*,180)
180    FORMAT('RANGE IN MM- '\)
      READ(*,183) RANGE
183    FORMAT(F5.1)
      WRITE(*,185)
185    FORMAT('HOW MANY STEPS- '\)
      READ(*,110) ISTEP
      STEP=FLOAT(ISTEP)
      PULSE=(RANGE/STEP)/(0.0127)
      IPULSE=INT(PULSE)
      RANGE=((FLOAT(IPULSE))*0.0127)*STEP
      WRITE(*,187) 'RANGE=',RANGE
187    FORMAT(A,F5.1)
      FORE(0,0)=FLOAT(IDIOD)
      BACK(0,0)=FLOAT(IDIOD)
      FMB(0,0)=FLOAT(IDIOD)
      FORE(0,1)=FLOAT(ISTEP)
      BACK(0,1)=FLOAT(ISTEP)
      FMB(0,1)=FLOAT(ISTEP)
      FORE(0,2)=RANGE
      BACK(0,2)=RANGE
      FMB(0,2)=RANGE
      FORE(0,3)=PULSE
      BACK(0,3)=PULSE
      FMB(0,3)=PULSE

      IPULSE=INT(PULSE)
      WRITE(*,190)
190    FORMAT('NUMBER OF SCANS- '\)
      READ(*,110) ISCN
200    CALL HOME
      PRINT*,'FOREGROUND(1)'
      PRINT*,'BACKGROUND(2)'
      PRINT*,'CHANGE PARAMETERS(3)'
      PRINT*,'RETURN TO MENU(4)'
      PRINT*,' '
      PRINT*,' '
      WRITE(*,210)
210    FORMAT('WHAT WOULD YOU LIKE TO DO- '\)
      READ(*,110) N
      IF (N.EQ.1) CALL MPROFF
      IF (N.EQ.2) CALL MPROFE
      IF (N.EQ.3) GO TO 90
      IF (N.EQ.4) GO TO 500

```

```

      IF (N.EQ.1) IX=1
      IF (N.EQ.2) IY=1
      GO TO 200
400   DO 404 I=1,50
      DO 402 J=1,150
      FMB(I,J)=0.0
402   CONTINUE
404   CONTINUE
      DO 420 I=1,IDIOD
      DO 410 J=1,1STEP
      FMB(I,J)=FORE(I,J)-BACK(I,J)
410   CONTINUE
420   CONTINUE
      GO TO 510
500   IZ=IX + IY
      IF (IZ.EQ.2) GO TO 400
510   FORE(0,0)=FLOAT(IDIOD)
      BACK(0,0)=FLOAT(IDIOD)
      FMB(0,0)=FLOAT(IDIOD)
      FORE(0,1)=FLOAT(1STEP)
      BACK(0,1)=FLOAT(1STEP)
      FMB(0,1)=FLOAT(1STEP)
      FORE(0,2)=RANGE
      BACK(0,2)=RANGE
      FMB(0,2)=RANGE
      FORE(0,3)=PULSE
      BACK(0,3)=PULSE
      FMB(0,3)=PULSE
      DO 575 J=1,IDIOD
      FORE(J,0)=IDN(J)
      BACK(J,0)=IDN(J)
      FMB(J,0)=IDN(J)
575   CONTINUE

      RETURN
      END
*****
      SUBROUTINE MAROFF
      EXTERNAL PD495A
      REAL FORE(0:50,0:150),BACK(0:50,0:150),FMB(0:50,0:150)
      INTEGER*2 SPECTA(4096),IDIO,IDIOF
      INTEGER*2 IDN(51),IDNE(51),IDIOD,1STEP,1SCN,1PULSE,N,K,L,N
      INTEGER*1 INTT
      COMMON FORE,BACK,FMB,IDIO,IDIOF,INTT
      COMMON /BL1/ IDN,IDIOD,1STEP,1SCN,1PULSE

      DO 4 I=1,50
      DO 2 J=1,150
      FORE(I,J)=0.0
2     CONTINUE
4     CONTINUE

      Z=(FLOAT(1STEP)*(0.5))*1PULSE
      N=INT(Z)
      DO 10 I=1,N
      CALL TRSTGE
10    CONTINUE
      CALL HOME
      DO 200 J=1,1STEP
110   FORMAT(I4)

      DO 115 KL=1,IDIOD
      IDNE(KL)=IDN(KL)
115   CONTINUE

      WRITE(*,120) 'STEP ',J,' OF ',1STEP

```

```

120      FORMAT (A,13,A,13)
      DO 130 K=1, ISON
      CALL PD496A(SPECTA(0), IDIOD)

      IF (K.GT.1) GOTO 128
      DO 126 M=1,3
      DO 124 L=1, IDIOD
      IF (SPECTA(IDN(L)).LT.SPECTA(IDN(L)+1)) IDN(L)=IDN(L)+1
      IF (SPECTA(IDN(L)).LT.SPECTA(IDN(L)-1)) IDN(L)=IDN(L)-1
124      CONTINUE
126      CONTINUE
128      CONTINUE

      DO 140 I=1, IDIOD
      FORE(I,J) = FORE(I,J) + FLOAT(SPECTA(IDN(I)))
140      CONTINUE
      WRITE(*,110) K
130      CONTINUE
      DO 150 M=1, IPULSE
      CALL TRSTGE
150      CONTINUE
      CALL HOME
      CONTINUE
200      Z=(FLOAT(ISTEP)*0.5)*IPULSE
      N=INT(Z)
      DO 300 I=1,N
      CALL TRSTGE
300      CONTINUE

      DO 400 I=1, IDIOD
      DO 350 J=1, ISTEP
      FORE(I,J)=FORE(I,J)/FLOAT(ISON)
350      CONTINUE
400      CONTINUE

      RETURN
      END
*****
      SUBROUTINE MPROBE
      EXTERNAL PD496A
      REAL FORE(0:50,0:150),BACK(0:50,0:150),FMB(0:50,0:150)
      INTEGER*2 SPECT(4096), IDIO, IDIOD
      INTEGER*2 IDN(51), IDIOD, ISTEP, ISON, IPULSE, N, M, L, K
      INTEGER*1 INTT
      COMMON FORE, BACK, FMB, IDIO, IDIOD, INTT
      COMMON /BL1/ IDN, IDIOD, ISTEP, ISON, IPULSE

      DO 4 I=1,50
      DO 8 J=1,150
      BACK(I,J)=0.0
2      CONTINUE
4      CONTINUE

      Z=(FLOAT(ISTEP)*(0.5))*IPULSE
      N=INT(Z)
      DO 10 I=1,N
      CALL TRSTGE
10      CONTINUE
      CALL HOME
      DO 200 J=1, ISTEP
110      FORMAT(14)

      WRITE(*,120) 'STEP ',J,' OF ',ISTEP
120      FORMAT(A,13,A,13)
      DO 130 K=1, ISON
      CALL PD496A(SPECT(0), IDIOD)

```

```

DO 140 I=1, IDIOD
BACK(I,J) = BACK(I,J) + FLOAT(SPECT(IDN(I)))
140 CONTINUE
WRITE(*,110) K
130 CONTINUE
DO 150 M=1, IPULSE
CALL TRSTGF
150 CONTINUE
CALL HOME
200 CONTINUE
Z=(FLOAT(ISTEP)*0.5)*IPULSE
N=INT(Z)

DO 300 I=1,N
CALL TRSTGF
300 CONTINUE

DO 400 I=1, IDIOD
DO 350 J=1, ISTEP
BACK(I,J)=BACK(I,J)/FLOAT(ISCN)
350 CONTINUE
400 CONTINUE
RETURN
END
*****
SUBROUTINE RFDISC
REAL FORE(0:50,0:150),BACK(0:50,0:150),FMB(0:50,0:150)
INTEGER*2 IDIO, IDIOP
INTEGER*1 INTT
COMMON FORE, BACK, FMB, IDIO, IDIOP, INTT
CHARACTER*8 DFNAME, DISC*2, FILNAM*14, TYPE*4
DISC='A:'
DO 6 I=0,50
DO 5 J=0,150
FORE(I,J)=0
BACK(I,J)=0
FMB(I,J)=0
5 CONTINUE
6 CONTINUE
WRITE(*,10)
10 FORMAT('NAME OF FILE TO BE READ- '\)
READ(*,20) DFNAME
20 FORMAT(A)
PRINT*, ' '
PRINT*, ' '
25 PRINT*, 'FOREGROUND(1)'
PRINT*, 'BACKGROUND(2)'
PRINT*, 'FOREGROUND - BACKGROUND(3)'
PRINT*, 'RETURN TO MENU(4)'
PRINT*, ' '
PRINT*, ' '
30 WRITE(*,35)
35 FORMAT('SPECTRA TO BE READ- '\)
READ(*,40) M
40 FORMAT(I4)
WRITE(*,50)
50 FORMAT('NUMBER OF PATCHES- '\)
READ(*,40) K
WRITE(*,60)
60 FORMAT('NUMBER OF STEPS- '\)
READ(*,40) L
IF (M.EQ.1) GO TO 100
IF (M.EQ.2) GO TO 300
IF (M.EQ.3) GO TO 300
IF (M.EQ.4) GO TO 900

```

```

      GO TO 30
100   TYPE='.FGR'
      FILNAM=DISC//DFNAME//TYPE
      OPEN(3,FILE=FILNAM)
      READ(3,500) ((FORE(I,J),I=0,K),J=0,L)
190   GO TO 600
200   TYPE='.BGR'
      FILNAM=DISC//DFNAME//TYPE
      OPEN(3,FILE=FILNAM)
      READ(3,500) ((BACK(I,J),I=0,K),J=0,L)
290   GO TO 600
300   TYPE='.FMB'
      FILNAM=DISC//DFNAME//TYPE
      OPEN(3,FILE=FILNAM)
      READ(3,500) ((FMB(I,J),I=0,K),J=0,L)
390   GO TO 600
500   FORMAT(8E10.4)
600   CLOSE(3)
      CALL HOME
      GO TO 25
900   RETURN
      END
*****
      SUBROUTINE STORE
      REAL FORE(0:50,0:150),BACK(0:50,0:150),FMB(0:50,0:150)
      INTEGER*2 IDIO,IDIOP,IDN(51),IDIOD,ISTEP,ISCN,IPULSE
      INTEGER*1 INTT
      COMMON FORE,BACK,FMB,IDIO,IDIOP,INTT
      CHARACTER*12 FNAME,DFNAME*8,TYPE*4,DISC*2,FILNAM*14,DATE*17,DESCR*306
      INTEGER ILN,IRN,IRN1,IRN2,IRN3,IRN4,IRN5,IRN6,IRN7,IRN8
      DISC='A:'
      WRITE(*,10)
      FORMAT('FILENAME- '\)
10    READ(*,20) DFNAME
20    FORMAT(A)
      WRITE(*,100)
100   FORMAT('NUMBER OF PATCHES- '\)
      READ(*,110) K
110   FORMAT(I4)
      WRITE(*,120)
120   FORMAT('NUMBER OF STEPS- '\)
      READ(*,110) L
150   PRINT*,' '
      PRINT*,' '
195   PRINT*, ' FOREGROUND(1)'
      PRINT*, ' BACKGROUND(2)'
      PRINT*, ' FOREGROUND - BACKGROUND(3)'
      PRINT*, ' RETURN TO MENU(4)'
      PRINT*,' '
      PRINT*,' '
      WRITE(*,200)
200   FORMAT('SPECTRA TO BE STORED- '\)
      READ(*,110) N
      IF (N.EQ.1) GO TO 300
      IF (N.EQ.2) GO TO 400
      IF (N.EQ.3) GO TO 500
      IF (N.EQ.4) GO TO 900
      GO TO 190
300   TYPE='.FGR'
      FILNAM=DISC//DFNAME//TYPE
      FNAME=FILNAM(3:14)
      OPEN(4,FILE=FILNAM,STATUS='NEW')
      WRITE(4,320) ((FORE(I,J),I=0,K),J=0,L)
320   FORMAT(8E10.4)
      GO TO 700
400   TYPE='.BGR'

```

```

FILNAM=DISC//DFNAME//TYPE
FNAME=FILNAM(3:14)
OPEN(4,FILE=FILNAM,STATUS='NEW')
WRITE(4,320)((BACK(I,J), I=0,K), J=0,L)
GO TO 700
500 TYPE='.FMB'
FILNAM=DISC//DFNAME//TYPE
FNAME=FILNAM(3:14)
OPEN(4,FILE=FILNAM,STATUS='NEW')
WRITE(4,320)((FMB(I,J), I=0,K), J=0,L)
700 CLOSE(4)
900 CONTINUE
END
*****
SUBROUTINE PLOT
REAL FORE(0:50,0:150),BACK(0:50,0:150),FMB(0:50,0:150)
REAL DATA(0:50,0:150)
INTEGER*2 IDIO, IDIOP, PATCHS, STEPS, Z, IX, IY, IXA
INTEGER*1 INTT
INTEGER*4 IADDR, IVAL*1
COMMON FORE, BACK, FMB, IDIO, IDIOP, INTT

5 CALL HOME
PRINT*, 'FOREGROUND(1)'
PRINT*, 'BACKGROUND(2)'
PRINT*, 'FOREGROUND - BACKGROUND (3)'
PRINT*, 'RETURN TO MENU (4)'
PRINT*, ' '
WRITE(*,10)
10 FORMAT('SPECTRA TO BE PLOTTED - '\)
READ(*,20) M
20 FORMAT(I4)

WRITE(*,30)
30 FORMAT('SCALE FACTOR (STORED/SCALE = RESULT) '\)
READ(*,40) SF
40 FORMAT(F5.2)

IF(M.EQ.1) GO TO 100
IF(M.EQ.2) GO TO 200
IF(M.EQ.3) GO TO 300
IF(M.EQ.4) GO TO 1000
GO TO 5

100 PATCHS = NINT(FORE(0,0))
STEPS = NINT(FORE(0,1))
DO 120 I = 0, PATCHS
DO 110 J = 0, STEPS
DATA(I,J) = FORE(I,J) / SF
110 CONTINUE
120 CONTINUE
GO TO 400

200 PATCHS = NINT(BACK(0,0))
STEPS = NINT(BACK(0,1))
DO 220 I = 0, PATCHS
DO 210 J = 0, STEPS
DATA(I,J) = BACK(I,J) / SF
210 CONTINUE
220 CONTINUE
GO TO 400

300 PATCHS = NINT(FMB(0,0))
STEPS = NINT(FMB(0,1))
DO 320 I = 0, PATCHS
DO 310 J = 0, STEPS

```

```

      DATA(1,J) = FMB(1,J) / SF
310    CONTINUE
320    CONTINUE
      GO TO 400

400    CALL HOME
      PRINT*, 'PLOT (1)'
      PRINT*, 'LIST ON PRINTER (2)'
      PRINT*, 'RETURN TO MENU (3)'
      PRINT*, ' '
      WRITE(*,410)
410    FORMAT('SELECT A NUMBER '\)
      READ(*,20) M

      IF (M.EQ.1) GO TO 500
      IF (M.EQ.2) GO TO 600
      IF (M.EQ.3) GO TO 1000
      IF (M.GT.3) GO TO 400

500    PRINT*, 'THE AREA OF THE PLOTTER EXTENDS FROM X,Y = 0,0 '
      PRINT*, 'TO X,Y = 3600,2600'
      WRITE (*,510)
510    FORMAT('INPUT THE START OF PLOT X COORDINATE '\)
      READ (*,520) IX
520    FORMAT(I4)
      WRITE(*,525)
525    FORMAT('INPUT Y COORDINATE '\)
      READ(*,530) IY
      WRITE(*,530)
530    FORMAT('PATCH TO BE PLOTTED '\)
      READ(*,540) IP
540    FORMAT (I2)

      DMAX = DATA(IP,1)
      DO 550 J = 2, STEPS
      IF (DATA(IP,J).GT.DMAX) DMAX = DATA(IP,J)
550    CONTINUE
      WRITE(*,560) DMAX
560    FORMAT('THE MAXIMUM IS ',F10.3)
      SC = (2600.0-IY)/DMAX
      WRITE(*,570) SC
570    FORMAT('TO FIT PLOT MUST SCALE BY ',F10.5)

      PRINT*, 'AUTO SCALE (1)'
      PRINT*, 'YOUR CHOICE (2)'
      PRINT*, 'NO SCALE (3) '
      WRITE (*,580)
580    FORMAT('SELECT A NUMBER '\)
      READ(*,590) M
590    FORMAT(I1)

      GO TO (640,610,600), M

600    SC = 1.0
      GO TO 640
610    WRITE(*,620)
620    FORMAT('YOUR CHOICE OF SCALING FACTOR IS '\)
      READ(*,630) SC
630    FORMAT(F10.5)
640    WRITE(*,650) SC
650    FORMAT('SCALING FACTOR IS ',F10.5)

      WRITE(*,660)
660    FORMAT('X AXIS SCALING FACTOR (1 TO 5) '\)
      READ(*,670) IXA
670    FORMAT(I1)

```

```

IADDR = $F9CDE
IVAL = $00
CALL POKE (IADDR, IVAL)
IADDR = $F9D0F
IVAL = $00
CALL POKE (IADDR, IVAL)
OPEN(6, FILE='LST:', STATUS='NEW')

WRITE(6, 700) ' '
700  FORMAT(A)
WRITE(6, 710) 'M', IX, ', ', IY
710  FORMAT(A, I4, A, I4)

IX = 0
IY = INT (DATA(IP, 1)*SC)
WRITE(6, 710) 'I', IX, ', ', IY
DO 750 J = 2, STEPS
IX = IXA
IY = INT((DATA(IP, J) - DATA(IP, J-1)) * SC)
WRITE (6, 710) 'I', 0, ', ', IY
WRITE (6, 710) 'I', IX, ', ', 0
750  CONTINUE

WRITE(6, 700) 'H'

CLOSE(6)
IADDR = $F9CDE
IVAL = $04
CALL POKE (IADDR, IVAL)
IADDR = $F9D0F
IVAL = $04
CALL POKE (IADDR, IVAL)

GO TO 400

* PRINTING THE DATA *
800  OPEN(6, FILE='LST:', STATUS='NEW')
805  PRINT*, 'GIVE START AND END OF DUMP '
WRITE(*, 810)
810  FORMAT('START - '\)
READ(*, 820) K
820  FORMAT(I4)
WRITE(*, 830)
830  FORMAT(' END - '\)
READ(*, 820) L
WRITE(*, 850)
850  FORMAT('PATCH NUMBER -'\)
READ(*, 860) IP
860  FORMAT (I2)

IF(K.LT.0) GO TO 805
IF(K.GT.STEPS) GO TO 805
IF(L.LT.K) GO TO 805
IF(L.GT.STEPS) GO TO 805
IF(IP.LT.0) GO TO 805
IF(IP.GT.PATCHS) GO TO 805

865  PRINT*, ' '
PRINT*, ' '
PRINT*, 'DUMP TO SCREEN (1)'
PRINT*, 'DUMP TO PRINTER (2)'
WRITE(*, 870)
870  FORMAT('DESTINATION OF DUMP -'\)
READ(*, 880) N
880  FORMAT(I1)

```



```

        IF (N.EQ.1) GO TO 890
        IF (N.EQ.2) GO TO 900
        GO TO 865

890      Z = 0
        GO TO 910
900      Z = 6
910      WRITE(Z,920)

920      FORMAT('DATA')
        DO 950 I = K,L
        WRITE(Z,930) I, DATA(IP,I)
930      FORMAT(I4,F15.4)
950      CONTINUE

        IF (Z.EQ.6) GO TO 980
        WRITE(*,960)
960      FORMAT('INPUT INTEGER TO CONTINUE '\)
        READ(*,970)M
970      FORMAT(I2)

980      CLOSE(6)

        GO TO 400

1000     RETURN
        END

*****
SUBROUTINE INTTIM
REAL FORE(0:50,0:150),BACK(0:50,0:150),FMB(0:50,0:150)
INTEGER*2 IDIC,IDIOF
INTEGER*1 INTT
COMMON FORE,BACK,FMB,IDIC,IDIOF,INTT
EXTERNAL STATUS
INTEGER*4 IADDR
INTEGER*1 IVAL
IVAL=$04
IADDR=$FF0017
CALL POKE(IADDR,IVAL)
IADDR=$FF0012
CALL HOME
IF (INTT.LT.0) JVAL=-1-INTT
IF (INTT.GE.0) JVAL=255-INTT
WRITE(*,110) 'INT TIME=',JVAL
10      CALL STATUS
        IX=IPEEK($FF00FC)
C        HEX 0B TO INCREASE AND HEX 16 TO DECREASE
        IF (IX.EQ.$0B) GO TO 100
        IF (IX.EQ.$16) GO TO 200
        GO TO 900
100      IF (JVAL.EQ.255) GO TO 105
        INTT=INTT-1
        PRINT*,INTT
        IF (INTT.LT.0) JVAL=-1-INTT
        IF (INTT.GE.0) JVAL=255-INTT
        IVAL=INTT
        CALL POKE(IADDR,IVAL)
105      CALL HOME
        WRITE(*,110) 'INT TIME=',JVAL
110      FORMAT(A9,I3)
        GO TO 10
200      IF (JVAL.EQ.1) GO TO 105
        INTT=INTT+1
        PRINT*,INT

```

```

        IF (INT1.L1.0) JVAL=-1-INT1
        IF (INTT.GE.0) JVAL=255-INTT
        IVAL=INTT
        CALL POKE(IADDR, IVAL)
        GO TO 105
900     RETURN
        END
*****
        SUBROUTINE TRSTG
        INTEGER*4 IADDR
        INTEGER*1 IVAL
10      PRINT*, 'MOVE FORWARD(1)'
        PRINT*, 'MOVE BACK(2)'
        PRINT*, 'RETURN TO MENU(3)'
        PRINT*, ' '
        PRINT*, ' '
90      WRITE(*,100)
100     FORMAT('WHAT WOULD YOU LIKE TO DO?- '\)
        READ(*,110) K
        IF (K.EQ.3) GO TO 900
110     FORMAT(I4)
        PRINT*, ' '
        PRINT*, ' '
        WRITE(*,120)
120     FORMAT('HOW MANY MM- '\)
        READ(*,115) RMM
        IPULSE=INT(RMM/.0127)
115     FORMAT(F5.1)
        IADDR=$FF0017
        IVAL=$00
        CALL POKE(IADDR, IVAL)
        IF (K.EQ.1) GO TO 200
        IF (K.EQ.2) GO TO 300
        GO TO 90
200     IADDR=$FF0012
        DO 230 I=1, IPULSE
        IVAL=$FD
        CALL POKE(IADDR, IVAL)
        CALL DELAY
        IVAL=$FF
        CALL POKE(IADDR, IVAL)
        CALL DELAY
230     CONTINUE
        CALL HOME
        IVAL=$04
        IADDR=$FF0017
        CALL POKE(IADDR, IVAL)
        GO TO 10
300     IADDR=$FF0012
        DO 330 I=1, IPULSE
        IVAL=$FE
        CALL POKE(IADDR, IVAL)
        CALL DELAY
        IVAL=$FF
        CALL POKE(IADDR, IVAL)
        CALL DELAY
330     CONTINUE
        CALL HOME
        IVAL=$04
        IADDR=$FF0017
        CALL POKE(IADDR, IVAL)
        GO TO 10
900     RETURN
        END
*****
        SUBROUTINE DELAY

```

```

      DO 20 I=1,5
      D=(2.303)*FLOAT(I)
20    CONTINUE
      RETURN
      END

```

```

SUBROUTINE TRSTGB
INTEGER*4 IADDR
INTEGER*1 IVAL
IADDR=$FF0017
IVAL=$00
CALL POKE(IADDR,IVAL)
IADDR=$FF0012
IVAL=$FE
CALL POKE(IADDR,IVAL)
CALL DELAY
IVAL=$FF
CALL POKE(IADDR,IVAL)
CALL DELAY
IVAL=$04
IADDR=$FF0017
CALL POKE(IADDR,IVAL)
RETURN
END

```

```

SUBROUTINE TRSTGF
INTEGER*4 IADDR
INTEGER*1 IVAL
IADDR=$FF0017
IVAL=$00
CALL POKE(IADDR,IVAL)
IADDR=$FF0012
IVAL=$FD
CALL POKE(IADDR,IVAL)
CALL DELAY
IVAL=$FF
CALL POKE(IADDR,IVAL)
CALL DELAY
IADDR=$FF0017
IVAL=$04
CALL POKE(IADDR,IVAL)
RETURN
END

```

APPENDIX B

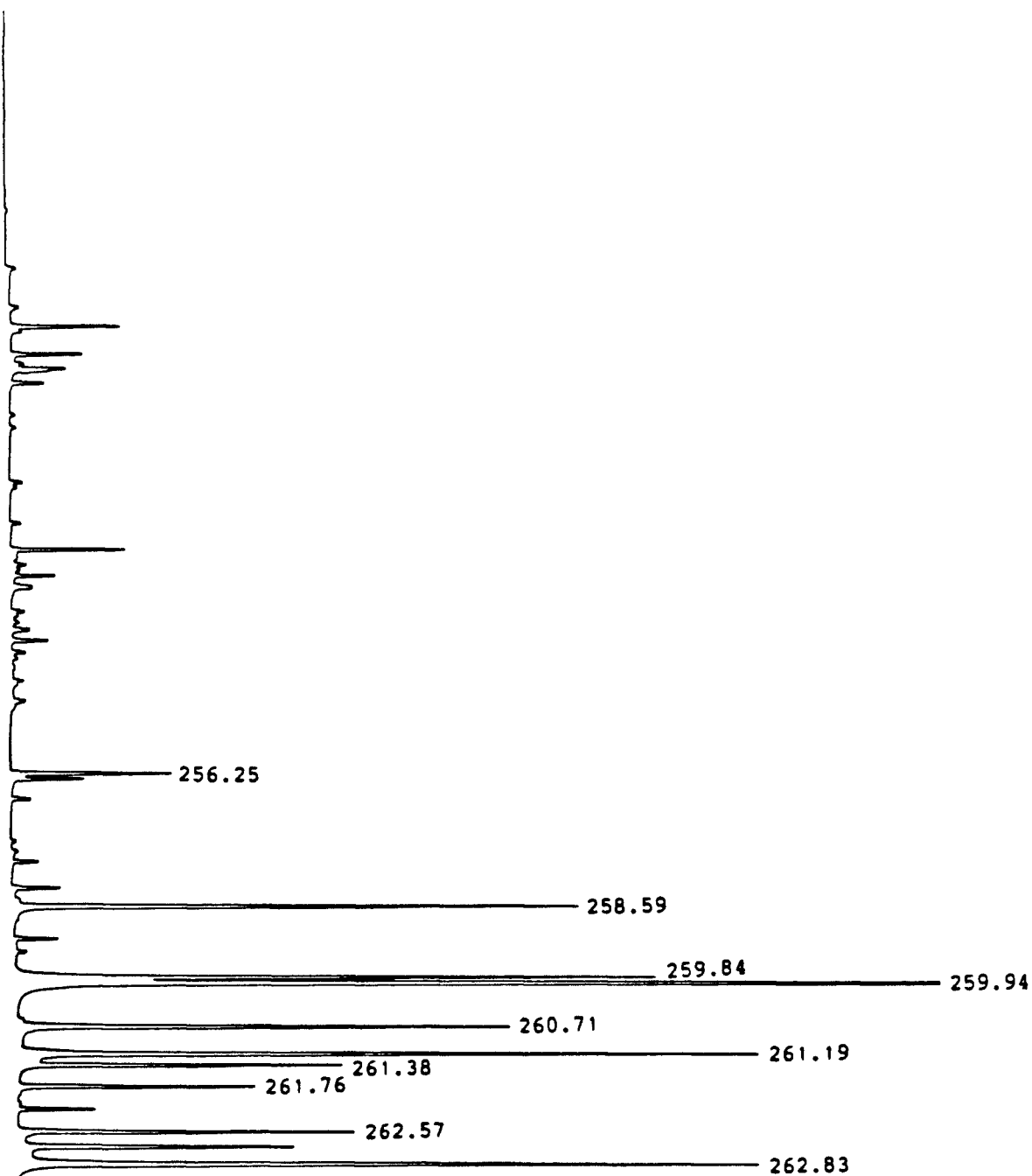
Fe spectra collected at an rf input power of 1.25 kW and a vertical height of 16 mm above the load coil are presented in parts A,B,C,D,E,F,G and H. The wavelength range of each spectrum and the emission lines contained within are listed in the following table. In order to see weak, high energy lines, the intensity axis have been expanded by the appropriate scale factor.

<u>Part</u>	<u>Wavelength Range (nm)</u>	<u>FeI Line</u>	<u>FeII Line</u>	<u>Scale Factor</u>
A	242.80 - 267.10		256.25	6.0
			258.59	
			259.84	
			259.94	
			260.71	
			261.19	
			261.38	
			261.76	
			262.57	
			262.83	
B	242.80 - 267.10		256.35	60.0
			256.69	
			258.26	
			259.15	
			262.17	
			266.47	
			266.66	
C	267.30 - 290.80		271.44	6.0
			272.75	
			273.96	
			274.32	
			274.65	
			275.33	

<u>Part</u>	<u>Wavelength Range (nm)</u>	<u>FeI Line</u>	<u>FeII Line</u>	<u>Scale Factor</u>
D	267.30 - 290.80		273.07 275.57 276.18	60.0
E	343.30 - 367.10	356.54 357.01 358.12 360.89 361.88		2.0
F	343.30 - 367.30	355.37 360.55 360.67 365.15		30.0
G	367.10 - 391.00	371.99 373.49 373.71 374.95 381.58 382.04 382.59 382.78 385.99 388.63		2.0
H	367.10 - 391.00	368.22 376.55 388.85		30.0

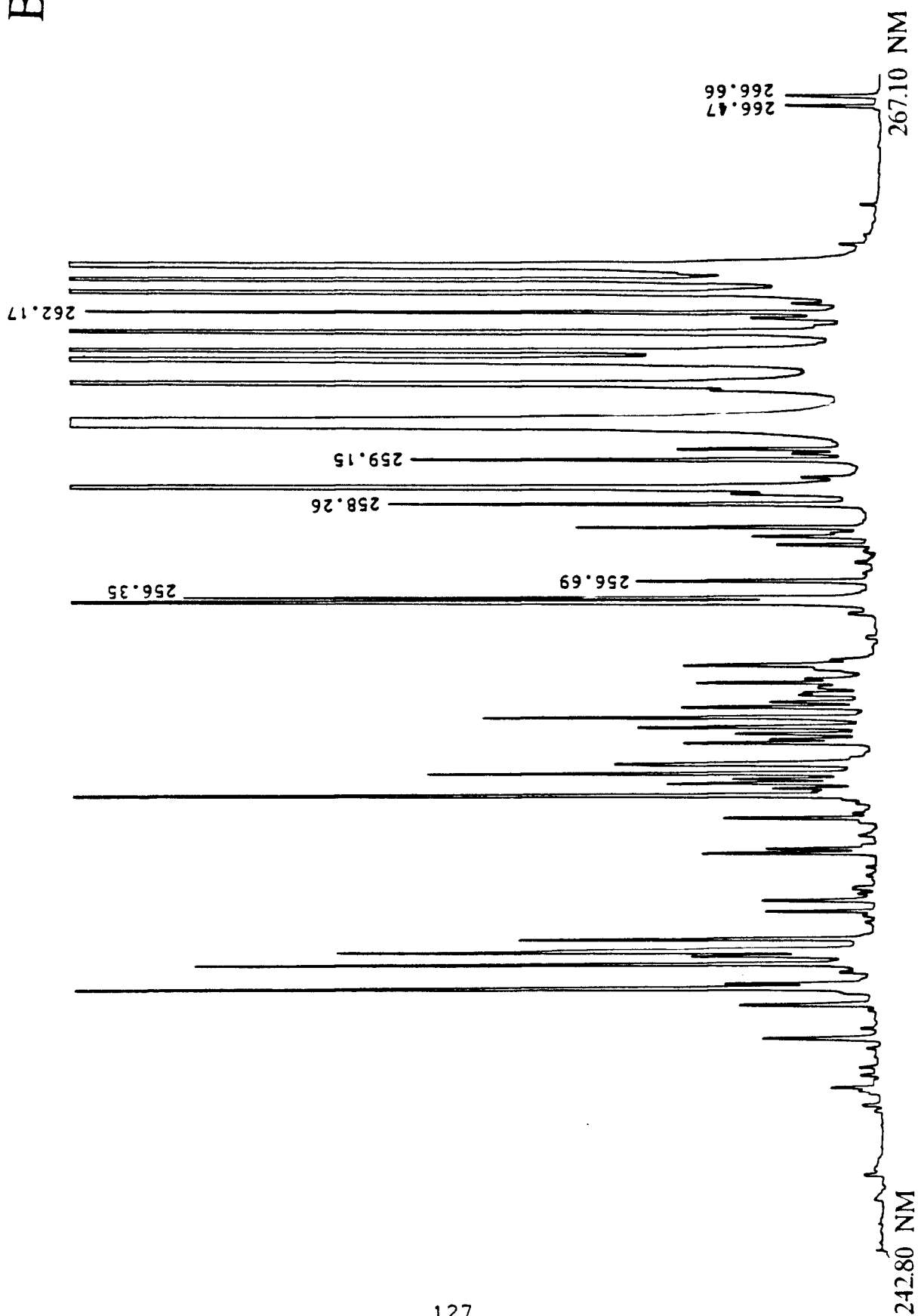
242.80 NM

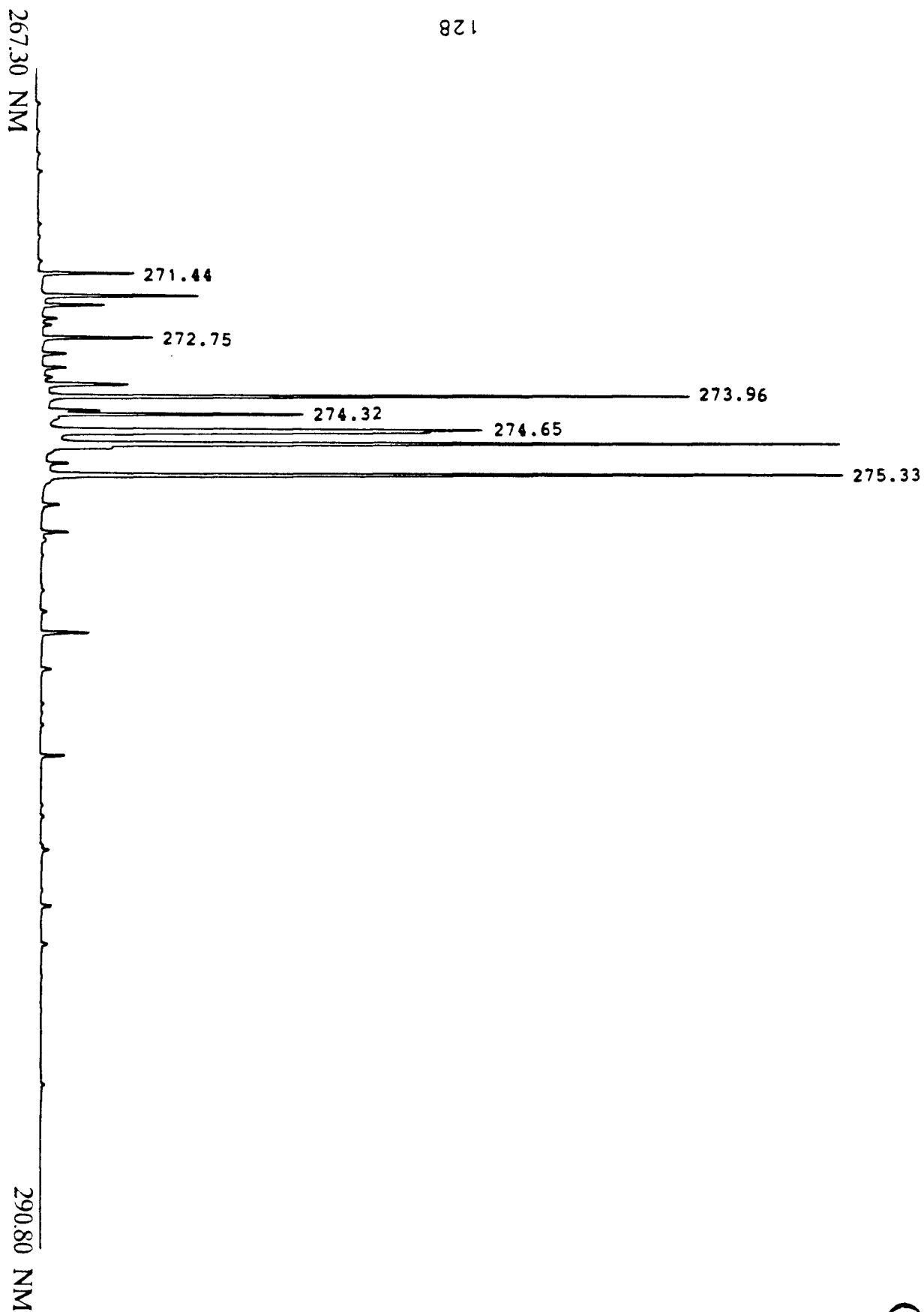
267.10 NM



A

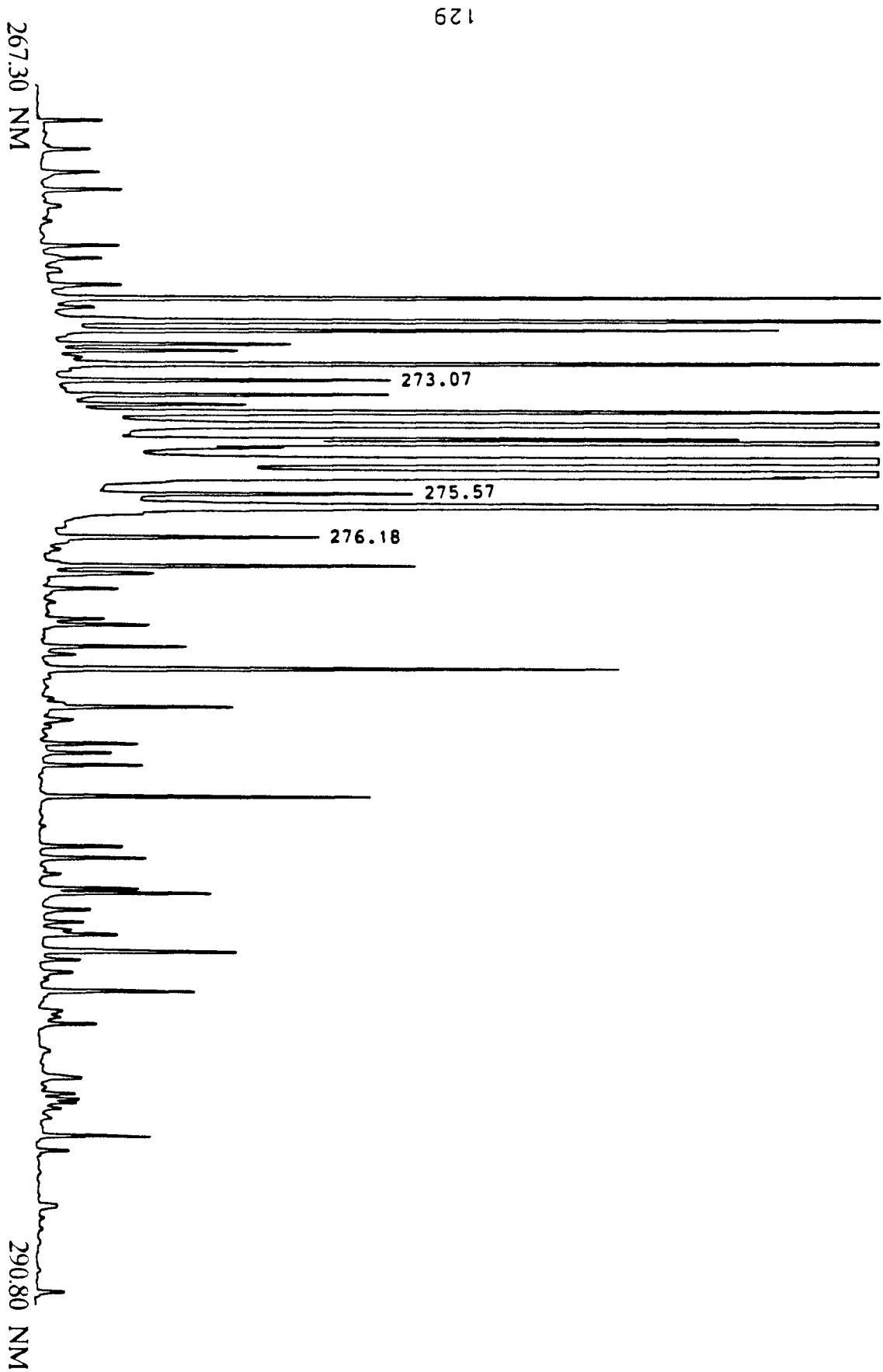
B



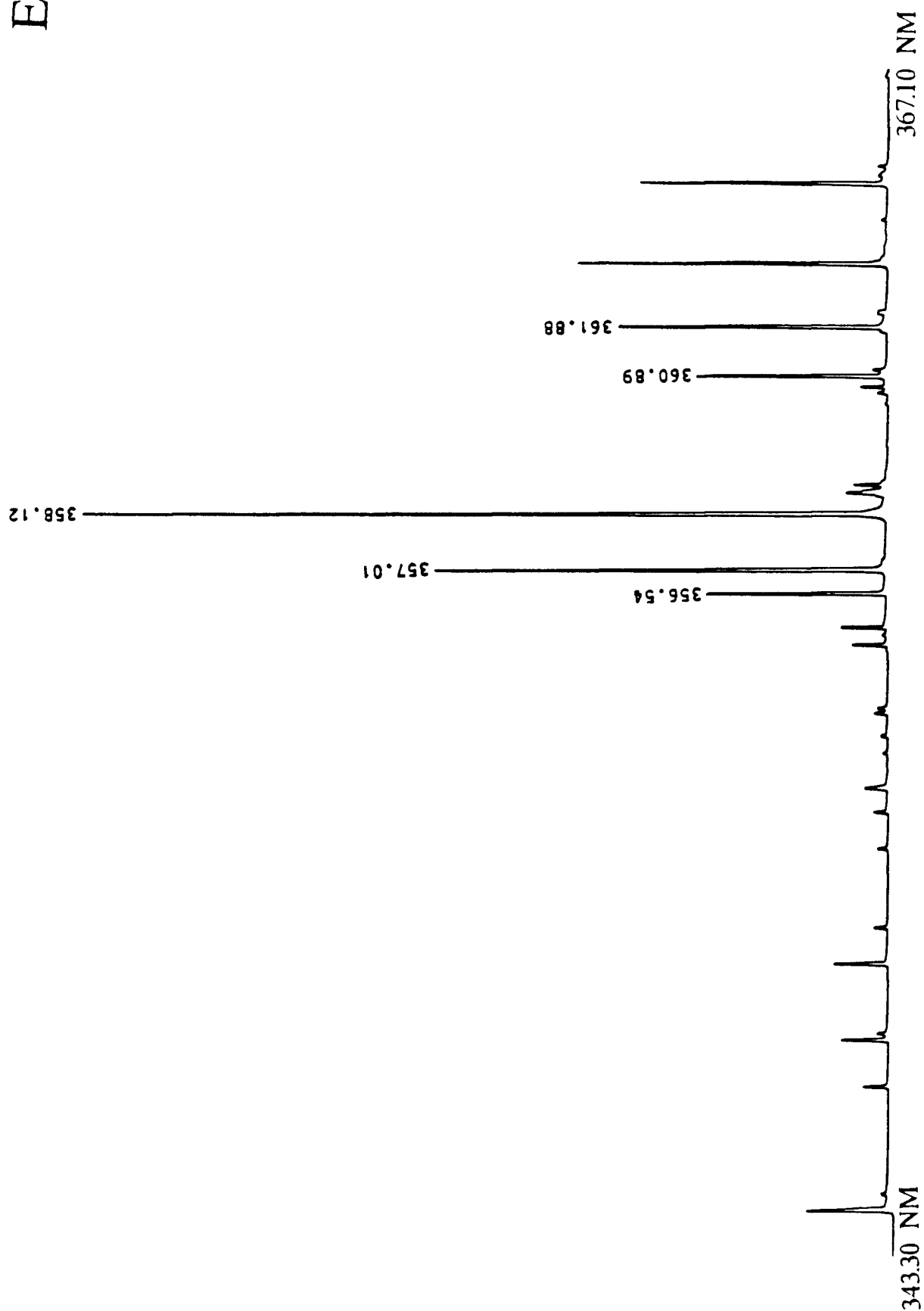


C

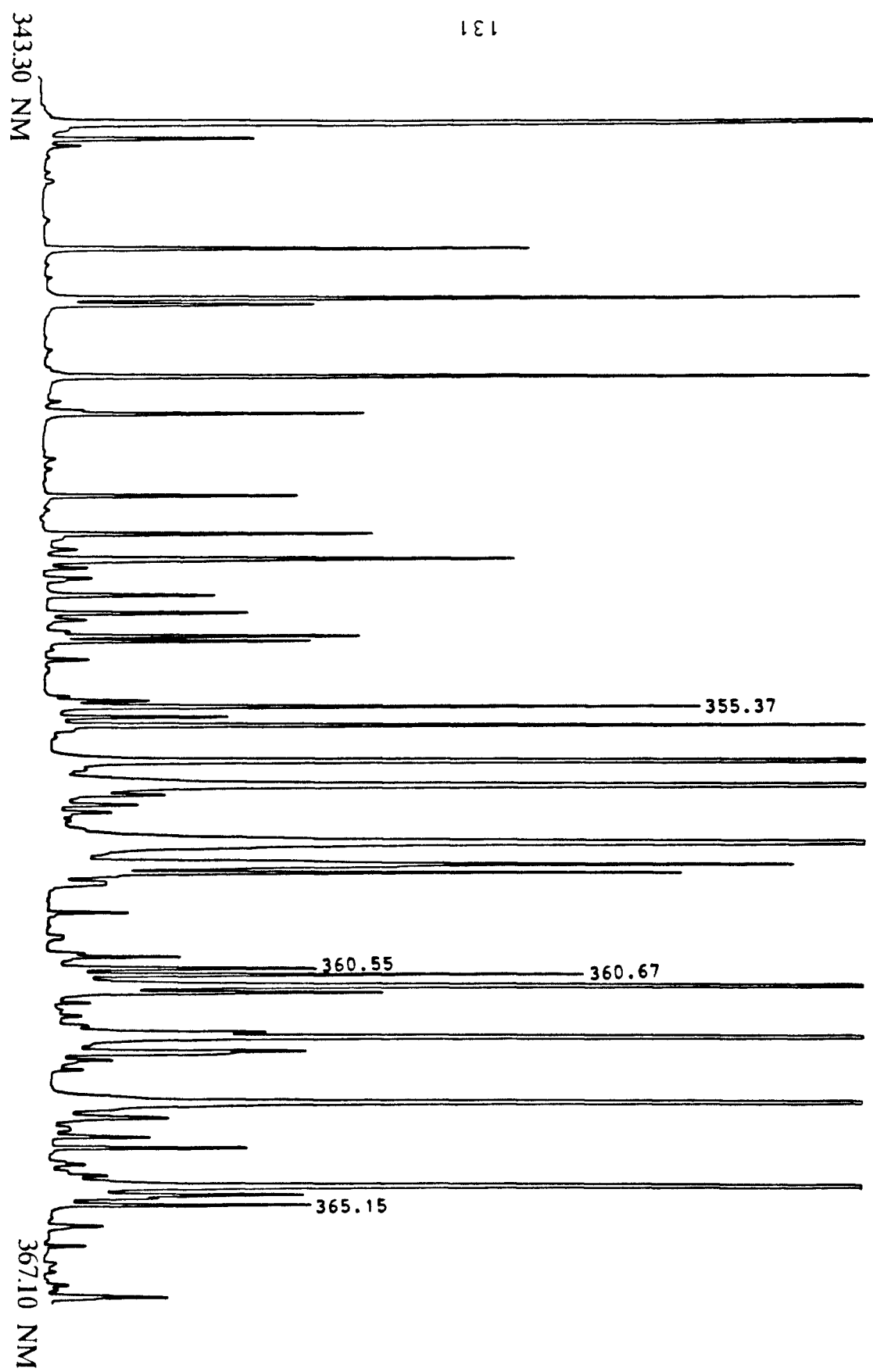
D



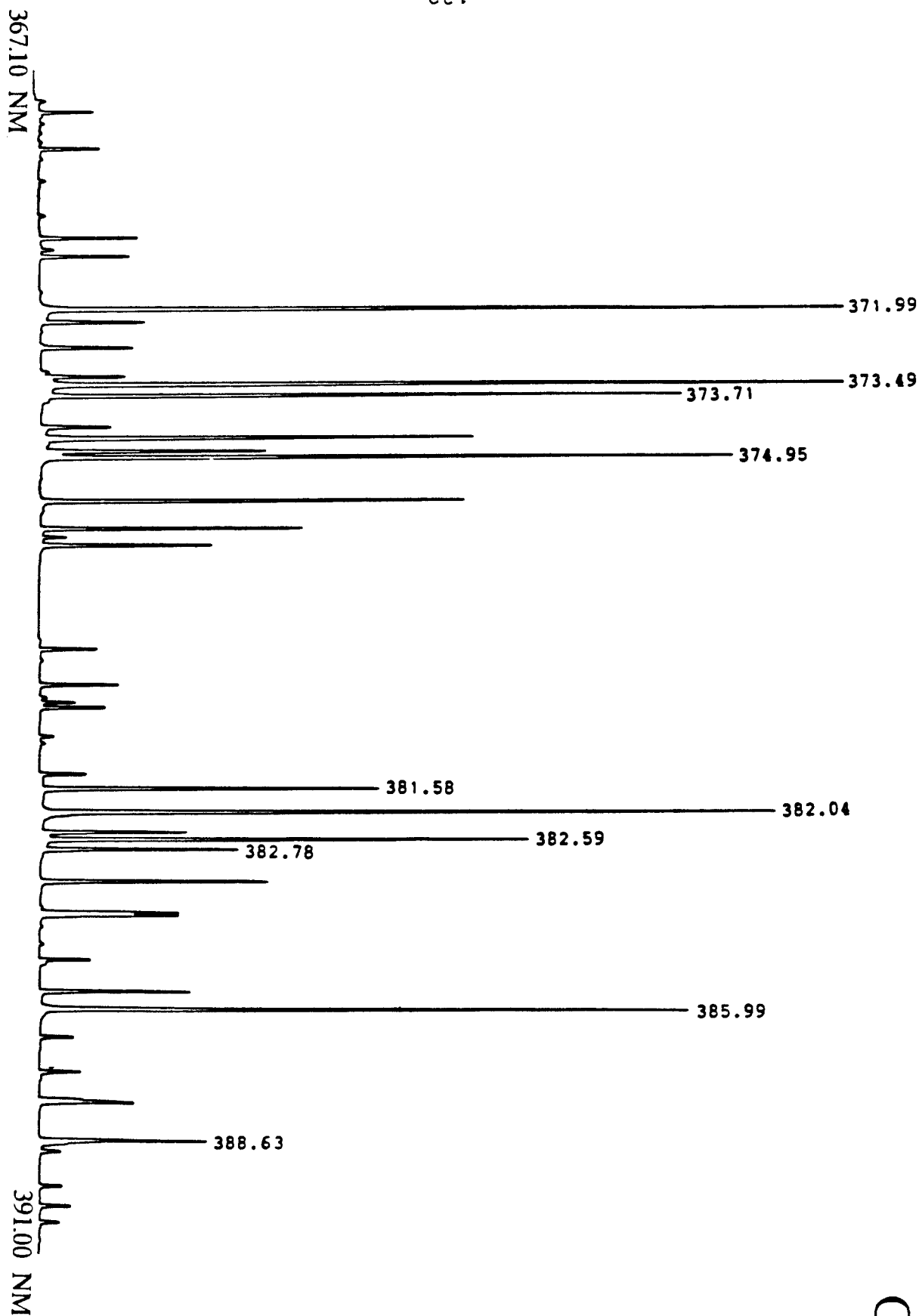
E



F

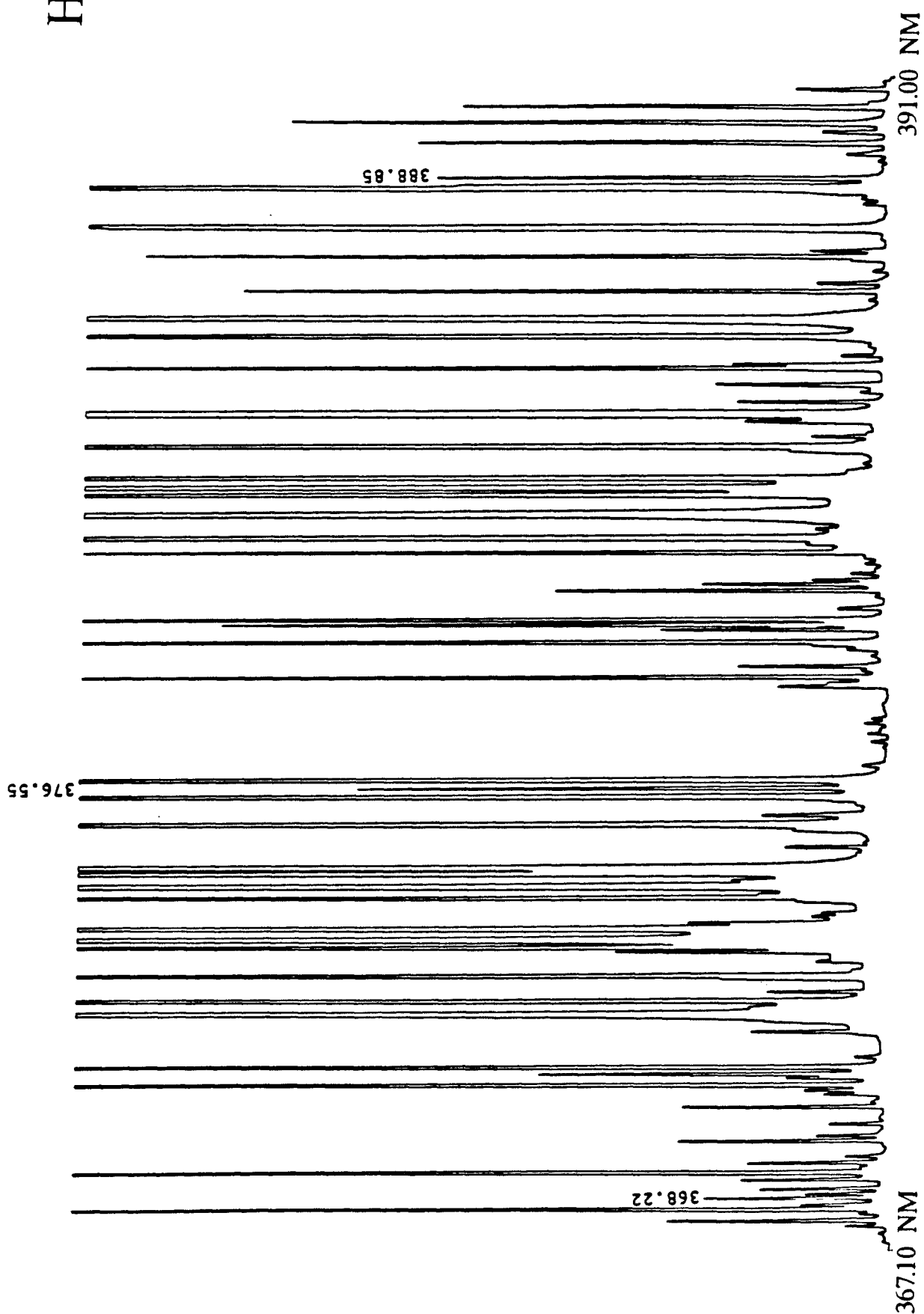


132



G

H

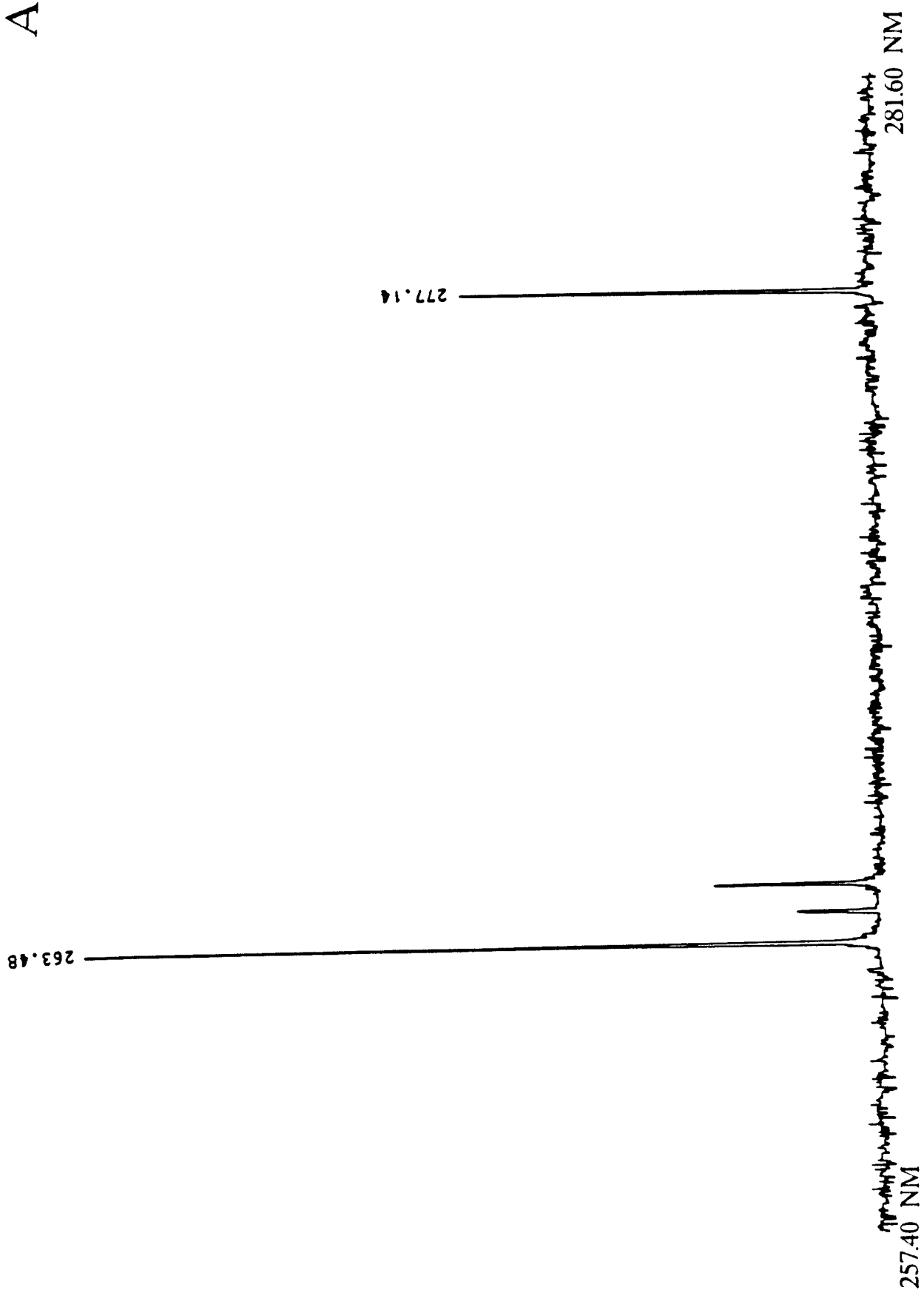


APPENDIX C

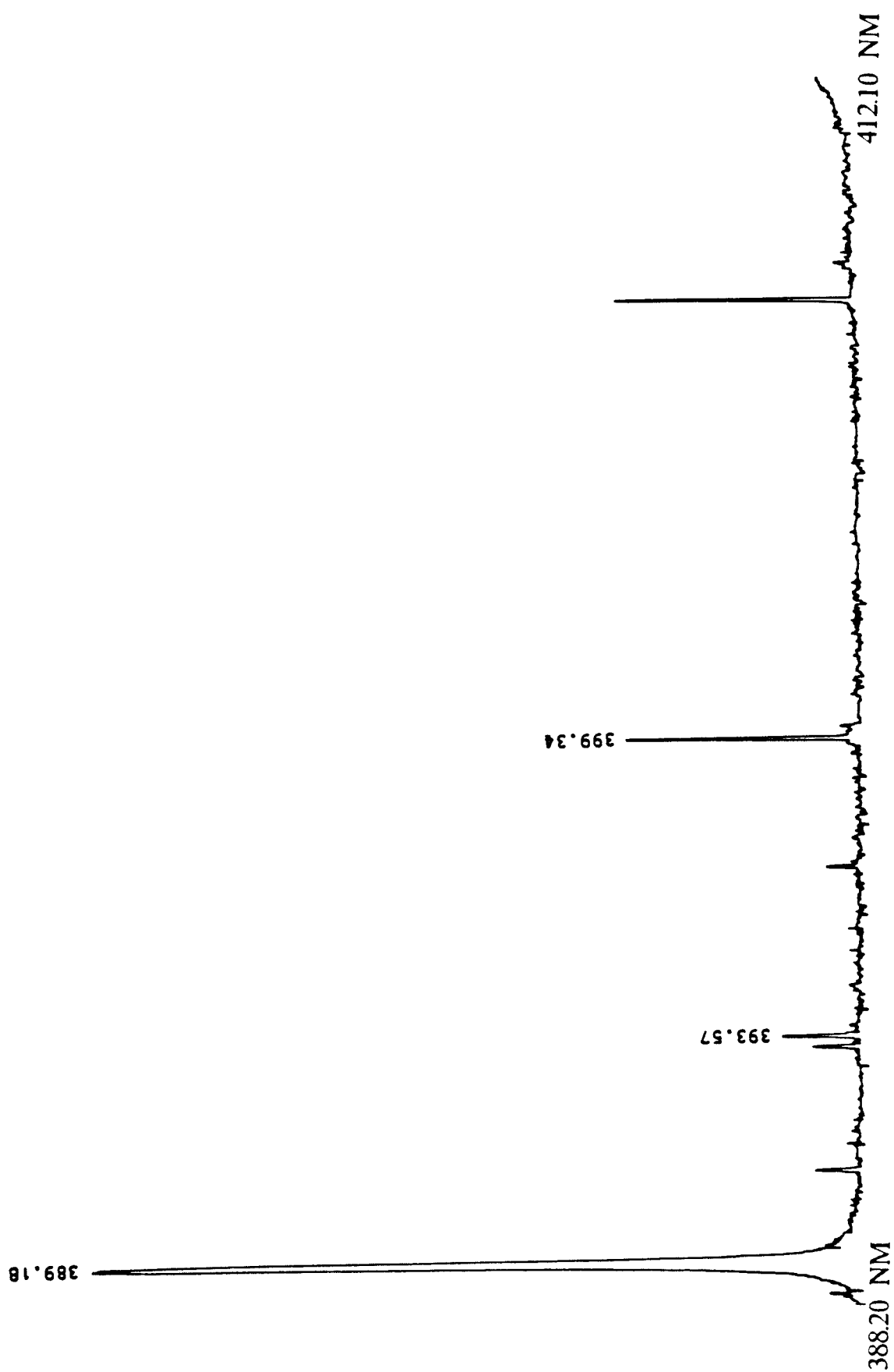
Ba spectra collected at an rf input power of 1.25 kW and a vertical height of 16 mm above the load coil are presented in parts A,B,C,D,E and F. The wavelength range of each spectrum and the emission lines contained within are listed in the following table. In order to see weak, high energy lines, the spectra have been expanded by the appropriate scale factor.

<u>Part</u>	<u>Wavelength Range (nm)</u>	<u>BaI Line</u>	<u>BaII Line</u>	<u>Scale Factor</u>
A	257.40 - 281.60		263.48 277.14	150.0
B	388.20 - 412.10	393.57 399.34	389.18	125.0
C	412.10 - 435.03	428.31 435.03	413.07 416.60	125.0
D	448.65 - 472.50		452.49 455.40	1.0
E	472.30 - 495.10		490.00 493.41	1.0
F	575.90 - 597.50	577.76 582.63 590.76 597.17	585.37	150.0

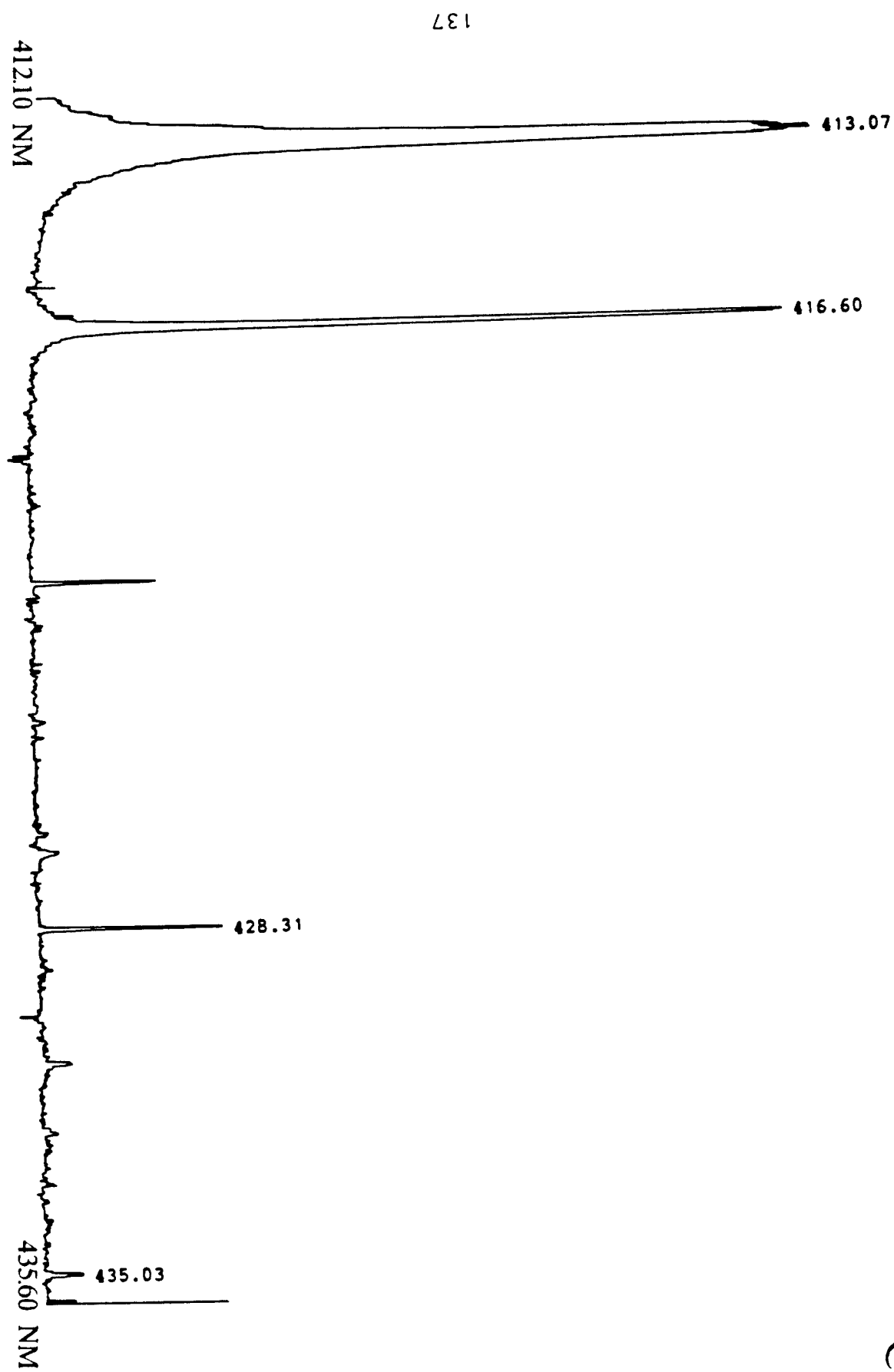
A



B

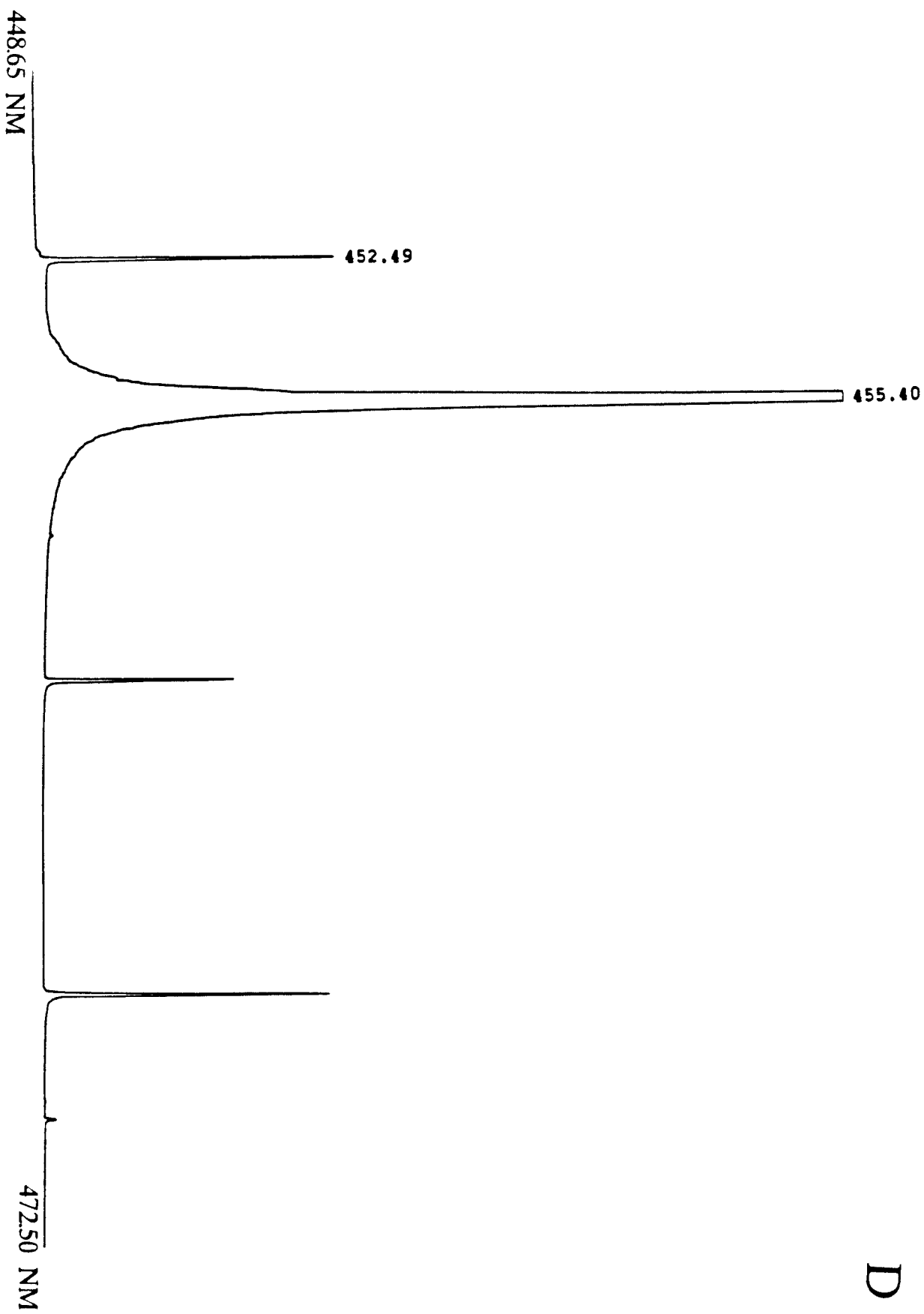


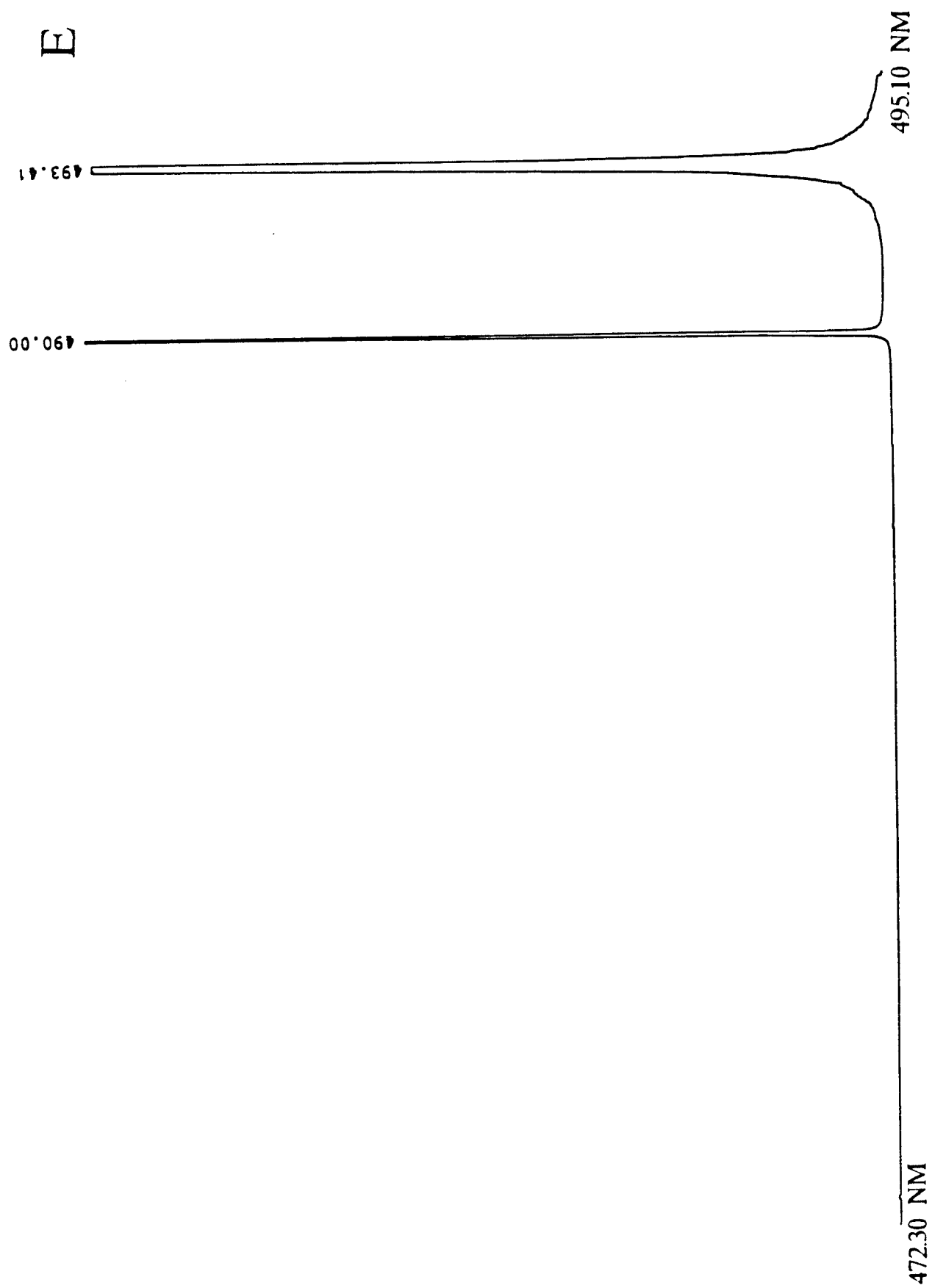
C



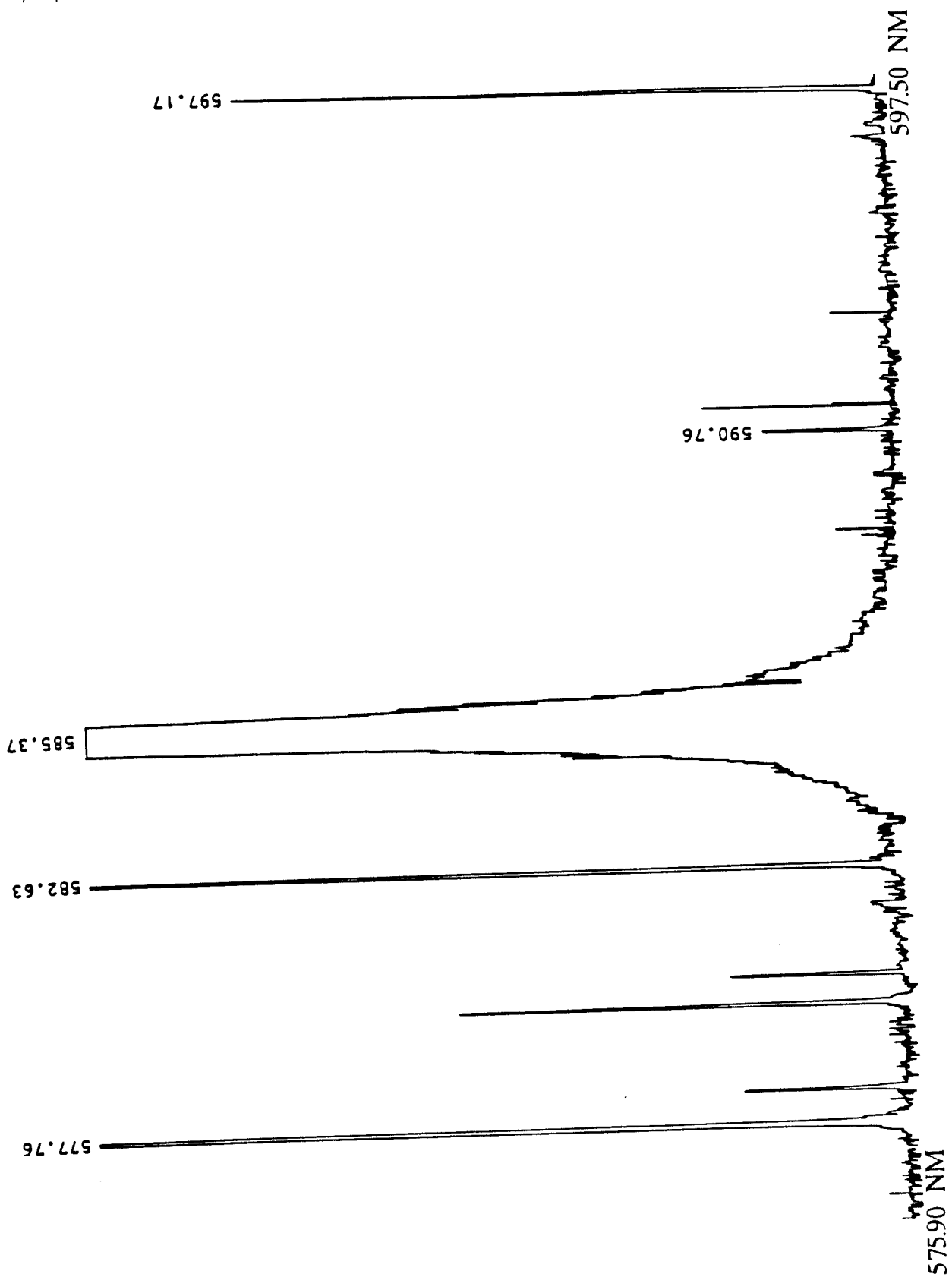
D

138





F



APPENDIX D

Cr spectra collected at an rf input power of 1.25 kW and a vertical height of 16 mm above the load coil are presented in parts A,B,C,D,E and F. The wavelength range of each spectrum and the emission lines contained within are listed in the following table. In order to see weak, high energy lines, the spectra have been expanded by the appropriate scale factor.

<u>Part</u>	<u>Wavelength Range (nm)</u>	<u>CrI Line</u>	<u>CrII Line</u>	<u>Scale Factor</u>
A	245.80 - 270.10		265.36 265.86 266.60	1.0
B	269.60 - 294.70		284.98 286.26 287.04	1.0
C	269.60 - 294.70	272.65 273.19 276.99 290.91	277.81 292.71	100.0
D	285.00 - 309.20	297.55 299.66 300.09 300.51 302.16 302.44 305.39	297.19 297.97 304.09 305.01	3.0
E	309.30 - 333.30		311.87 312.04 318.07 323.41	0.75

<u>Part</u>	<u>Wavelength Range (nm)</u>	<u>CrI Line</u>	<u>CrII Line</u>	<u>Scale Factor</u>
F	421.10 - 444.60	425.44 427.48 428.97 434.45 435.18		

A

143

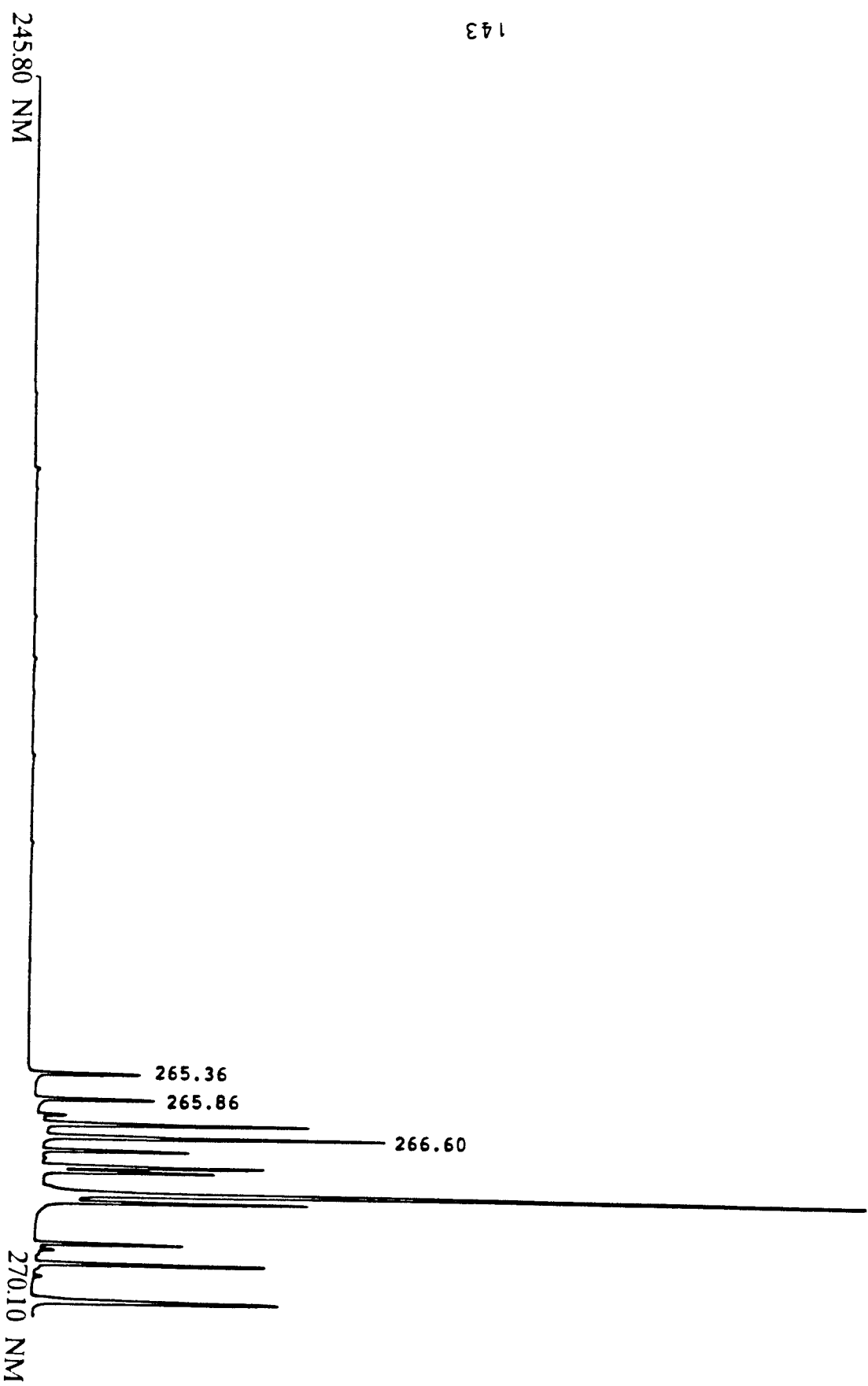
245.80 NM

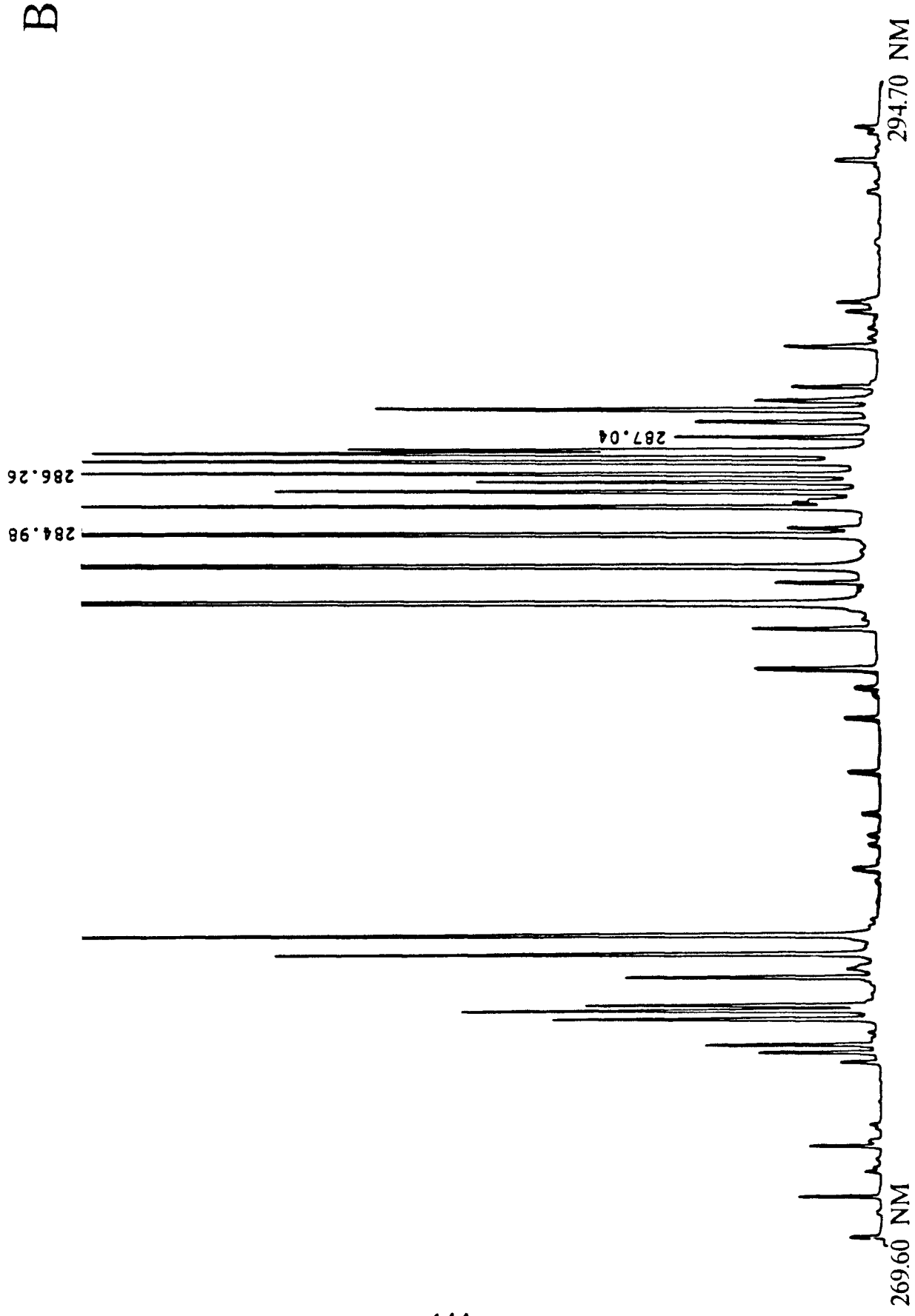
265.36

265.86

266.60

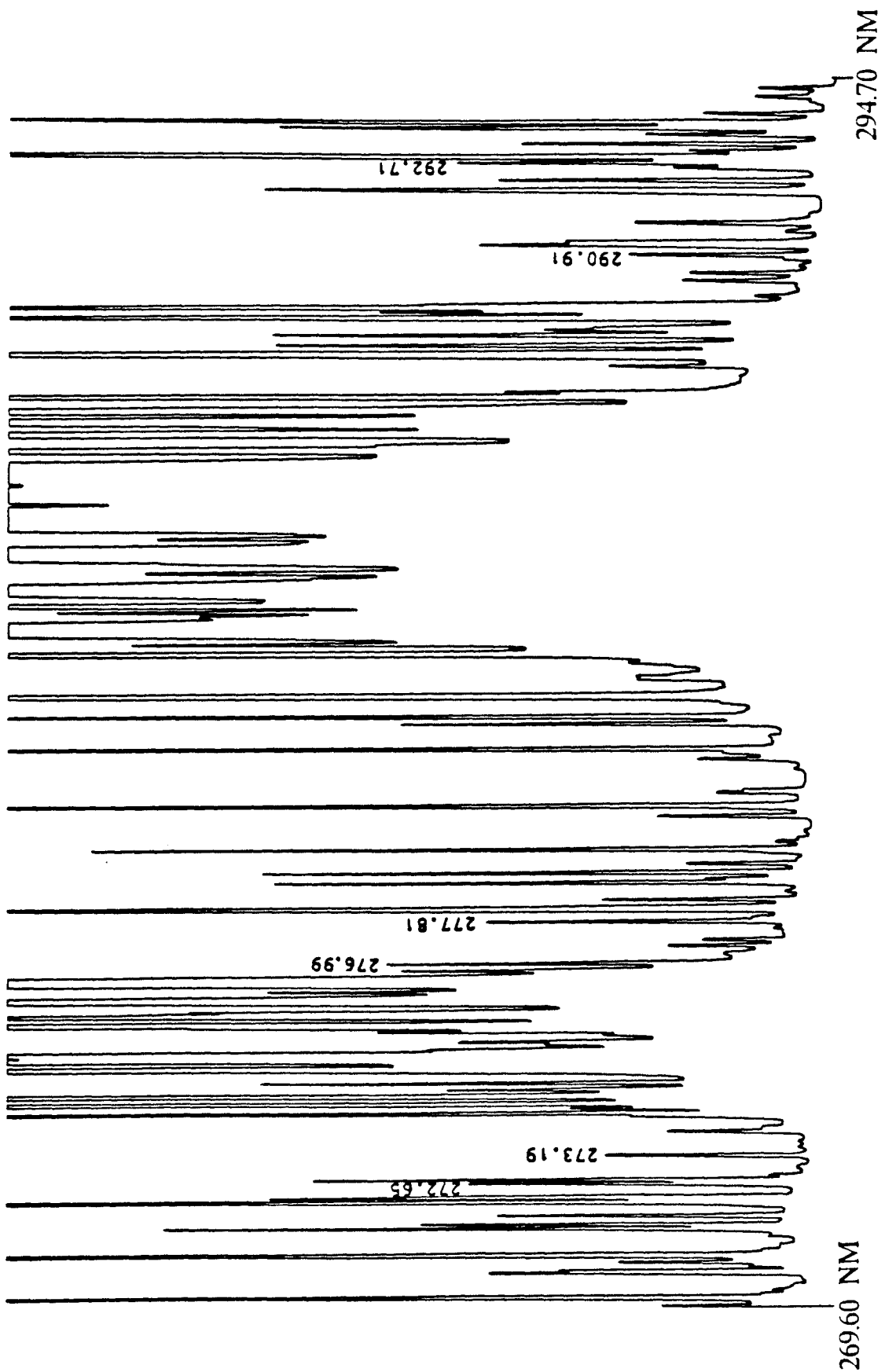
270.10 NM

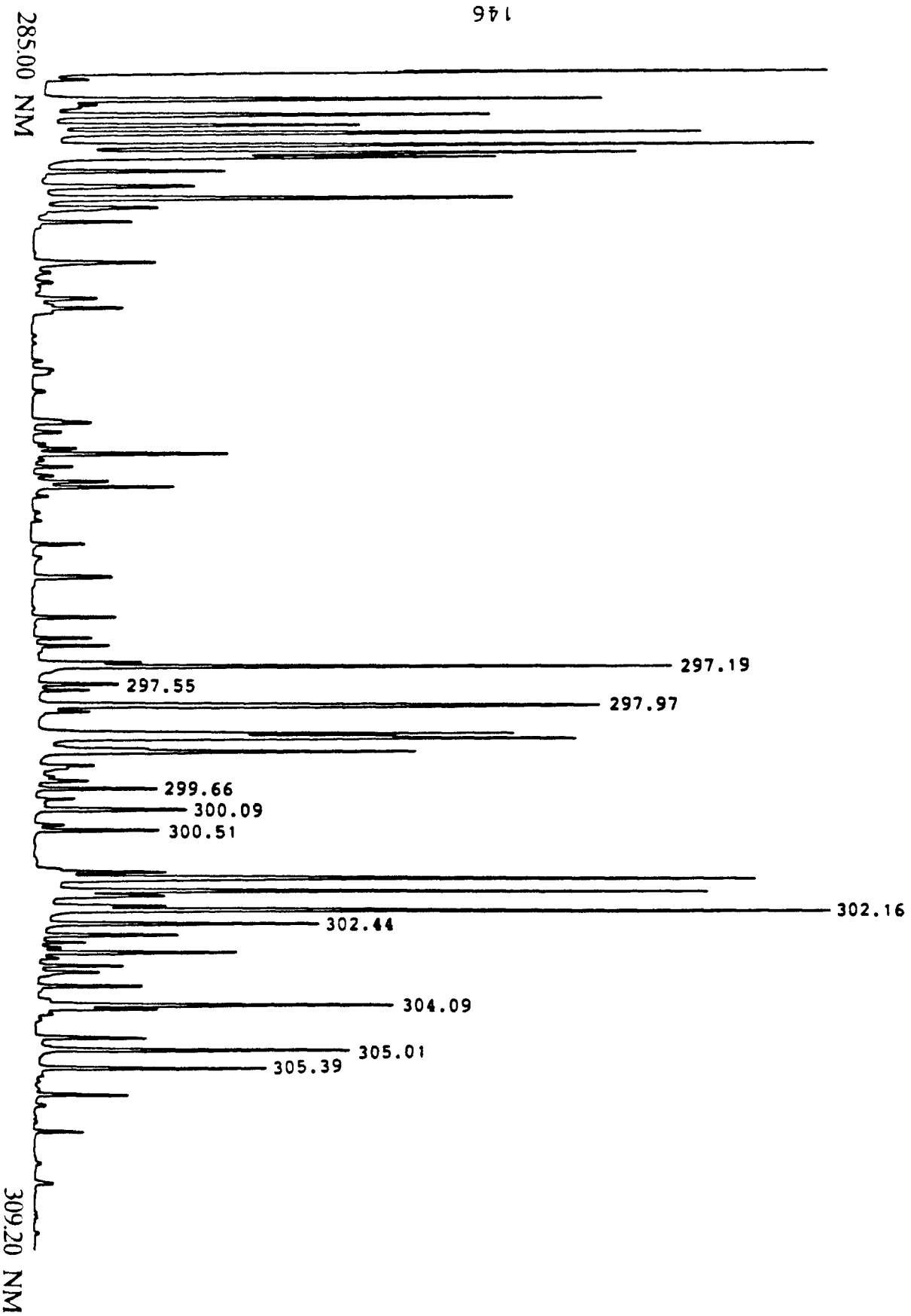




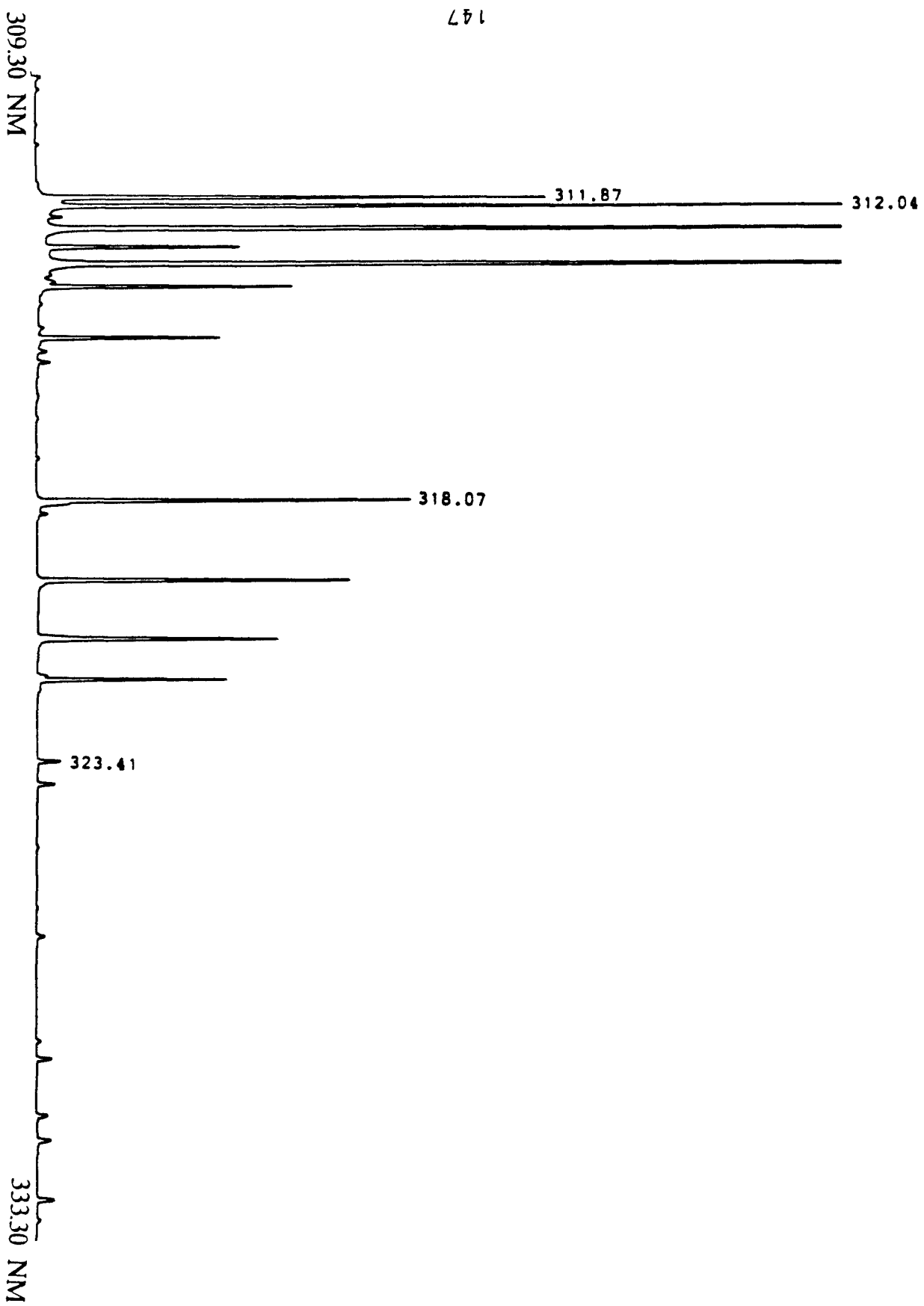
B

C





D



E

421.10 NM

148

425.44

427.48

428.97

434.45

435.18

444.60 NM

F